

**NOVEL CONTROL AND COMMUNICATION APPROACHES
FOR PERFORMANCE IMPROVEMENT
IN NETWORKED CONTROL SYSTEMS**

Ph.D. THESIS

Ahmet KUZU

Department of Control and Automation Engineering

Control and Automation Engineering Programme

FEBRUARY 2015

**NOVEL CONTROL AND COMMUNICATION APPROACHES
FOR PERFORMANCE IMPROVEMENT
IN NETWORKED CONTROL SYSTEMS**

Ph.D. THESIS

**Ahmet KUZU
(504062108)**

Department of Control and Automation Engineering

Control and Automation Engineering Programme

Thesis Advisor: Prof. Dr. Metin GÖKAŞAN

FEBRUARY 2015

**AĞ ÜZERİNDEN KONTROL SİSTEMLERİNİN
PERFORMANS İYİLEŞTİRMESİ İÇİN
YENİ KONTROL VE HABERLEŞME YAKLAŞIMLARI**

DOKTORA TEZİ

**Ahmet KUZU
(504062108)**

Kontrol ve Otomasyon Mühendisliği Anabilim Dalı

Kontrol ve Otomasyon Mühendisliği Programı

Tez Danışmanı: Prof. Dr. Metin GÖKAŞAN

ŞUBAT 2015

Ahmet KUZU, a Ph.D. student of ITU Graduate School of Science Engineering and Technology 504062108 successfully defended the thesis entitled “**NOVEL CONTROL AND COMMUNICATION APPROACHES FOR PERFORMANCE IMPROVEMENT IN NETWORKED CONTROL SYSTEMS**”, which he/she prepared after fulfilling the requirements specified in the associated legislations, before the jury whose signatures are below.

Thesis Advisor : **Prof. Dr. Metin GÖKAŞAN**
Istanbul Technical University

Co-advisor : **Prof. Dr. Seta BOĞOSYAN**
Istanbul Technical University

Jury Members : **Prof. Dr. Asif SABANOVIC**
Sabancı University

Prof. Dr. İbrahim EKSİN
Istanbul Technical University

Prof. Dr. Hakan TEMELTAŞ
Istanbul Technical University

Assoc. Prof. Kemalettin ERBATUR
Sabancı University

Asst. Prof. Özgür Turay KAYMAKÇI
Yıldız Technical University

Date of Submission : **30 Aralık 2014**

Date of Defense : **20 February 2015**

To my family,

FOREWORD

I would like to gratefully acknowledge the supervision of Prof. Dr. Metin Gokařan and Prof. Dr. Seta Boęosyan for their important support and constructive comments throughout this work. I would like to express my deep and sincere gratitude to Prof. Dr. Asıf Sabanovic for his constructive criticism and excellent advices during the preparation of this thesis. I would also like to thank the members of my thesis committee; Prof. Dr. İbrahim Eksin and Prof. Dr. Hakan Temeltař for their guidance and valuable advices. My special thanks go to my colleague; Sabri Yılmaz, for his cooperation.

I would like to thank Mechatronics Education and Research Center (MEAM) family, especially to Alev Keskin and Reyhan Kenan, who are the very talented technicians, for their practical contributions.

I would like to thank Sabancı University family, especially to Dr. Eray Baran, for his support and cooperation.

Also, I would like to thank University of Alaska Fairbanks family, especially to Rex Estrada, for his friendliness, kind support and cooperation.

Finally, I would like to thank deeply my son Aybars Kuzu, my wife Ebru Kuzu, my mother Aliye Kuzu, and my father Mustafa Kuzu for their unconditional love, support and belief in me throughout my PhD.

February 2015

Ahmet KUZU
(MSc.)

TABLE OF CONTENTS

	<u>Page</u>
FOREWORD.....	ix
TABLE OF CONTENTS.....	xi
ABBREVIATIONS	xiii
LIST OF TABLES	xv
LIST OF FIGURES.....	xvii
SUMMARY	xix
ÖZET	xxi
1. INTRODUCTION	1
1.1 Motivation.....	1
1.2 Purpose of the Thesis.....	4
1.3 Contributions of the Thesis.....	5
1.4 Thesis Outline.....	6
2. NETWORKED CONTROL CORE SOLUTION.....	7
2.1 System Configuration	8
2.2 Design of Delay Regulator	9
2.3 Design Of Control And Estimation Schemes For The Master-Slave System	10
2.3.1 Astrom’s Smith Predictor (ASP) on master side	10
2.3.2 Sliding Mode Observer (SMO) on master side	14
2.4 Design of Model Tracking Control Scheme on Slave Side	18
2.5 Experimental Results With Proposed Methods For The Two Master-Slave Configurations	25
2.6 Conclusions and Future Directions	27
3. IMPROVEMENTS IN FORWARD PATH.....	33
3.1 Network Protocol Constraints	34
3.2 Delay Regulator.....	37
3.3 Development of Control Signal Entropy Conservation (CSCS) Scheme.....	38
3.4 Simulation Results.....	44
3.5 NIL Results.....	46
3.6 Conclusion.....	49
4. EXTENDING TO MULTI-DOF	53
4.1 A Configuration for the Networked Control System.....	53
4.2 Experimental System and Results	54
4.3 Conclusion.....	56
5. THROUGHPUT IMPROVEMENT USING COMPRESSION.....	61
5.1 DFT Based Benchmark Compression System	63
5.2 Wavelet Packet Transform.....	65
5.3 WPT Based Compression System for Bilateral Control	67

5.4 DFT vs DWT Experimental Compression Results.....	68
5.5 DWT Basis Functions.....	70
5.5.1 Haar	71
5.5.2 Coiflets.....	72
5.5.3 Daubechies	73
5.5.4 Bior.....	74
5.5.5 Rbior.....	74
5.6 Detailed WPT Experimental Analysis.....	75
5.6.1 Experiment Set-1	77
5.6.2 Experiment Set-2.....	79
5.6.3 Experiment Set-3	80
5.7 Discussion.....	80
5.8 Conclusion	83
6. SYNCHRONIZATION IMPROVEMENT USING OPERATOR MOTION ESTIMATION.....	85
6.1 Taylor based PIDC as Benchmark System	86
6.2 Grey based PIDC.....	86
6.3 Experimental System and Results	89
6.4 Conclusion.....	93
7. ADDING FORCE FEEDBACK INTO LOOP.....	95
7.1 System Configuration	95
7.2 Reaction Force Observer (RFOB)	98
7.3 Environment Parameter Estimator (EPE).....	99
7.4 Reaction Force Generator (RFG)	100
7.5 Experimental Results.....	100
7.6 Conclusions	104
8. CONCLUSIONS AND FUTURE WORKS.....	107
8.1 Conclusions	107
8.2 Future Works	109
REFERENCES.....	111
CURRICULUM VITAE.....	119

ABBREVIATIONS

ASP	: Astrom's Smith Predictor
IP	: Internet Protocol
MTC	: Model Tracking Control
DFT	: Discrete Fourier Transform
DWT	: Discrete Wavelet Transform
DR	: Delay Regulator
NIL	: Network in the Loop
PIDC	: Predictive Input Delay Compensator
TCP	: Transmission Control Protocol
SMO	: Sliding Mode Observer
UDP	: User Datagram Protocol
WPT	: Wavelet Packet Tree
WSP	: Watanebe's Smith Protocol

LIST OF TABLES

	<u>Page</u>
Table 2.1 : HIL Experiment Parameters.....	26
Table 3.1 : TCP Communication Sequence.	35
Table 3.2 : UDP Communication Sequence.....	37
Table 3.3 : Ordinary Case of CSCS.....	42
Table 3.4 : Just with Packetloss Case of CSCS.....	42
Table 3.5 : Just with Permutations Case of CSCS.	43
Table 3.6 : Both with Permutations and Packetloss Case of CSCS.	43

LIST OF FIGURES

	<u>Page</u>
Figure 2.1 : Configuration of the bilateral control system with communication delays both in control and feedback paths.	8
Figure 2.2 : Delay Regulator Sample Signal Flow Diagram.....	9
Figure 2.3 : Astrom’s Smith Predictor.	11
Figure 2.4 : Nyquist Diagram of Loop Function.....	13
Figure 2.5 : Diagram of Sliding Mode Observer.....	14
Figure 2.6 : Architecture of Model Tracking Control at Slave side.....	18
Figure 2.7 : Modified SP and MTC based master-slave configuration.	23
Figure 2.8 : SMO and MTC based master-slave configuration.....	24
Figure 2.9 : Varying Delay Scheme used in Simulations.....	25
Figure 2.10 : Reference tracking performance of slave with the ASP based configuration a) under no load (delay effect displayed), b) zoomed version of performance.	27
Figure 2.11 : Reference tracking performance of slave with the SMO based configuration a) under no load (delay effect displayed), b) zoomed version of performance.	28
Figure 2.12 : Reference tracking performance of slave with the ASP based configuration a) under sinusoidal disturbance (delay effect displayed), b) zoomed version of performance.....	29
Figure 2.13 : Reference tracking performance of slave with the SMO based configuration a) under sinusoidal load (delay effect displayed), b) zoomed version of performance.....	30
Figure 3.1 : Top: Cross Atlantic round trip time delay between Georgia Tech, Atlanta and Metz, France using TCP [1]	36
Figure 3.2 : Top: Cross Atlantic round trip time delay between Georgia Tech, Atlanta and Metz, France using UDP [1].....	37
Figure 3.3 : Delay Regulator Sample Signal Flow Diagram.....	38
Figure 3.4 : Teleoperation Control Signal Correction Scheme.	40
Figure 3.5 : Configuration Diagram for Teleoperation Simulations.	44
Figure 3.6 : Angular Displacements while 30s Internet Break a-)at constant delay b-)at variable delay.	44
Figure 3.7 : Control Torques while 30s Internet Break a-)reference b-)at constant delay c-)at variable delay.	45
Figure 3.8 : Control Input Transmission Results.	47
Figure 3.9 : Angular Displacement Tracking Results.....	48
Figure 3.10 : NIL Setup Diagram.	49
Figure 3.11 : NIL Angular Displacement Results a-)DR only b-)DR+CSCS.	50

Figure 3.12: NIL Control Torque Results a-)Torque at Master Side b-)Torque at Slave Side for DR only configuration c-)Torque at Slave Side for DR+CSCS configuration.	51
Figure 4.1 : Multi-DOF Position Control Scheme.	55
Figure 4.2 : Multi-Dof MTC; a) Symbol, b) Block Diagram.	56
Figure 4.3 : Multi-Dof ASP; a) Symbol, b) Block Diagram.	57
Figure 4.4 : Setup for Multi-Dof Experiment.	58
Figure 4.5 : Multi-DOF Position Control joint displacements for sine reference.	58
Figure 4.6 : Multi-DOF Position Control joint displacements for pulse reference.	59
Figure 4.7 : Multi-DOF Position Control joint displacements for arbitrary reference.	59
Figure 5.1 : Benchmark DFT Based Compression-Decompression Scheme.	63
Figure 5.2 : Wavelet Decomposition Algorithm.	66
Figure 5.3 : Wavelet Reconstruction Algorithm.	66
Figure 5.4 : Wavelet Packet Transform Tree; a) Decomposition, b) Reconstruction.	67
Figure 5.5 : Proposed DWT Based Compression-Decompression Scheme.	68
Figure 5.6 : Experimental Setup.	69
Figure 5.7 : Original Signal Used for Compression-Decompression.	70
Figure 5.8 : Reconstructions from the Original Signal.	71
Figure 5.9 : Reconstruction Power Errors.	72
Figure 5.10: General Shapes of Wavelet Basis Functions.	72
Figure 5.11: Filter Length of Wavelets.	75
Figure 5.12: Original Signal Used for Compression-Decompression.	76
Figure 5.13: Comparison of Wavelet Families With Respect to Vanishing Moments and Compression Levels.	78
Figure 5.14: Comparison of Wavelet Families With Respect to Buffer Size.	79
Figure 5.15: Comparison of Wavelet Families With Respect to Compression Ratio.	80
Figure 5.16: Position Tracking Responses of the Master and Slave Systems.	82
Figure 5.17: Wavelet Position and Force Tracking Results under Hard Contact.	83
Figure 6.1 : Extended Control Scheme of Networked Control for Grey Prediction.	90
Figure 6.2 : Experimental Setup for Grey Prediction.	91
Figure 6.3 : Measured and Predicted Angular Positions of each joint and zoomed versions a) joint 1, b) zoomed area of joint 1, c) joint 2, d) zoomed area of joint 2, e) joint 3, f) zoomed area of joint 3.	92
Figure 7.1 : Configuration of the bilateral control system with communication delays both in control and feedback paths.	96
Figure 7.2 : Interaction between object and slave manipulator.	96
Figure 7.3 : Bilateral Control Architecture Block Diagram.	97
Figure 7.4 : Structure of the Reaction Force Observer.	98
Figure 7.5 : Experimental Setup for Bilateral Control.	101
Figure 7.6 : No-contact Force Feedback Results; a) Forces, b) Displacements.	102
Figure 7.7 : Soft-contact Force Feedback Results; a) Forces, b) Displacements.	103
Figure 7.8 : Hard-contact Force Feedback Results; a) Forces, b) Displacements.	104

NOVEL CONTROL AND COMMUNICATION APPROACHES FOR PERFORMANCE IMPROVEMENT IN NETWORKED CONTROL SYSTEMS

SUMMARY

Teleoperation stands for controlling mobile or non-mobile manipulators from a geographically distant location. Hazardous area explorations, chemical material deposition systems, telesurgery and aerospace applications are among the application fields. Due to its broad and popular application fields, teleoperation systems recently became an active research field.

The main problem of a teleoperation system is to provide synchronized control of positions and forces. This synchronization problem is directly related to communication channel between geographically separated motion control systems. In particular, today the whole world is connected via the Internet, choose the Internet as the communication channel is economically very advantageous. Fakat, bununla birlikte İnternetin dezavantajları da yok değildir. Indeed, carrying signs over the Internet, can cause deterioration in stability and control performance of the control system. This problem is due to the delay characteristic of Internet medium. Except for the time delay, the inverse relationship between bandwidth and sampling rate are also negatively affects the performance. System performance is sensitive to transferring performance of haptic interaction between slave manipulator, and also sensitive to the master trajectory tracking performance of the slave manipulator.

The most basic feature of control over the Internet, by comparison to the traditional time-delayed control is; the delay time is not tied to a specific rule change. This feature creates a new disturbance effect on the system. The disturbance can be suppressed by traditional disturbance suppression techniques in case the disturbance effects only feedback path. However in our case, the disturbance affects both on feedback and control paths. Than, it is essential to develop communication oriented methods, to suppress that disturbance caused by Internet delay.

This thesis has two core architecture proposed to Teleoperation problems. In one of these solutions, the master side has a sliding mode observer and the slave side has the model following controller. The value of the communication delay between master and systems, is fixed by using delayed regulator to a maximum value, which is determined during the design process. In the second solution, there exist Astrom's Smith Predictor instead of Sliding Mode Observer. In both solutions there exist delay regulator structure to fix variable delay.

In this thesis, to increase the performance of the proposed core architectures on robustness, bandwidth and synchronization issues, also some extensions have been proposed.

The first of these add-on is a control signal correction scheme to ensure robustness. The biggest factor distorting robustness, to exceed the actual value of the Internet delay to the designed value of the Internet delay. Then, the delay regulator can no longer

fix to the designed maximum delay value. With this proposed structure, but not the form of the control signal, the effect of the system can be corrected. Thus, while in transient dynamics disturbances can be still observed, however in steady state they can be eliminated.

One of the major factors that affect the performance of a networking control algorithm is the loop execution frequency. The fact from Nyquist theory implies that the shorter sampling period yields the wider bandwidth of the signal. Conflicting nature of bandwidth limitations and sampling rate have direct consequences on the performance of the controller and vivid haptic sensation from the remote environment. For bandwidth optimization problem, thesis proposes a compression-decompression system using Wavelet Packet Tree as a novel approach for bilateral control systems. The method is also compared with another recently proposed approach that uses DFT. Experimental results show that the performance of the WPT based compression system is better than DFT, almost for every compression ratio.

Third add-on focuses on synchronization problem. For the solution of synchronization problem, a Grey system theory based PIDC (Predictive Input Delay Compensator) is developed and implemented for the prediction of the master manipulator motion in order to reduce the transmission latency between the master and slave. Our philosophy is to reduce the latency in every way possible within our capability, considering network latency is unavoidable and random.

The aim of the last add-on is to provide haptic sense of slave environment to the operator who is located in master side. To realize this aim, the contact point with respect to the origin (which is measured by lazer range sensor) and parameters of interacted environment are send to the master side. In master side, those data coming from slave side and master manipulator position with respect to the origin are fused, and reaction force is generated for applying operator. This method is two advantageous. The bandwidth requirement is less than the other force control methods, because the parameters doesn't vary frequently. The second advantageous is that, while the lazer range sensor can measure the contact position with respect to the origin before contact occurs, the reaction force can be applied to the operator pro-actively before the contact occurs.

Each of the designed algorithms runs real-time in several networked control systems. There is no need to be a exact best solution which solves all problems. Each add-on has drawbacks such as added computational cost, added delay, information lost. Here, It can be said that, we propose a set of tools which can be glued to a core solution, so the designer can optimize it for his needs.

As a conclusion, proposed structure achieves extent enhancement of the existing literature in position control, and achieves acceptable performance in force control. Also, for both in position control and force control, low bandwidth requirement of the proposed architecture makes it superior than the similar works in the literature.

AĞ ÜZERİNDEN KONTROL SİSTEMLERİNİN PERFORMANS İYİLEŞTİRMESİ İÇİN YENİ KONTROL VE HABERLEŞME YAKLAŞIMLARI

ÖZET

Teleoperasyon mobil veya sabit bir manipülatörü coğrafi olarak uzak bir noktadan kontrol etme anlamına gelmektedir. Tehlikeli bölgelerde arama/tarama, kimyasal madde işleme sistemleri, uzaktan ameliyat sistemleri ve uzay robotiği sistemleri günümüzde teleoperasyon uygulama alanları arasında sayılabilir. Uygulama alanlarının bu kadar geniş ve popüler bir yelpaze oluşturmaları teleoperasyon konusunu aktif bir araştırma alanı haline getirmiştir.

Teleoperasyonun en temel problemi coğrafi olarak uzak sistemlerin senkronize edilmesidir. Bu senkronizasyon problemi coğrafi olarak uzakta bulunan bu iki sistemi birleştiren haberleşme kanalı ile doğrudan ilintilidir. Özellikle, günümüzde tüm dünya, Internet üzerinden birbirine bağlı olduğundan, haberleşme kanalı olarak Internet'i tercih etmek ekonomik olarak çok avantajlıdır. Fakat, bununla birlikte Internet'in dezavantajları da yok değildir. Nitekim, Internet üzerinden işaret taşıma, kontrol sistemlerinin kararlılığında ve kontrol performansında bozulmalara neden olabilir. Bu probleme Internet ortamındaki zaman gecikmesi sebep olur. Zaman gecikmesi haricinde, performans band genişliği ve örnekleme hızı arasındaki ters ilişkidende olumsuz olarak etkilenmektedir. Sistem performansı ayrıca efendi taraftaki operatörün köle taraftaki manipülatörün etkileşimde olduğu çevreyi dokunarak algılama başarımına, köle taraftaki manipülatörün de efendi taraftaki manipülatörün yörünge takip başarımından da fazlaca etkilenmektedir.

Internet üzerinden kontrolü, geleneksel zaman gecikmeli kontrolden ayıran en temel özellik, zamanda gecikme süresinin belli bir kurala bağlı kalmadan değişiyor olmasıdır. Bu özellik sistemde yeni bir bozucu etkisi yaratır. Geliştirilen efendi-köle mimarisi öncelikle bu bozucuyu bastırmalıdır. Bozucunun sadece geribesleme hattında olması durumunda olumsuz etki geleneksel bozucu bastırma yöntemleri ile bastırılabilirken, bozucunun kontrol işareti hattında da etkili olması haberleşme kaynaklı bozucu bastırma yöntemlerinin geliştirilmesini gerektirmektedir.

Bu tezde teleoperasyon problemine iki çekirdek mimari önerilmiştir. Bu çözümlerin birinde, efendi tarafta kayma kipli bir gözleyici ve köle tarafta model izleyen bir kontrolör bulunmaktadır. Haberleşme gecikmesinin değeri, hem efendi sistemden köle sistem yönüne, hem de köle sistemden efendi sistem yönüne gecikme doğrultucusu ile tasarım sürecinde belirlenen bir maksimum değere sabitlenmiştir. İkinci çözümde ise, efendi sistem tarafında Astrom'un Smith Predictor yapısı, ve köle sistem tarafında yine model izleyen kontrolör bulunmaktadır. Gecikme regülatörleri bu çözümde de kullanılmaktadır.

Tezde, yukarıda sunulan çekirdek mimari yapısının dayanıklılık, bandgenişliği ve senkronizasyon performansının arttırımını sağlayacak eklentiler de önerilmiştir.

Bu eklentilerden birincisi dayanıklılığı garanti altına almak için önerilen kontrol işaret düzeltme yapısıdır. Dayanıklılığın en büyük engeli gecikmenin tasarlanan değerin üstüne çıkması ve gecikme regülatörlerinin gecikmeyi sabitleyememesidir. Bu önerilen yapı ile kontrol işaretinin kendisi değil, sisteme olan etkisi düzeltilebilmektedir. Böylelikle geçici rejim dinamiğinde bozukluklar görülmesine rağmen sürekli halde bu bozukluklar ortadan kalkmaktadır.

Ayrıca haberleşme hattının çıktı hızı da çözülmesi gereken başka bir problem kaynağıdır. İkinci eklenti bu problemi çözmektedir. Çıktı hızının limiti kontrol sistemini mekanik sistemin dinamiğinin limitlediğinden daha düşük bir Nyquist frekansında çalışmaya zorlar. Bu nedenle örnekleme hızı belirlenirken sadece mekanik sistem değil, aynı zamanda haberleşme ortamının çıkış hızı da dikkate alınmalıdır. Çıktı hızına uyum sağlamak için örnekleme frekansını düşürmek kontrol sisteminin doğruluğunu da beraberinde düşürecektir. Ayrıca örnekleme hızını düşürme sisteme eklenebilecek olan EKF gibi yüksek örnekleme frekansı gerektiren modern gözleyicilerin de kullanımını kısıtlar. Bu tezde, ayrıca, bu tip problemleri çözebilecek ağ haberleşmesi kaynaklı yaklaşımlar da önerilmektedir. Çıktı hızını en iyileme problemi için tezde Wavelet Paket Ağacı (Wavelet Packet Tree-WPT) dönüşümünü temel alan yeni bir sıkıştırma yapısı önerilmiştir. Bu yapı literatürdeki DFT tabanlı yapı ile karşılaştırılmıştır. Yaptığımız deneyler WPT tabanlı yapınının hemen hemen her sıkıştırma oranında DFT tabanlı algoritmadan daha iyi sonuç verdiğini göstermiştir.

Üçüncü eklenti, senkronizasyon problemini hedeflemektedir. Efendi ve köle taraf arasındaki senkronizasyonu etkileyen en önemli unsur doğal olarak ağ gecikmesinin büyüklüğüdür. Genelde teleoperasyon problemi hep kararlılık açısından ele alınmıştır. Oysaki sadece kararlılığa odaklanmış algoritmaların coğrafi olarak uzak mesafedeki sistemlerin senkronizasyon problemlerini de çözdüğünü söylemek pek mümkün değildir. Bu senkronizasyonu iyileştirmek için performansı belirleyen diğer bileşenleri de dikkate almak gerekir. Teleoperasyonda, referans işareti genel olarak operatör diye adlandırılan bir insan tarafından oluşturulmaktadır. İnsanın doğasını düşündüğümüzde, band genişliği entegre sisteme oranla çok küçüktür. Senkronizasyon probleminin çözümü için tezde Grey Teori tabanlı bir kestrici önerilmiş, ve efendi manipulatörde gerçek referans yörüngesi oluşmadan bir kestrim yörüngesi oluşturulmuştur. Böylelikle efendiden köleye etki süresinin kısaltılması hedeflenmiştir. Bizim buradaki felsefemiz, ağ kaynaklı gecikmelerin kaçınılmaz ve rastgele olduğunu bilip, imkanlar dahilinde diğer tüm gecikmeleri azaltmaktır.

Son eklenti köle taraftaki manüplatörün çevreyle olan etkileşimini operatörün de hissetmesini sağlamak için yapılan eklentidir. Bunun için kantağın başladığı nokta (lazer mesafe sensörü ile ölçülür), ve etkileşilen çevrenin mekanik parametreleri efendi tarafa yollanır. Orada efendi manüplatörün pozisyon bilgisi ve alınan parametreler kullanılarak operatör için tepki kuvveti oluşturulur. Bu yöntemin iki avantajı vardır. Bunlardan ilki parametreler yavaş değiştiğinden (hatta pek değişmediğinden) diğer kuvvet geri beslemeli sistemlere oranla bandgenişliği ihtiyacı daha azdır. İkinci avantajı, kontak noktasının lazer mesafe sensörü ile önceden ölçüldüğünden dolayı, tepki kuvvetini operatöre yansıtmak için kantağın olmasını beklemeye gerek kalmamasıdır.

Tasarlanan algoritmalar birçok deney düzeneğinde gerçek zamanlı olarak denenmiştir. Bu çalışmada her problemi en iyi şekilde cevaplayacak bir çözümde ziyade,

tasarımcıların kendi spesifik problemlerine uygun bir alt küme seçebilmelerini sağlayacak bir çözüm kümesi araştırılmıştır.

Önerilen herbir eklentinin önemli yararları olduğu gibi, işlem yükü, gecikme maliyeti, bilgi kaybı gibi sakıncaları da vardır. Amacımız tasarımcının kendine en uygun çözümü seçebilmesidir.

Özetle, genel olarak bakıldığında önerdiğimiz yapı mevcut literatür ile karşılaştırıldığında pozisyon kontrolünde önemli ölçüde iyileştirme, kuvvet kontrolünde ise kabul edilebilir bir performans sağlamaktadır. Ayrıca band genişliği ihtiyacı da hem pozisyon işaretinin sıkıştırılarak yollanması sebebiyle, hem de kuvvet bilgisinin parametrik olarak yollanmasından dolayı literatürdeki emsallerine göre daha başarılı ve özgündür.

1. INTRODUCTION

1.1 Motivation

Teleoperation and bilateral control systems have been attracting significant interest due to their potential to contribute to human life; i.e. teleoperated robots that contribute to safety [2] and security [3, 4] in hazardous environments or exploration in remote areas [5], or medical robots that can perform telesurgery [6, 7]. Irrespective of the application, bilateral control is faced, to some extent, with problems resulting from uncertainties on the slave side and unpredictable network delays, which becomes significant when internet is used as the communication media.

Numerous studies have been performed for time delay compensation in bilateral control systems. The scattering variables approach [8], is a passivity based approach, using transmission line theories. In this approach, the data transfer between systems is designed in a way to avoid losses, hence ensuring passivity. The method has been initially designed for constant delay, and further extended to variable delay. However, although stability is guaranteed according to the passivity theory, no transparency analysis is provided with the scattering variables method. The wave variables method in [9] is also derived from the scattering variables theory, based on the addition of a damping term to ensure stability in terms of passivity. However, in this method transparency and stability are conflicting performance parameters. This issue is often addressed by the adaptive tuning of damping.

There are also sliding-mode control (SMC) approaches as in [10, 11]. In the field of medicine, for example, there is active research on time-delay compensation using SMC framework [12]. Other examples are [13], which uses SMC as a base for developing an efficient and robust adaptive fuzzy controller; in [14], equivalent control based SMC is used mainly for control delay compensation; in [15] the master control is performed via an impedance controller and the slave control via SMC controller. A recent study

has proposed an SMC framework to simplify the interpretation of tasks in a multibody mechanical system, applicable to bilateral and multilateral control [16].

Sliding-mode control (SMC) based approaches in bilateral control often consider the delay effects as a disturbance, hence seek ways to make the system robust to such disturbances via control. The well-known chattering problem associated with the standard SMC concept can only be reduced with very high switching frequencies, which naturally conflicts with the conditions of time delay systems. To address this issue, chattering-free SMCs are proposed, but the high gain requirement of such systems is a major cause for instability under time-delay conditions, yielding an acceptable performance mostly under short time-delay (shorter than the sampling interval).

Smith-Predictor (SP) based applications perform time delay compensation by using the system model and time delay model. Hence, the standard Smith Predictor [17] will provide a good performance under known model and delay conditions, but will perform very poorly under random network delay, model and load uncertainties, inherent for bilateral control systems. If we ignore measurement path, we see that there is a model and controller closed loop on the master side. The controller feeds both model system and slave system. If both model and slave are the same, then the output of the slave system tracks the output of the model system with a time delay. Because the output of the model system tracks the reference signal, it can be assumed that plant will also track the reference with the same time delay if the modeling of the plant is accurate. However, when there exists mismatch between the model and plant, there will be an error at the plant output. The measurement path is used to suppress that error. The output of the model is artificially delayed as long as the network delay and subtracted from the measurement signal coming from the plant at master side. That difference is added to the reference based on a set point regulator structure. Here, we see two bottlenecks; one is model plant which is used in the generation of control signal of the actual slave plant. Its model mismatch can be modeled as a disturbance and that disturbance increases by the mismatch amount. The other bottleneck is the artificial delay for synchronizing measurement coming from the slave side to master side through Internet. The mismatch between actual network delay length and artificially generated delay length is also an other disturbance source.

Moreover, in this control structure, there is just one controller which should satisfy tracking constraints and disturbance suppression. To overcome that problem Astrom adds an other controller to the standard Smith predictor. As a result, the degree of freedom of the controller increases and the objectives of tracking performance and disturbance rejection because of mismatches are shared between those two controllers. Consequently, Astrom's Smith Predictor [18] improves SP's performance to some extent in the face of uncertainties, however, for an acceptable performance in bilateral control applications like the one in consideration, additional measures should be taken for delay regulation and disturbance rejection.

A more recent approach in bilateral control is the consideration of the communication delay effect as a disturbance, which is further addressed by the design of an observer, namely, a communication delay observer (CDOB). The method is shown to be more effective than the Smith-predictor approach due to its independence of modeling errors and capability to handle variable delays as normally expected with the internet. Moreover this method is as applicable to a SISO system as it is to MIMO systems [19], [20]. The CDOB approach lumps the delays in the control and measurement loop and proposes a 1st-order observer derived under the assumption of a linear system. The approach is based on the empirical determination of the cutoff, ω_c , and more recently, of the time constant, T . Although performing well under constant delay, the authors mention ongoing problems in practical applications under variable time delay and slave uncertainties.

The weight of the studies in the literature appear to be clustered around passivity, CDOB, and Smith Predictor based approaches. Other methods remain weak and redundant. However, these three more established methods also have issue:

Passivity based approaches transform distributed parameter circuits approach from electronics domain to mechanical domain. Here, both master and slave manipulators are modeled by a one port network, and the Internet communication medium is modeled by a transmission line. Under those assumptions, passivity-based control systems behave as an adaptive impedance matching circuit, which aims to supply passivity constraints or suppress scattering. While transforming from electrical concepts to mechanical concepts, potential-flow classification is used [21]. In potential-flow classification, voltage counterpart is force/torque, and current

counterpart is velocity/angular velocity. Then we can say that the control aims is to minimize the error between master side and slave side velocities, and master side and slave side forces. Because making the velocity error zero is the primary objective of the control (and not the position error), initial transient response and also numerical roundoff errors cause position mismatch errors. Moreover, the force control performance is highly sensitive to bandwidth. [1]

Smith Predictor based methods give rise to steady state error due to model mismatch. Such approaches can provide moderate force and moderate position tracking performance, however the performance is strictly delay dependent. [22]

Disturbance observer based methods have also steady state error, again because of model mismatch [23]. Despite providing good force tracking, the position tracking performance is quite poor. This can impact the ultimate performance poorly by causing the application of a correctly estimated force to an inaccurately estimated point. Its stability is not depend on delay. It was proven under real intercontinental Internet delay experiments. However the performance of CDOB approach deteriorates under low bandwidth constraint. Therefore this approach needs a networking infrastructure which can supply high bandwidth, to give satisfactory results. [22,24]

1.2 Purpose of the Thesis

The purpose of this thesis is the design and implementation of novel control and communication approaches for performance improvement in networked controlled systems, predominantly by addressing the above discussed issues, not adequately addressed in the literature so far. Networked control is different from the traditional time delay control since in that case delay time is varying by the time. This phenomena results in an additional disturbance being injected into the system. The developed configurations should solve firstly the effects of that disturbance. For the effects in the feedback path, traditional disturbance suppression techniques can be used. However, the effects of the delay on the control (forward) path, and the network throughput are two other important issues to be taken into consideration; i.e. A network bandwidth that is slower than the system dynamics will determine the Nyquist frequency of the system for adequate control performance. Therefore the sampling time should be reduced. Reducing sample time causes decreased accuracy, and can

render some modern observers useless. The purpose of the thesis is to develop and experimentally test communication, estimation, prediction, and control approaches which address some problems of networked control systems that have significant effect on the performance. A detailed description of each problem and solution is given in related sections.

1.3 Contributions of the Thesis

In this thesis, our main contribution is solving the teleoperation problem with a novel combination of known methods Astrom Smith Predictor (ASP), Delay Regulator (DR), and Model Tracking Control (MTC). Neither of these structures alone, nor any combination of two of those structures can resolve the main teleoperation problem. However, by our proposed novel model based proposed structure, which is an integration of these structures, addresses the teleoperation problem adequately with no steady state error, and very good position tracking. Moreover it demonstrates perfect position tracking performance under maximum assumed delay, while maintaining stability even when the maximum assumed delay is exceeded. In this thesis, this solution will be called core solution. This novel core networked control architecture will be discussed in Chapter 2 in detail. The main contribution of the thesis is the design of a master-slave core configuration that has the following positive attributes;

- The core architecture has the capability to compensate for time varying delay problems under maximum delay assumption.
- The core architecture is made resilient to model mismatch via the design of a Model Tracking Control (MTC).
- The core architecture has increased availability against Internet disconnections with long duration. While this capability is limited with a maximum delay value, when the Internet connection is re- established after a long disconnection, the system can start working without any initialization procedure. This is an important advantage for real-life practical applications of teleoperation.

Another novel contribution is the design of the Control Signal Correction Scheme (CSCS) add-on. This add-on can be easily glued to the core architecture, and supplies

robustness against the case of exceeding the maximum delay constraint. Another contribution is achieved through the design of the compression add-on. This add-on can be easily glued to the core architecture again to reduce the effect of sampling frequency because of throughput limits. This allows the capability for higher sample rates at both master and slave side. One other contribution is the design of the Predictive Input Delay Compensator (PIDC) add-on. This add-on predicts the operator motion trajectory by using operator trajectory measurements by using Grey Theory. Another novel contribution is the design of the pre-contact environment estimation scheme. This add-on provides a force feedback without the need for high bandwidth. The approach is based on measuring the contact point position with respect to origin before the contact occurs. As a result, the upcoming force sense is provided to the operator before the actual contact occurs in slave side, hence eliminating the effects of network delay.

1.4 Thesis Outline

This thesis is organized as follows. Chapter 2 introduces the proposed networked control system core solution with experimental results. Chapter 3 focuses on the control signal path problem, and proposes a solution that we have named Control Signal Correction Scheme (CSCS). The benefits are demonstrated with the use of simulated extreme network conditions. Chapter 4 shows how the proposed architecture can be applied on a multi-DOF system by experimenting core solution and control signal conservation add-on . An intercontinental experiment was conducted to this aim using two multi-DOF industrial manipulators. Chapter 5 focuses on the throughput problem, and proposes a DWT based novel compression scheme, and demonstrates its performance by experiments. Chapter 6 focuses on synchronization, and for that purpose, proposes a Predictive Input Delay Compensator (PIDC). Chapter 7 discusses the design of the pre-contact force feedback estimation scheme with experimental results. Finally, the thesis contributions are recapped and conclusions are presented in Chapter 8.

2. NETWORKED CONTROL CORE SOLUTION

This chapter builds on the disturbance observer approach [10, 11] taken for the solution of network delays in bilateral control, and aims to address specifically the variable delay, variable load, and model mismatch problems of [10, 11].

The main contribution of this chapter is developing and practically implementing two novel master-slave system configurations that yield a significantly improved performance in position control. Each configuration consists of a delay regulator integrated with disturbance rejection schemes on both master and slave sides. More specifically, the following two configurations are developed and tested under variable network delay, and the model mismatch problems of bilateral control systems: 1) Sliding mode observer (SMO) to compensate for measurement delay on the master side, and a Model Tracking Controller (MTC) on the slave side to reduce the effects of load uncertainties and model mismatch between master and slave. 2) Astrom's Smith-Predictor (ASP) to compensate for the effects of network delay on the master side and MTC against slave side uncertainties. Both configurations use the same delay regulator approach [25], which contributes significantly to the disturbance rejection performances of the SMO and ASP, as will be demonstrated with experimental results.

The proposed observer-regulator-controller configurations are tested for step type and bidirectional type load and reference trajectories under random network delays. Throughout the experiments, the emulated random delay is varied between 100-400 milliseconds, based on the network delay measured in [1] , for a networking implementation between country-region France and place country-region USA using UDP/IP internet protocol.

The organization of the chapter is as follows. Section 2.1 introduces general system configuration. Section 2.2, 2.3 and 2.4 discusses the functional blocks used in proposed topologies, delay regulator, estimation schemes and model tracking control

consequently. Section 2.5 shows their experimental results , with conclusions and future directions in Section 2.6.

2.1 System Configuration

The general configuration of the master-slave system considered in this study is given in Fig. 7.2. In this master-slave configuration, the human operator forces the master manipulator, which is in compliance mode, and generates a reference trajectory on the master side. This reference trajectory, together with the trajectory data coming from the slave side through Internet is considered by the master controller in the generation of the control signal is generated to be sent to the slave side. On the slave side, the control signal coming from the master side through Internet and the actual slave trajectory data is processed by the slave controller and actual control signal that is generated. The information sent from the master side to the slave side is a message package containing the tapped control input signal (the reference current value) and a sequence ID. On slave side, more specifically, on the received side of the slave regulator, this information is processed to get the actual current input signal to be applied as reference to the slave side. As a result of this process, the input current signal is now compensated for data losses and the delay is regulated to a constant value.

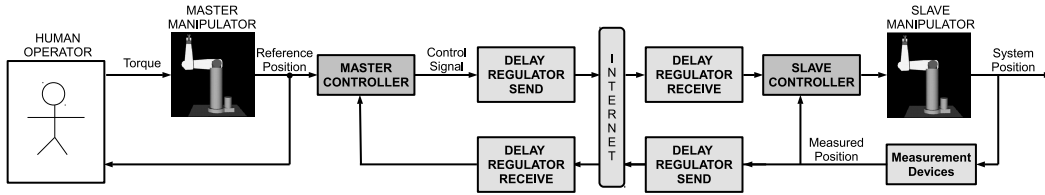


Figure 2.1 : Configuration of the bilateral control system with communication delays both in control and feedback paths.

The equation of motion for a direct-drive single link arm with load can be given as follows:

$$\dot{\theta}(t) = \omega(t) \quad (2.1)$$

$$\dot{\omega}(t) = \frac{K_t}{J}u(t) - \frac{B}{J}\omega(t) - \frac{T_L}{J} \quad (2.2)$$

where K_t is torque constant ($N - m/A$), J is system inertia ($kg - m^2$), B is viscous friction ($N - ms/rad$), $u = i_q$ is control current (A), T_L is the gravitational load.

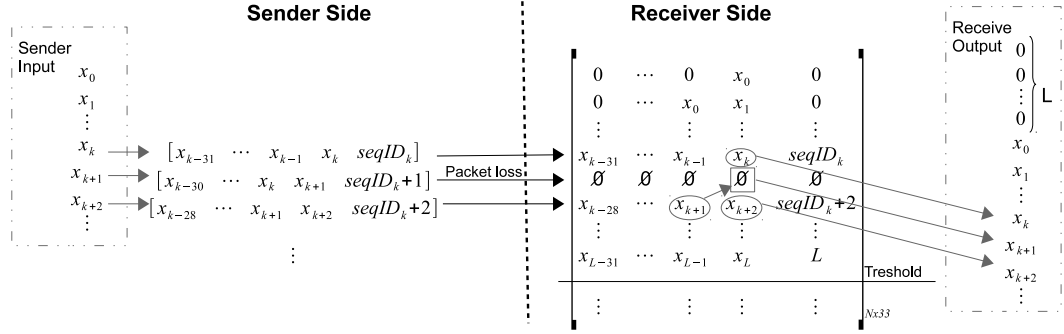


Figure 2.2 : Delay Regulator Sample Signal Flow Diagram.

2.2 Design of Delay Regulator

For bilateral control systems using the internet as the communication medium, it is necessary to consider the delay characteristics of different Internet Protocols. Currently, the more commonly used IPs (Internet Protocols) are the Transport Control Protocol (TCP/IP) and the User Datagram Protocol (UDP). TCP provides a point-to-point channel for applications that require reliable communication. It is a higher-level protocol that manages to robustly string together data packets, sorting them and retransmitting them as necessary to reliably retransmit data. Further, TCP/IP is confirmation based, i.e. it transmits data and waits for confirmation from the other side. If not fulfilled, it retransmits the data. With TCP/IP, there is no data loss.

The UDP protocol does not guarantee communication between two applications on the network. While TCP/IP is connection based, UDP is just a simple serial communication channel. Much like sending a letter through mail, and unlike TCP/IP, UDP does not confirm arrival, hence eliminating data re-transmission. On the other hand, while its faster transmission rate may make UDP more preferable for most real-time control applications, some delay regulation measure is also necessary to minimize the data loss.

The delay regulator works based on the following principle: Each transmitted UDP packet consist of the current plus 31 previous data samples, in addition to a sequence ID. Once transmitted to the slave side, this packet is stored into a memory cell identified by the packet's sequence ID. The number of stored packets on the receiving end is

limited with the buffer size, N . During the very first send-receive process, stored packets are not fed to the related control process (to master for feedback or to slave for control) until a selected $L < N$ threshold is reached. This L/T value determines the selected regulation period, which when exceeded, the first data, $x(k)$ is fed to related control process, and this memory cell is labelled as $null(\emptyset)$. In the next sample time x_{k+1} will be fed to the control process until we face a data loss, in which case x_{k+2} will be null. In this case the algorithm checks the next memory cell and then, the next one until a non-corrupted x_{k+2} value is founded in the memory cells below. [25, 26] The figure of a sample signal flow is seen in Fig. 7.5

2.3 Design Of Control And Estimation Schemes For The Master-Slave System

Two control approaches are developed for the master side, one based on Smith Predictor principles, and one using Sliding Mode concepts. A discussion of both will be provided in this section.

2.3.1 Astrom's Smith Predictor (ASP) on master side

The Smith Predictor (SP) concept [17] is based on the design of a controller that can predict how the effects of system changes will affect the controlled variable (system output) in the future. The standard SP configuration, which requires the time delay to be constant (or, known) has the shortcoming of poor disturbance rejection. Watanabe's Smith predictor (WSP) [27] and the Astrom's Smith predictor (ASP) [18], given in Fig. 2.3, have been proposed to overcome this problem. While both ASP and WSP are two degree of freedom Modified Smith Predictors, Here we prefer Astrom's Smith Predictor. Because, contrary to Watanabe's Smith Predictor, effect of auxiliary controller doesn't degrade main controller performance. [18]

Astrom's Smith Predictor (ASP) decouples the disturbance response from the reference response, allowing the two to be independently optimized. Furthermore, its structure provides the designer with more freedom to choose the transfer function, $M_{asp}(s)$. Considering the developed delay regulator, and the slave-side disturbance rejection scheme (to be discussed in the next section), an ASP based master control appears to be well-suited for the targeted performance standards in this study. Within this configuration, the human operator generates the master trajectory, which then leads

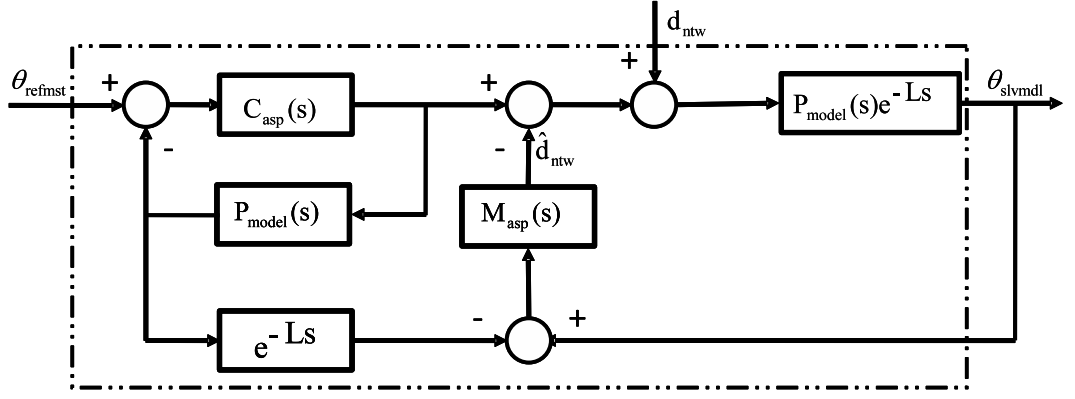


Figure 2.3 : Astrom's Smith Predictor.

to the generation of the control input current to be transmitted to the slave side as explained in Section 2. At the slave side, the delayed control signal coming from the master side (through the Internet) and the actual slave feedback data are processed by the slave controller and the actual control signal is generated and applied to the slave. The ASP is expected to compensate for disturbances caused by communication discrepancies between master and slave, when the buffer side is exceeded. Fig. 2.3 presents the designed ASP within the proposed master-slave.

For the determination of the transfer function, $M_{asp}(s)$ of the ASP, the reference-to-output and disturbance-to-output transfer functions should first be taken into consideration for the system. With the given structure and with the assumption that the delay is constant, L , the reference-to-output transfer function will be independent of $M_{asp}(s)$. [28, 29]

$$\frac{\theta_{slvmdl}(s)}{\theta_{refmst}(s)} = \frac{C_{asp}(s)P_{model}(s)e^{-sL}}{1 + C_{asp}(s)P_{model}(s)} \times \frac{1 + M_{asp}(s)P_{model}(s)e^{-sL}}{1 + M_{asp}(s)P_{model}(s)e^{-sL}} \quad (2.3)$$

$$\frac{\theta_{slvmdl}(s)}{\theta_{refmst}(s)} = \frac{C_{asp}(s)P_{model}(s)e^{-sL}}{1 + C_{asp}(s)P_{model}(s)} \quad (2.4)$$

Here C_{asp} is the main controller whose parameters are designed by ignoring network delay. In this work we choose C_{asp} as a *PID* controller whose parameters are k_{PCasp} , k_{ICasp} , and k_{DCasp}

On the other hand, the disturbance response is as follows:

$$\frac{\theta_{slvmdl}(s)}{d_{ntw}(s)} = \frac{P_{model}(s)e^{-sL}}{1 + M_{asp}(s)P_{model}(s)e^{-sL}} \quad (2.5)$$

Where,

$$P_{model}(s) = \frac{K_{tn}}{s(J_n s + B_n)} \quad (2.6)$$

Also K_{tn} , J_n , B_n are the rated parameter values of K_t , J and B respectively.

To suppress the disturbance \hat{d}_{ntw} should track d_{ntw} in Fig. 2.3. The transfer function from d_{ntw} to \hat{d}_{ntw} is

$$\frac{\hat{d}_{ntw}(s)}{d_{ntw}(s)} = \frac{M_{asp}(s)P_{model}(s)e^{-sL}}{1 + M_{asp}(s)P_{model}(s)e^{-sL}} \quad (2.7)$$

Then

$$M_{asp}(s) = k_{PMasp} + sk_{DMasp} \quad (2.8)$$

Here loop transfer function is

$$G_l(s) = M_{asp}(s)P_{model}(s)e^{-sL} \quad (2.9)$$

$$G_l(s) = (k_{PMasp} + sk_{DMasp}) \left(\frac{K_{tn}}{s(J_n s + B_n)} \right) e^{-sL} \quad (2.10)$$

if we rearrange the equations

$$G_l(s) = \left(\frac{k_{PMasp} + sk_{DMasp}}{s} \right) \left(\frac{K_{tn}}{(J_n s + B_n)} \right) e^{-sL} \quad (2.11)$$

and define

$$M'_{asp}(s) = \frac{k_{PMasp} + sk_{DMasp}(s)}{s} \quad (2.12)$$

$$= k'_{PMasp} + \frac{k'_{lMasp}}{s} \quad (2.13)$$

and

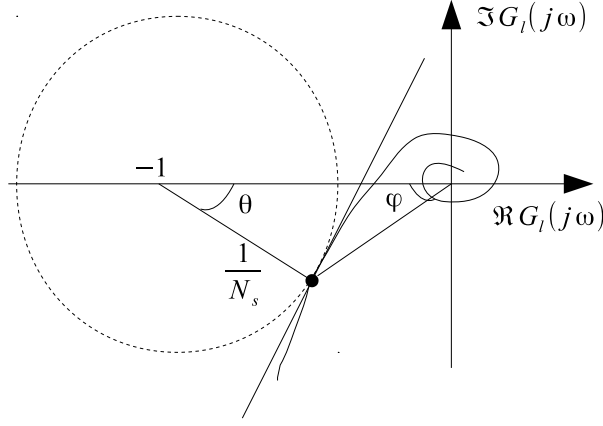


Figure 2.4 : Nyquist Diagram of Loop Function.

$$P'_{model}(s) = \frac{K_{tn}}{(J_n s + B_n)} e^{-sL} \quad (2.14)$$

where $k'_{IMasp} = k_{PMasp}$ and $k'_{PMasp} = k_{DMasp}$

Due to this PD-PI relation above, it is possible to design a PD controller for the position control problem in consideration, using the guidelines of the PI design in [30] given based on the system's sensitivity requirements dictated by N_s , and derived for a velocity control system, different from our position control system.

$$k_{DMasp} = \frac{1}{L} \left(1.451 - \frac{1.508}{N_s} \right) \frac{J_n}{K_{tn}} \quad (2.15)$$

$$k_{PMasp} = \frac{1}{L} \left(1.451 - \frac{1.508}{N_s} \right) \frac{B_n}{K_{tn}} \quad (2.16)$$

Here, N_s is determined by the desired sensitivity specification and is defined as

$$N_s = \max_{0 \leq \omega < \infty} \frac{1}{L} \left| \frac{1}{1 + P_{model}(j\omega)M(j\omega)} \right| \quad (2.17)$$

N_s can also be defined as the inverse of the shortest distance of the open loop transfer function from the Nyquist curve as seen in Fig. 2.4. The major advantages of N_s is that, by selecting N_s , performance factors

$$A_m > \frac{N_s}{N_s - 1} \quad (2.18)$$

$$\varphi_m > 2 \arcsin \frac{1}{2N_s} \quad (2.19)$$

$$\dot{\omega}_e(t) = \frac{K_{tn}}{J_n} u_{slv}(t) - \frac{B_n}{J_n} \omega_e(t) + u_o(t) \quad (2.23)$$

$X = [\theta_e \ \omega_e]^T$ are observer states. u_o is control input of the observer (to be determined based on SM theory).

Slave states measured on the master side which is the output of delay regulator: $\theta_{dlyregout}$, $\omega_{dlyregout}$

$$\theta_{dlyregout}(kT) = \theta_{slvmdl}(kT - L) \quad (2.24)$$

$$\omega_{dlyregout}(kT) = \omega_{slvmdl}(kT - L) \quad (2.25)$$

where, L is the regulated delay.

The control input applied to the slave also deviates from the actual control input by the same delay as

$$u_{slv}(kT) = u_{mst}(kT - L) \quad (2.26)$$

Next, for the design of the observer, the sliding manifold is selected as

$$\sigma(t) = c_{smo} e_{smo}(t) + \dot{e}_{smo}(t) \quad (2.27)$$

where, $e_{smo}(t)$ and $\dot{e}_{smo}(t)$ are as follows:

$$e_{smo}(t) = \theta_{dlyregout}(t) - \theta_e(t - L) \quad (2.28)$$

$$\dot{e}_{smo}(t) = \omega_{dlyregout}(t) - \omega_e(t - L) \quad (2.29)$$

With a properly selected Lyapunov candidate, a control will be designed for the SM based observer that will force the observed states, $\theta_e(kT - L)$ and $\omega_e(kT - L)$ to the measured $\theta_{dlyregout}$, $\omega_{dlyregout}$. As given in (2.24) and (2.25), this actually indicates that the actual slave state values (before the delay) have been reached for use in the master controller.

The Lyapunov candidate and its derivative are selected as follows to satisfy the following conditions:

$$V(t) = \sigma^2(t) \quad (2.30)$$

$$\dot{V}(t) = \sigma(t) \dot{\sigma}(t) = -d_{smo} \sigma^2(t) \quad (2.31)$$

where

$$\dot{\sigma}(t) = c_{smo} \dot{e}_{smo}(t) + \dot{\omega}_{dlyregout}(t) - \dot{\omega}_e(t-L) \quad (2.32)$$

(2.31) and (2.32) are used to derive the SM control law as follows [10]:

$$\dot{\sigma}(t) = -d_{smo} \sigma(t) \quad (2.33)$$

By substituting (2.20), (2.21), (2.22), (2.23), and (2.27) into (2.32),

$$\begin{aligned} \dot{\sigma}(t) = c_{smo} \dot{e}_{smo}(t) + \dot{\omega}_{dlyregout}(t) \\ - \frac{K_{tn}}{J_n} u_{mst}(t-L) + \frac{B_n}{J_n} \omega_e(t-L) - u_o(t) \end{aligned} \quad (2.34)$$

Next, we define,

$$\begin{aligned} [u_o(t)]_{eq} = c_{smo} \dot{e}_{smo}(t) + \dot{\omega}_{dlyregout}(t) \\ + \frac{B_n}{J_n} \omega_e(t-L) - \frac{K_{tn}}{J_n} u_{mst}(t-L) \end{aligned} \quad (2.35)$$

which converts (2.34) into,

$$\dot{\sigma}(t) = [u_o(t)]_{eq} - u_o(t) \quad (2.36)$$

If $u_o(t) = [u_o(t)]_{eq}$, then $\dot{\sigma} = 0$, and per (2.33), $\sigma = 0$.

To calculate the observer control, we discretize $\dot{\sigma}$ under the assumption of a very high sampling rate, hence, (2.36) becomes

$$u_o(kT - T) - [u_o(kT - T)]_{eq} = \frac{\sigma(kT) - \sigma(kT - T)}{T} \quad (2.37)$$

and also

$$u_0(kT) - [u_o(kT)]_{eq} = -d_{smo}\sigma(kT) \quad (2.38)$$

Assuming $[u_o(k)]_{eq}$ does not change between two sampling periods,

$$[u_o(kT)]_{eq} = [u_o(kT - T)]_{eq} \quad (2.39)$$

By rearranging (2.38) and subtracting from (2.37) we get

$$u_o(k) = u_o(k - 1) + \left[\frac{(1 + d_{smo}T)\sigma(k) - \sigma(k - 1)}{T} \right] \quad (2.40)$$

The control in (2.40) will enforce the sliding mode to the selected manifold. With the application of this control, and with the consideration of

$$[u_o(t)]_{eq} = c_{smo}\dot{e}_{smo}(t) + \dot{\omega}_{dlyregout}(t) + \frac{B_n}{J_n}\omega_e(t - L) - \frac{K_{tn}}{J_n}u_{mst}(t - L) \quad (2.41)$$

the observer system in (2.22) and (2.23) can be re-written as,

$$\dot{\theta}_e(t - L) = \omega_e(t - L) \quad (2.42)$$

$$\begin{aligned} \dot{\omega}_e(t - L) = & -\frac{B_n}{J_n}\omega_e(t - L) + \frac{K_{tn}}{J_n}u_{mst}(t - L) \\ & + c_{smo}\dot{e}_{smo}(t) + \dot{\omega}_{dlyregout}(t) \\ & + \frac{B_n}{J_n}\omega_e(t - L) - \frac{K_{tn}}{J_n}u_{mst}(t - L) \end{aligned} \quad (2.43)$$

Which yields

$$\underbrace{[\dot{\omega}_{dlyregout}(t) - \dot{\omega}_e(t - L)]}_{\ddot{e}_{smo}(t)} + c_{smo}\dot{e}_{smo}(t) = 0 \quad (2.44)$$

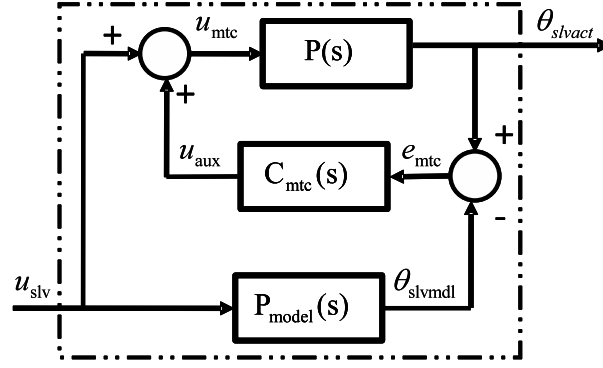


Figure 2.6 : Architecture of Model Tracking Control at Slave side.

Inspecting (2.33), it can be said that when $\dot{\sigma}(t) \rightarrow 0$ $\sigma(t) \rightarrow 0$. This indicates that $\dot{e}_{smo}(t) \rightarrow 0$, $c_{smo}e_{smo}(t) \rightarrow 0$; that is,

$$\omega_e(t-L) = \omega_{dlyregout}(t) = \omega_{slvmdl}(t-L) \quad (2.45)$$

$$\theta_e(t-L) = \theta_{dlyregout}(t) = \theta_{slvmdl}(t-L) \quad (2.46)$$

Block diagram of described Sliding Mode Observer is seen in Figure 5.

2.4 Design of Model Tracking Control Scheme on Slave Side

In this section, the design of the proposed Model Tracking Control(MTC) is discussed. The MTC based slave control system forces the actual slave system to track a desired slave model, hence achieving disturbance rejection in the face of parameter and load uncertainties. This model tracking scheme is represented in Fig. 2.6. [33,34] It should be noted that the slave feedback used on the master side is the output of the slave “model”, not the output of the actual slave. integrated master-slave system is the output of the model system. The use of the this model on both master and slave sides is an approach taken in this study that significantly improves master-slave tracking performance. With this approach, the master and slave controllers can also be designed separately.

To derive the model tracking controller, $C_{mtc}(s)$, the mathematical model of the actual plant, $P_{slv}(s)$ in Eq.2 is taken into consideration in the following form:

$$\frac{K_t}{J} (u_{slv} + u_{aux}) - \frac{T_L}{J} - \frac{B}{J} \omega_{slvact} = \dot{\omega}_{slvact} \quad (2.47)$$

Where;

- T_L : load torque $[Nm]$
- J : total moment of inertia $[kg\,m^2]$
- B : total viscous friction coefficient $[Nm\,s/rd]$
- ω_{slvact} : angular velocity $[rd/s]$
- K_t : torque constant $[Nm/A]$
- u_{slv} : control input to track the known part of the slave model
- u_{aux} : control input to compensate for slave model uncertainties

The model below represents the known portion of the slave model:

$$\frac{K_{tn}}{J_n} u_{slv} - \frac{B_n}{J_n} \omega_{slvmdl} = \dot{\omega}_{slvmdl} \quad (2.48)$$

Where all values reflect the known slave model parameters and variables, as below:

- J_n : moment of inertia of slave model $[kg\,m^2]$
- B_n : viscous friction coefficient of slave model $[Nm\,s/rd]$
- ω_{slvmdl} : angular velocity $[rd/s]$
- K_{tn} : torque constant $[Nm/A]$

With the aim of deriving the appropriate tracking controller, C_{mtc} , first the error between the actual plant and model plant outputs should be defined as:

$$e_{mtc} = \theta_{slvact} - \theta_{slvmdl} \quad (2.49)$$

$$\dot{e}_{mtc} = \omega_{slvact} - \omega_{slvmdl} \quad (2.50)$$

$$\ddot{e}_{mtc} = \dot{\omega}_{slvact} - \dot{\omega}_{slvmdl} \quad (2.51)$$

Using (2.47) and (2.48), the second derivative of the error is defined as,

$$\ddot{e}_{mtc} = \frac{-K_{tn}}{J_n} u_{slv} + \frac{B_n}{J_n} \omega_{slvmdl} + \frac{K_t}{J} (u_{slv} + u_{aux}) - \frac{T_L}{J} - \frac{B}{J} \omega_{slvact} \quad (2.52)$$

Defining the error between actual and model parameter values with the symbol, Δ as:

$$\frac{k_t}{J} = \frac{k_{tn}}{J_n} + \Delta \left(\frac{k_t}{J} \right) \quad \frac{B}{J} = \frac{B_n}{J_n} + \Delta \left(\frac{B}{J} \right) \quad (2.53)$$

(2.52) can be re-organized as below:

$$\ddot{e}_{mtc} = \frac{K_{tn}}{J_n} (-u_{slv} + u_{slv} + u_{aux}) + \Delta \left(\frac{K_t}{J} \right) (u_{slv} + u_{aux}) - \frac{B_n}{J_n} \dot{e}_{mtc} - \Delta \left(\frac{B}{J} \right) \omega_{slvact} - \frac{T_L}{J} \quad (2.54)$$

and

$$\ddot{e}_{mtc} + \frac{B_n}{J_n} \dot{e}_{mtc} = \frac{K_{tn}}{J_n} u_{aux} - \frac{T_L}{J} + \Delta \left(\frac{K_t}{J} \right) (u_{slv} + u_{aux}) - \Delta \left(\frac{B}{J} \right) \omega_{slvact} \quad (2.55)$$

Next, the load and parameter uncertainties are defined as d_{mtc}

$$\frac{1}{J_n} d_{mtc} \triangleq \frac{T_L}{J} - \Delta \left(\frac{K_t}{J} \right) (u_{slv} + u_{aux}) + \Delta \left(\frac{B}{J} \right) \omega_{slvact} \quad (2.56)$$

Here disturbance upper bound can also be defined as

$$[d_{mtc}]_{max} = \frac{J_n [T_L]_{max}}{[J]_{min}} - J_n \left[\Delta \left(\frac{K_t}{J} \right) \right]_{max} [u_{mtc}]_{max} + J_n \left[\Delta \left(\frac{B}{J} \right) \right]_{max} [\omega_{slvact}]_{max} \quad (2.57)$$

(2.56) when substituted in (2.55) will yield the following error dynamics:

$$\ddot{e}_{mtc} + \frac{B_n}{J_n} \dot{e}_{mtc} = \frac{1}{J_n} (K_{tn} u_{aux} - d_{mtc}) \quad (2.58)$$

Inspecting (2.58), it could be observed that when

$$u_{aux} \rightarrow \frac{d_{mtc}}{K_{tn}}, \dot{e}_{mtc} \rightarrow 0 \text{ while } e_{mtc} \rightarrow \text{constant} \quad (2.59)$$

For $e_{mtc} \rightarrow 0$, the following error dynamics should be derived:

$$\ddot{e}_{mtc} + \frac{B_n}{J_n} \dot{e}_{mtc} + k_{mtc} e_{mtc} = 0 \quad (2.60)$$

This condition requires the following term:

$$\frac{1}{J_n} (K_{tn} u_{aux} - d_{mtc}) = -k_{mtc} e_{mtc} \quad (2.61)$$

which results in the following relationships:

$$d_{mtc} = k_{tn} u_{aux} + k_{mtc} J_n e_{mtc} \quad (2.62)$$

$$u_{aux} = \frac{d_{mtc} - k_{mtc} J_n e_{mtc}}{K_{tn}} \quad (2.63)$$

Defining a new variable, z as:

$$z \triangleq d_{mtc} - k_{mtc} J_n e \rightarrow \dot{d} = \dot{z} + k_{mtc} J_n \dot{e}_{mtc} \quad (2.64)$$

Assuming d_{mtc} to have a very slow variation,

$$\dot{z} = -k_{mtc} J_n \dot{e}_{mtc} \quad \ddot{z} = -k_{mtc} J_n \ddot{e}_{mtc} \quad (2.65)$$

Re-writing (2.58) in terms of z :

$$\ddot{z} + \frac{B_n}{J_n} \dot{z} + k_{mtc} z = k_{mtc} d_{mtc} \quad (2.66)$$

Hence

$$\ddot{z} + \frac{B_n}{J_n} \dot{z} + k_{mtc} z = k_{mtc} (k_{mtc} J_n e_{mtc} + K_{tn} u_{aux}) \quad (2.67)$$

To derive $C_{mtc}(s)$, z in (2.67) is expressed in s-domain:

$$z(s) = \frac{k_{mtc}}{s^2 + \frac{B_n}{J_n}s + k_{mtc}} (k_{mtc}J_n e_{mtc} + K_{tn}u_{aux}) \quad (2.68)$$

which is substituted in d_{mtc} expression, yielding,

$$d_{mtc} = \frac{k_{mtc}}{s^2 + \frac{B_n}{J_n}s + k_{mtc}} (k_{mtc}J_n e_{mtc} + K_{tn}u_{aux}) + k_{mtc}J_n e_{mtc} \quad (2.69)$$

Replacing d_{mtc} with its definition in (2.62),

$$K_{tn}u_{aux} = \frac{k_{mtc}}{s^2 + \frac{B_n}{J_n}s + k_{mtc}} (k_{mtc}J_n e_{mtc} + K_{tn}u_{aux}) + k_{mtc}J_n e_{mtc} - k_{mtc}J_n e_{mtc} \quad (2.70)$$

Expressing (2.70) in terms of aux, the expression for the tracking control, $C_{mtc}(s)$ can be derived as follows:

$$\left(s^2 + \frac{B_n}{J_n}s + k_{mtc} \right) K_{tn}u_{aux} = k_{mtc}K_{tn}u_{aux} + k_{mtc}J_n (k_{mtc}e_{mtc}) \quad (2.71)$$

$$u_{aux} = \underbrace{\frac{J_n k_{mtc}^2}{s^2 + \frac{B_n}{J_n}s}}_{C_{mtc}(s)} e_{mtc}(s) \quad (2.72)$$

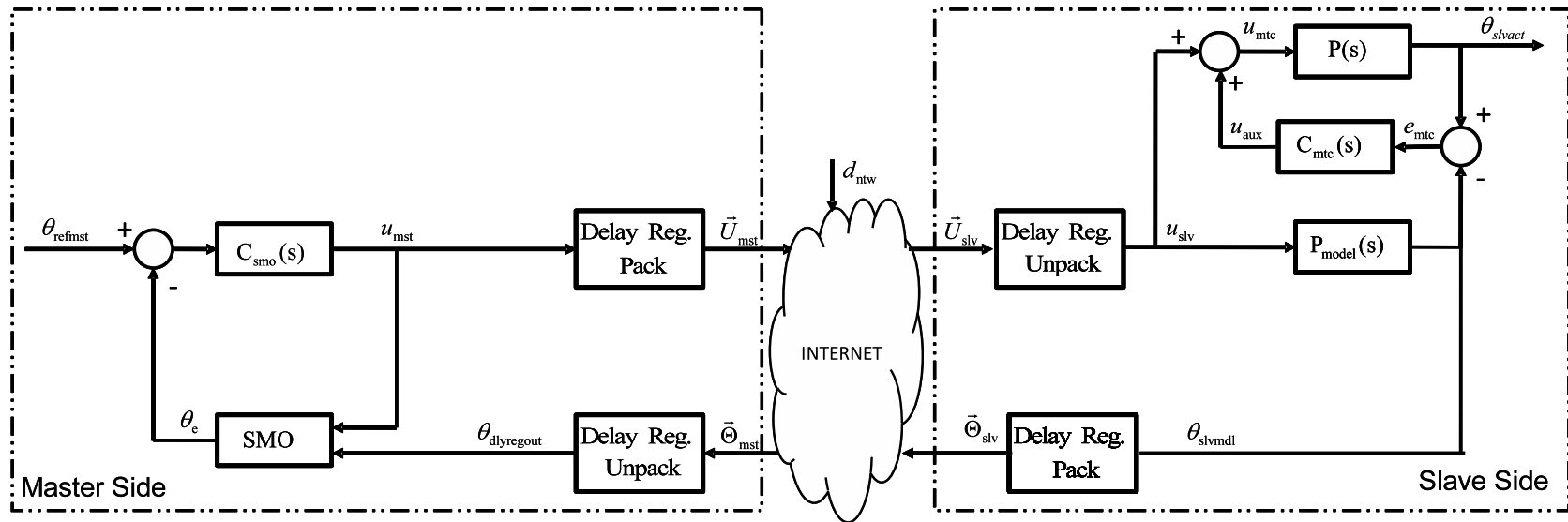


Figure 2.8 : SMO and MTC based master-slave configuration.

Here, the controller, $C_{mtc}(s)$, is configured as a compensator and its output is added on to the PD control generated, which is the constant time delayed version of the control signal generated on the master side.

2.5 Experimental Results With Proposed Methods For The Two Master-Slave Configurations

In this section, experimental results will be provided with the proposed schemes, which are presented as two configurations. The controller parameters are $c_{smo} = 0.0001$, $d_{smo} = 0.001$, $k_{PCasp} = k_{PCsmo} = 0.92$, $k_{ICasp} = K_{ICsmo} = 0.1$, $k_{DCasp} = k_{DCsmo} = 2$, $k_{PMasp} = .03$, $k_{DMasp} = .12$, and $k_{mtc} = 200$. Also Fig. 2.7 presents the master-slave configuration based on the modified SP and MTC, abbreviated as SP-MTC for brevity, and Fig. 2.8 presents the master-slave configuration based on the modified SMO and MTC. In both configurations, the developed model tracking controller (MTC) forces the slave to track the desired model, hence avoiding instability issues and increasing tracking accuracy despite parameter uncertainties and disturbances on the slave side. As demonstrated in Fig.2, the control input (a current signal) for the slave side is generated by the master side controller, which takes into consideration the reference trajectory and the slave feedback received from the model. This is an important contribution of this study, as in the previous studies of the authors [11] , it was demonstrated that the use of the actual slave plant feedback causes steady state error and drift in the slave performance.

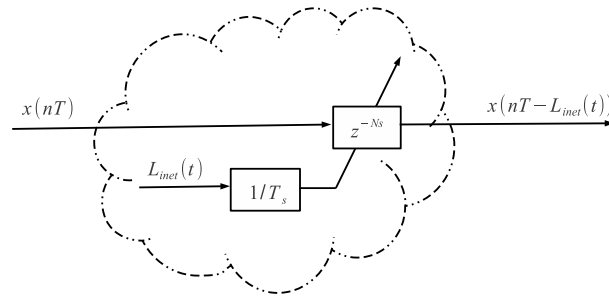


Figure 2.9 : Varying Delay Scheme used in Simulations.

The experimental results are obtained under random network delays both in the feedback and control loops. The schematic of simulated network delay is seen in 2.9. Here T_s denotes sampling time, and $L_{inet}(t)$ is positive white noise signal whose upper limit is L_{max} and lower limit is L_{min} . The paper [35] mention that delay is

irrelevant. Therefore, by using modeling methods, it is irresponsible to estimate the value of network time-delay. For the proper operation of the SMO and ASP schemes, a delay regulator is designed on both master and the slave sides to regulate these random delays to a constant delay value of 400ms. This value was obtained from the intercontinental network experiments presented in [25]. To further challenge the slave plant, the load disturbance on the slave and the reference trajectories are applied as sinusoidal functions and bi-directional trajectories, respectively, which sometimes gives rise to short spikes.

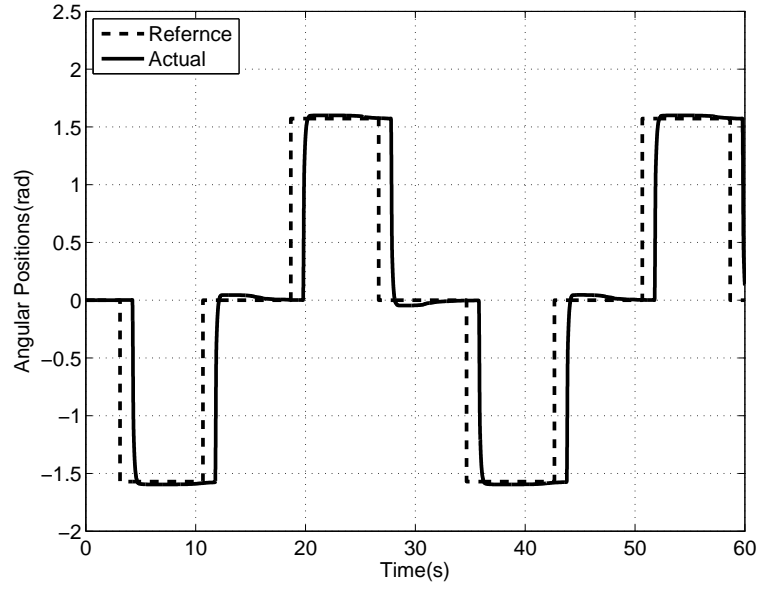
A direct-drive motor driven single-link arm is used in the experiments, the parameters of which are listed in Table 2.1. The delay is generated as a random signal varying between 100-400 milliseconds.

Table 2.1 : HIL Experiment Parameters.

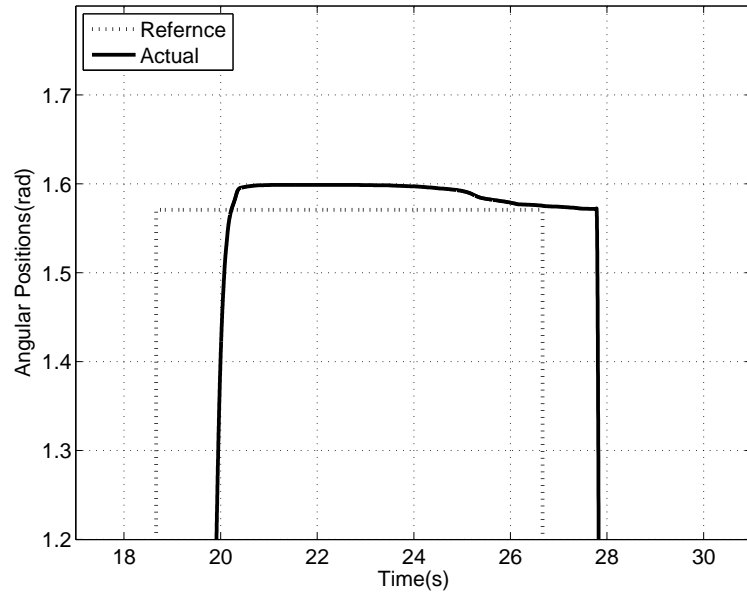
Parameter Name	Parameter Value	Description
V_{qn}	60V	Motor nominal voltage
i_{qn}	5A	Motor nominal current
R_q	0.6 Ω	Motor phase windings resistance
L_q	0.005H	Motor phase windings inductance
K_b	2.3Vsec/rad	Back e.m.f constant
T_{en}	10Nm	Motor nominal torque
K_{vi}	1A/V	Motor driver gain
ω_n	4 π rad/sec	Motor nominal speed
T_{em}	15Nm	Motor maximum torque
K_t	2Nm/A	Torque constant
J	0.012kg – m ²	Effective Inertia
B	0.207Nms/rad	Effective Viscous friction
T_L	10sin Θ Nm	Load torque
L_{min}	100ms	Minimum delay time
L_{max}	350ms	Maximum delay time

Fig. 2.10 and Fig. 2.11 represent the performance of the ASP and SMO based configurations, respectively, under no load on the slave. The figures demonstrate the delay effect in all cases. Inspecting the zoomed versions of the diagrams, one may note a slightly smoother performance of ASP based configuration.

Fig. 2.12 and Fig. 2.13 represent the performance of the ASP and SMO based configurations, respectively, under a sinusoidal load variation on the slave side. The figures demonstrate the delay effect in all cases. While a slightly



(a)



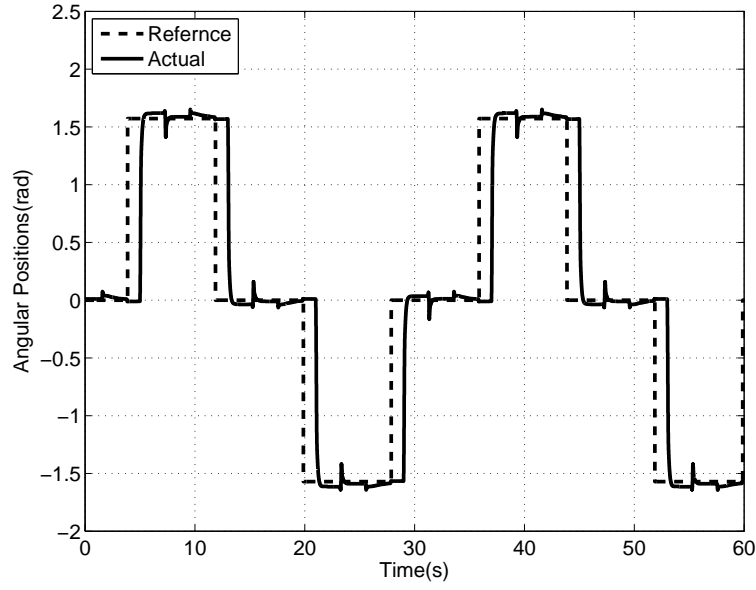
(b)

Figure 2.10 : Reference tracking performance of slave with the ASP based configuration a) under no load (delay effect displayed), b) zoomed version of performance.

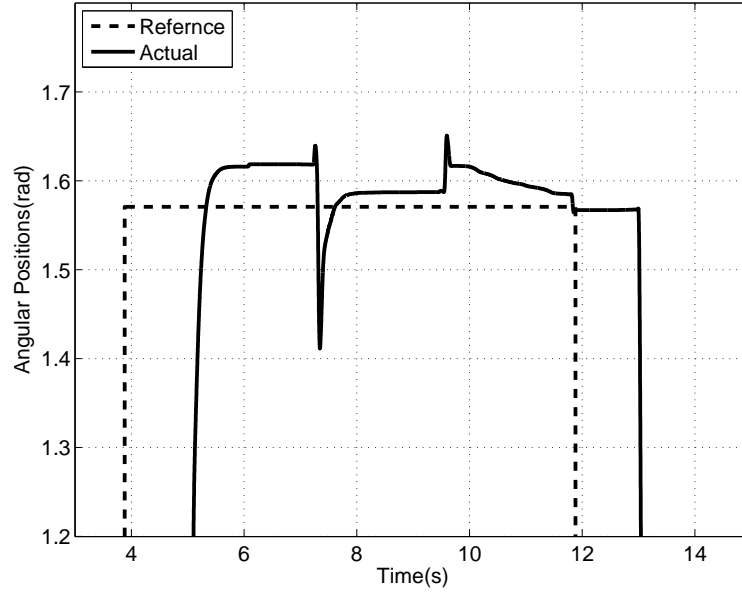
smoother performance is noted with ASP again, both configurations display similar performances in terms of tracking error.

2.6 Conclusions and Future Directions

This study builds on the disturbance observer based approach in bilateral control and contributes to significant improvements in both control and communication issues



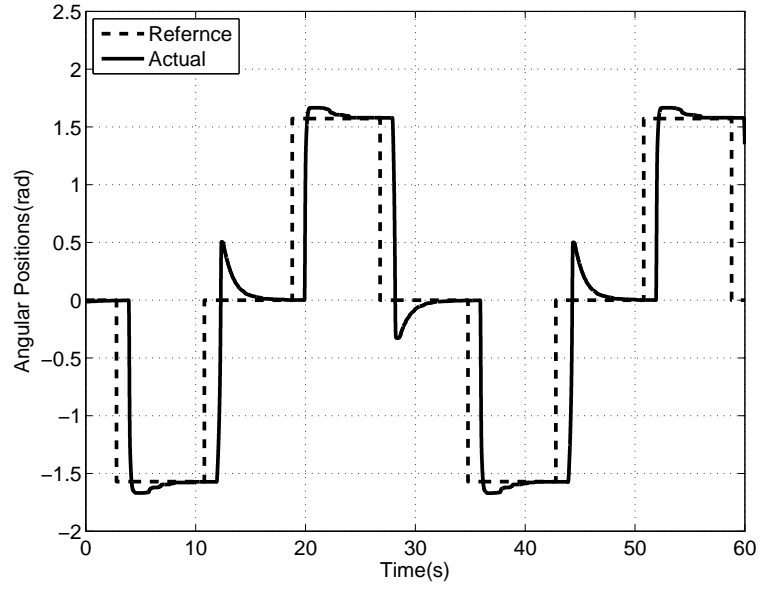
(a)



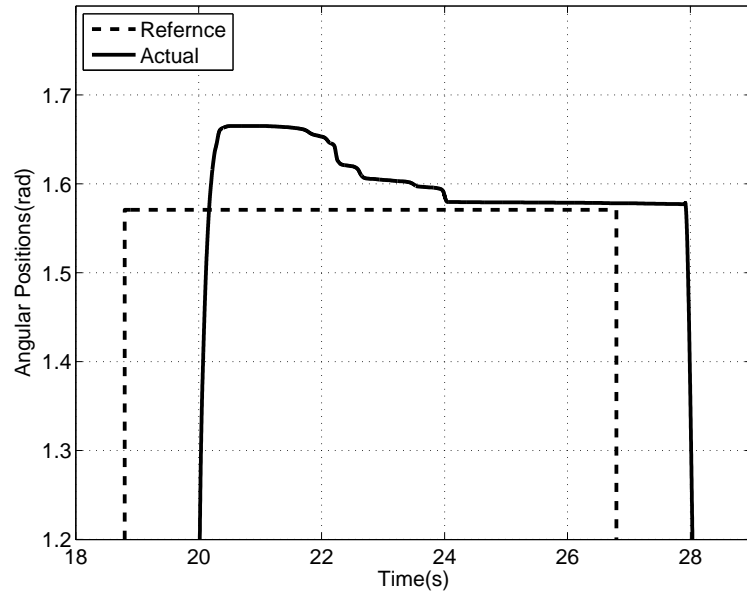
(b)

Figure 2.11 : Reference tracking performance of slave with the SMO based configuration a) under no load (delay effect displayed), b) zoomed version of performance.

faced with position control aspects of bilateral control systems. To this aim, two novel master-slave configurations are proposed, one based on a sliding-mode observer and model-tracking controller , and the other based on Astrom's Smith Predictor on the master side. Both configurations benefit from a delay regulator, which regulates the random network delay into a constant delay. Both configurations also use a MTC designed for the slave side disturbance rejection and trajectory tracking.



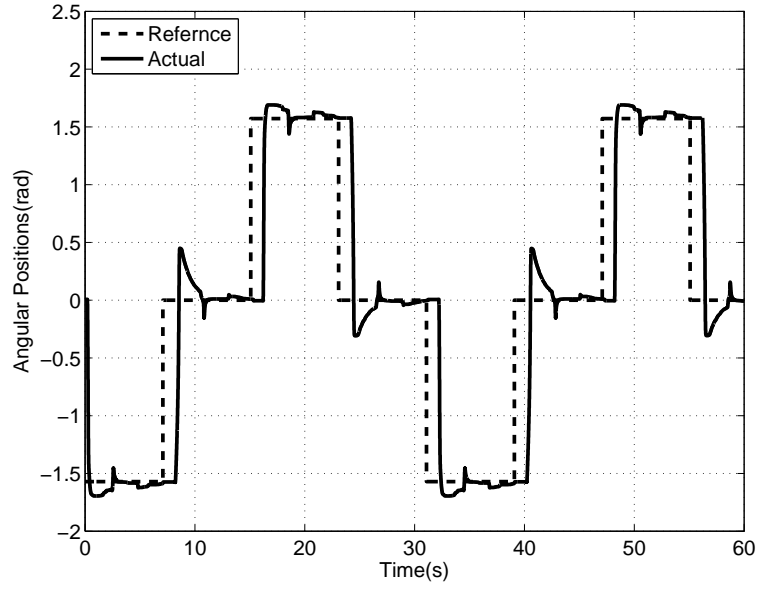
(a)



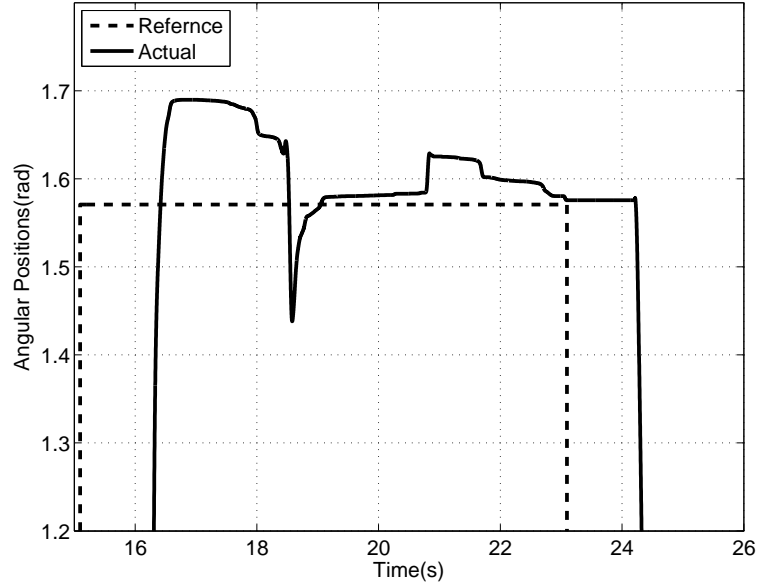
(b)

Figure 2.12 : Reference tracking performance of slave with the ASP based configuration a) under sinusoidal disturbance (delay effect displayed), b) zoomed version of performance.

Experiments are conducted on a single-link arm system under variable gravitational effects and a randomly varied network delay of 100-400 ms that impacts both the feedback and control loop. While the ASP is a more capable version of the standard SP against disturbances stemming from network and slave uncertainties, the much reduced system uncertainties via the proposed combination of the delay regulator and MTC contribute significantly to the overall performance.



(a)



(b)

Figure 2.13 : Reference tracking performance of slave with the SMO based configuration a) under sinusoidal load (delay effect displayed), b) zoomed version of performance.

The delay regulator and MTC have also benefited the SMO based configuration significantly, which has been shown to demonstrate a poor tracking performance under variable network and slave disturbances in the authors' previous studies, while achieving perfect tracking under no load and constant network delay. Hence, both configurations demonstrate a significantly improved tracking performance against model-mismatch and randomly varying network delay (within 100-400ms) and can handle feedback loop deteriorations arising from the limited buffer size of the delay

regulator. However, currently neither of the configurations can handle network delays exceeding 400ms in the control loop. This issue requires further attention and will be addressed in the following chapter.

3. IMPROVEMENTS IN FORWARD PATH

This chapter aims to focus on the control (forward) loop in networked motion control and teleoperation systems by performing a detailed analysis of network delay effects on the forward path (control path) and also proposes a novel control approach to improve the performance in the control path by compensating for IP quality problems as well as slave side uncertainties resulting from network delays. In the process, we also make use of existing approaches in the literature, such as the above mentioned delay regulator, which has originally been proposed to solve speed control problems under network delay [25]; however, its use for networked position control is a novel approach of this study, and has required additional control measures to eliminate the plant uncertainties and nonlinearities [34]. The performance of the modified delay regulator developed in this study is still limited with the buffer size, hence, requires further actions to be taken. This study addresses all these issues and introduces a novel approach to handle the negative outcomes of delay on the control signal by ensuring the conservation of energy (CSCS) between the original control signal (transmitted from the master side) and the control signal input to the slave. The proposed scheme builds upon the assumption that the actual plant will closely track a desired linear system model eg. via Model Reference Adaptive Control (MRAC) or Model Tracking Control (MTC) as demonstrated in [34, 36].

In this chapter, because our focus is on the forward path, only the control path of the integrated master-slave system presented in [34, 36] will be taken into consideration as separate path from the whole system. We propose the control signal energy conservation (CSCS) scheme for this path, and after analyzing and comparing the CSCS and delay regulation schemes separately, we also demonstrate the performance of the combined CSCS plus the delay regulator system.

The organization of the chapter is as follows: First, the master slave system's performance will be analyzed under network delay with no delay regulation and no CSCS schemes; next, the performance of delay regulation will be tested for

the case when the buffer limit is not exceeded and then, for the exceeded case. This will be followed by the discussion of the case with the implementation of CSCS alone. Finally, the combined system's (CSCS plus delay regulator combined) control path performance will be analyzed for the worst case, i.e. under random network delay and with buffer size exceeded. Section 3.1 describes the constraints of the Network Protocols, and reasons for the preference of UDP for teleoperation applications. Section 3.2, and 3.3 describe the delay regulator and proposed CSCS schemes, respectively. Section 3.4 analyzes and discusses the performance of the delay regulator and the CSCS scheme individually, and then as a combined scheme for different scenarios; i.e. under random network delay and with and without the buffer size exceeded with simulation results, which allows us to test the system under extreme conditions. Section 3.5 gives Network-in the-Loop (NIL) simulation results of the proposed structure under real network conditions. Finally, in Section 3.6, concluding remarks are provided.

3.1 Network Protocol Constraints

Considering the internet will be used as the communication medium for bilateral control, it is necessary to discuss the delay characteristic of different Internet Protocols. Currently, the most commonly used IP (Internet Protocols) are the Transport Control Protocol (TCP/IP) and the User Datagram Protocol (UDP). TCP provides a point-to-point channel for applications that require reliable communication. It is a higher-level protocol that manages to robustly string together data packets, sorting them and retransmitting them as necessary to reliably retransmit data. Further, TCP/IP is confirmation based, meaning it transmits data and waits for confirmation from the other side. If not, it retransmits. With TCP/IP there is no data loss. The illustration of this concept is shown in Table 3.1, with the following scenario. Assume that a message is sent at 400ms. The acknowledgement of the master's first message is received at 410ms. At this time, it can send its second message. This phenomena reduces the packet throughput. A different phenomena can be considered in the transmission of the second message with sequence id, Seq_2 . Assume that it is first sent at 420ms, but no acknowledgement is received because the sent message could not be received from the slave side. Then, the system goes into timeout and resends the package at 1000ms.

Table 3.1 : TCP Communication Sequence.

Time(ms)	Master		Slave	Time(ms)
0000	$Seq_1 + Data_1$	\rightarrow	$Seq_1 + Data_1$	0200
0410	Ack_1	\leftarrow	Ack_1	0210
0420	$Seq_2 + Data_2$	\rightarrow	$Seq_2 + Data_2$	—
timeout { \vdots				
1000	$Seq_2 + Data_2$	\rightarrow	$Seq_2 + Data_2$	1200
1410	Ack_2	\leftarrow	Ack_2	1210
1420	$Seq_3 + Data_3$	\rightarrow	$Seq_3 + Data_2$	1620
timeout { — \vdots	Ack_3	\leftarrow	Ack_3	1630
2000	$Seq_3 + Data_3$	\rightarrow	$Seq_3 + Data_2$	2010
2220	Ack_3	\leftarrow	Ack_3	2020

Yet, in another case, a third transmitted package is received from the slave side and the acknowledgement is sent, but in this case, the acknowledgement is lost and could not be received from the master side. Then, the master side goes into timeout and resends the message again at 0000ms.

In the above mentioned table, time intervals are simply selected for illustration of concepts. The real time experiment result for a cross Atlantic networking experiment between Georgia Tech, Atlanta, and Metz France demonstrates the performance given in Fig. 3.1. The figure on top depicts the round trip latency, and the bottom figure shows a sine wave sampled at 10 milliseconds, and sent back and forth by TCP/IP. The experiment was carried out on a typical workday during mid afternoon. It is easily seen that the delay varies substantially, ranging from 100 milliseconds to 3000 milliseconds. In the bottom figure, although no information is lost in the TCP/IP based communication, it can be noted from the figure that data sampled at different points in time gets lumped together along the way and arrives simultaneously at the destination, resulting in a deformed sine wave. These issues make TCP/IP based communication unfavorable for real-time control. [37]

The UDP protocol, on the other hand, does not guarantee communication between two applications on the network. While TCP/IP is connection based, UDP emulates just a simple serial communication channel. Much like sending a letter through mail, UDP does not confirm arrival. The sequence is illustrated with an example communication

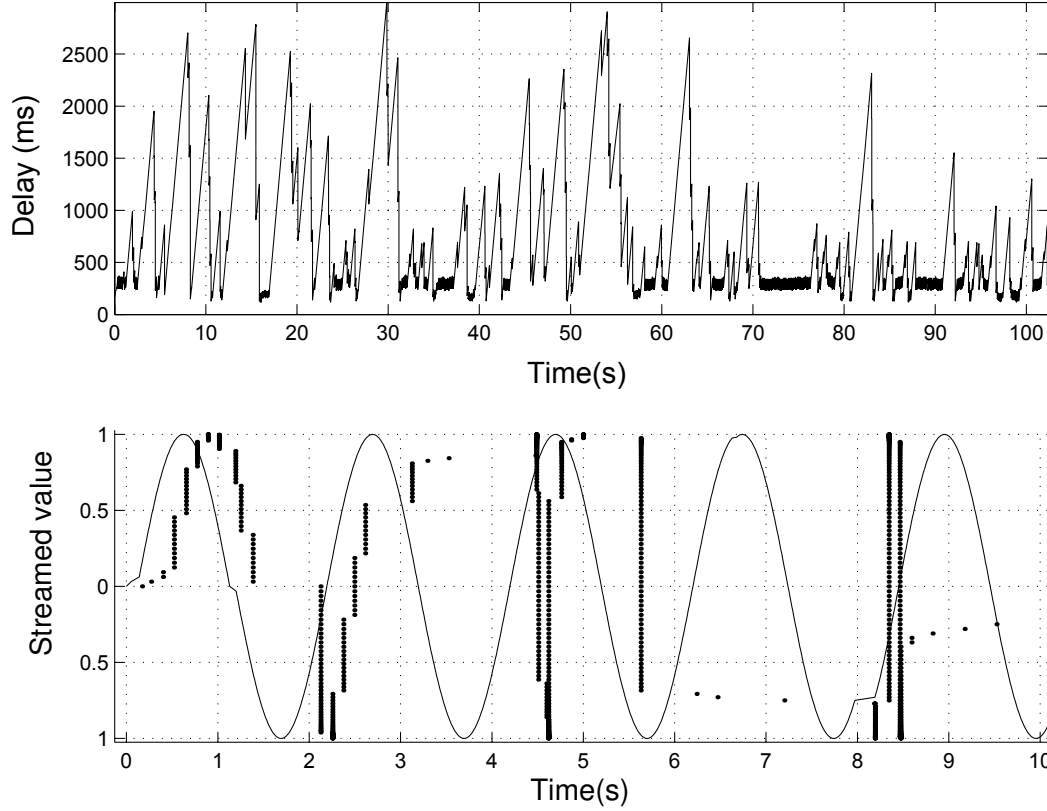


Figure 3.1 : Top: Cross Atlantic round trip time delay between Georgia Tech, Atlanta and Metz, France using TCP [1]

scenario in Table 3.2. Here, let's assume that the message sent from the master side at 0ms arrives at the slave side at 200ms with 200ms delay. The next message sent at 20ms is lost. Then, while the message sent at 30ms arrives at 250ms, the message sent at 50ms is received before the 30ms message, maybe due to different routers etc. In summary, UDP has two major properties; a) the protocol does not try to recover lost or corrupted packages, b) reception of messages does not follow the order of transmissions. Fig. 3.2 top demonstrates the performance of the above mentioned cross Atlantic communication experiment, this time for UDP/IP. The figure above depicts the cross Atlantic roundtrip latency between Georgia Tech, Atlanta, and Metz France, and the figure below shows a sine wave sampled at 10 milliseconds travel same way, both sent by UDP/IP. The experiment was carried out on a typical work day during mid afternoon. It is easily seen that the delay varies substantially, ranging 100 milliseconds to 250 milliseconds. It can be noted that the shape of the sine wave is maintained with much accuracy with UDP/IP than with TCP/IP. It can also be noted that a few datagrams have arrived simultaneously and some 12 to 16 percent of information is

Table 3.2 : UDP Communication Sequence.

Time(ms)	Master		Slave	Time(ms)
0	$Data_1$	\rightarrow	$Data_1$	200
20	$Data_2$	\rightarrow	$Data_2$	
30	$Data_3$	\rightarrow	$Data_3$	250
50	$Data_4$	\rightarrow	$Data_4$	230

lost along the way. Considering the overall performance, the reasons for UDP being the preferred protocol for real-time control becomes apparent [1].

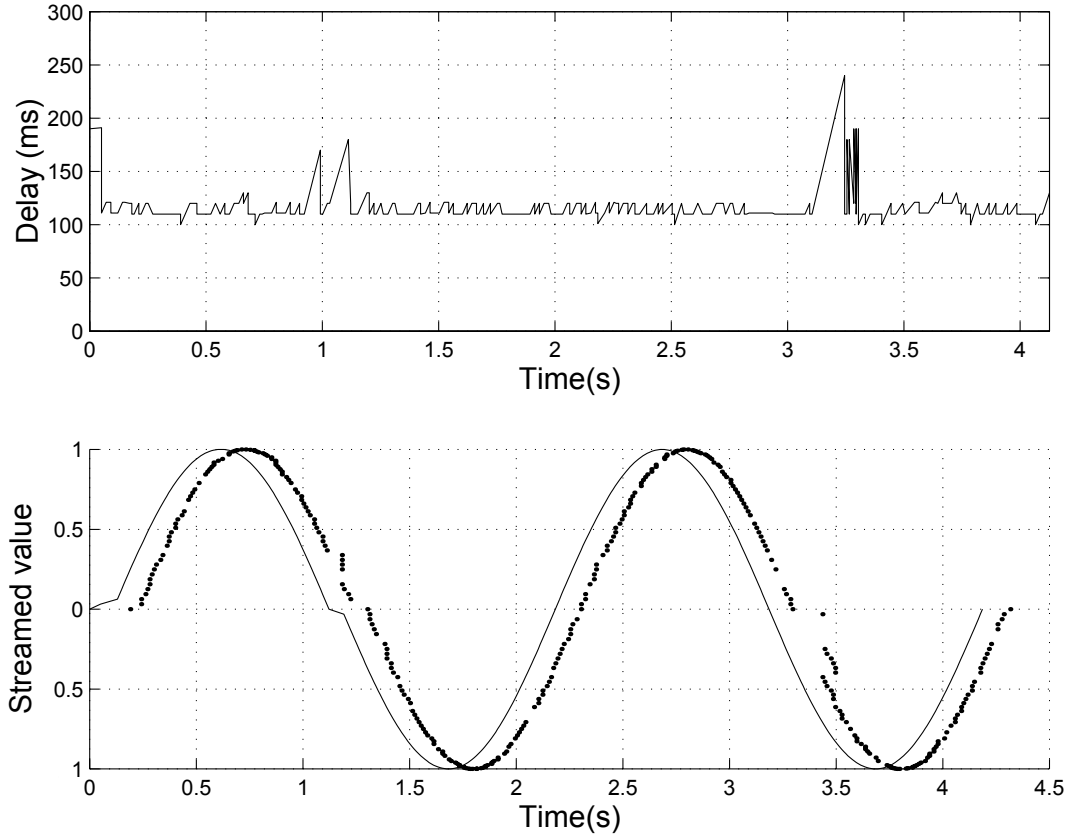


Figure 3.2 : Top: Cross Atlantic round trip time delay between Georgia Tech, Atlanta and Metz, France using UDP [1]

3.2 Delay Regulator

In the previous section, it was discussed that, while a faster transmission rate makes UDP more preferable for most real-time control applications, some delay regulation measure is also necessary to minimize the data loss.

The delay regulator is one such approach proposed in the literature [25, 34]. The delay regulator in [34] works based on the following principle, which is also illustrated in the diagram. Data is transmitted from master to slave and vice versa in packages. Each

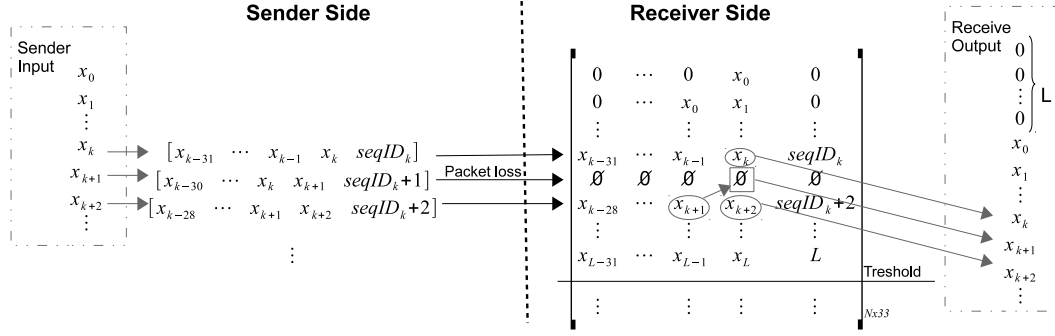


Figure 3.3 : Delay Regulator Sample Signal Flow Diagram.

transmitted UDP package consists of the 31 previous data samples in addition to the current sample, plus a sequence ID. Once transmitted to the slave side, this packet is stored into a memory cell identified by the packet's sequence ID. The number of stored packets on the receiving end is limited with the buffer size, N . During the send-receive process, stored packets are not fed to the related control process (to master for feedback or to slave for control) until a selected $L < N$ threshold is reached. This L value determines the selected regulation period, which when exceeded, the first data, $x(k)$ is fed to related control process, and this memory cell is labeled as $null(\emptyset)$. In the next sample time x_{k+1} will be fed to the control process until we face a data loss, say for the next sample, in which case x_{k+2} will be null. In this case, the algorithm checks the next memory cell and then the next, until a non-corrupted x_{k+2} value is found in the memory cells below. [25, 26] The delay regulator operation is illustrated with the signal flow diagram given in Fig. 7.5.

3.3 Development of Control Signal Entropy Conservation (CSCS) Scheme

As has been discussed in detail in the previous chapter and will be demonstrated with new test results in this chapter, the performance of the delay regulator is limited with the buffer size, N , which, when exceeded, results in performance deterioration on the slave side. The negative effects caused by this limitation in the feedback (measurement) loop is partially compensated by the Smith Predictor, or the Sliding Mode Observer, used in conjunction with the delay regulator. However, currently, no measures are offered against delay effects in the control loop (or, forward path). In this section, the proposed novel CSCS scheme will be presented after a brief discussion of its derivation based on the principles of linear, time-invariant systems. Note that in our

previously proposed master-slave configuration given in Fig. 3.5 (Here the feedback path through network is deleted for simplifying the concept), the slave manipulator, $P(s)$, is forced to track a 1st order linear system, $P_m(s)$, via the design of a model tracking controller, $C_2(s)$. Moreover, $C_1(s)$ is the controller which generates $P_m(s)$'s input signal at master side.

Hence, taking the slave manipulator as an LTI system driven by an electric motor, the position-current input relationship gets the following familiar form:

$$\theta = \frac{K_t}{s(Js + B)} i(s) \quad (3.1)$$

where ω represents the angular velocity, θ represents angular displacement, K_t represents torque constant, B represents viscous damping coefficient, J represents inertia and finally $i(s)$ represents armature current.

Discretizing the armature current,

$$i[n] = \sum_{k=0}^{\infty} i_k \delta[n-k] \quad (3.2)$$

and with

$$\theta[n] = i[n] * h[n] \quad (3.3)$$

$h(t)$: system's impulse response in continuous-time systems, $h[n]$ in discrete-time.

Finally, the system output, $\theta[n]$ can be written as follows, by taking the control input signal as a sum of scaled and time-shifted Kronecker delta functions:

$$\theta[n] = \sum_{k=0}^{\infty} h[n-k] * i_k \quad (3.4)$$

$$h[n] = K(1 - e^{-a(n-k)T}) \quad (3.5)$$

where $a = B/J$ and $K = K_t/B$

$$\theta[n] = \sum_{k=0}^n K(1 - e^{-a(n-k)T}) i_k \quad (3.6)$$

$$\lim_{n \rightarrow \infty} \theta[n] = \lim_{n \rightarrow \infty} \sum_{k=0}^n K(1 - e^{-a(n-k)T}) i_k \quad (3.7)$$

$$\lim_{n \rightarrow \infty} \theta[n] = \sum_{k=0}^{\infty} \lim_{n \rightarrow \infty} (K(1 - e^{-a(n-k)T}) i_k) \quad (3.8)$$

$$\theta_{\infty} \triangleq \lim_{n \rightarrow \infty} \theta[n] = \sum_{k=0}^{\infty} K i_k \quad (3.9)$$

Here, it should be noted that each control input contributes to the output value at infinity, θ_{∞} in proportion to its amplitude. This indicates that possible permutations in the control input sequence will not change the value of the output at the infinity.

On the other side other packet loss changes the output permanently θ_{∞} as seen in (3.9). This cause steady state error in closed loop system. [38]

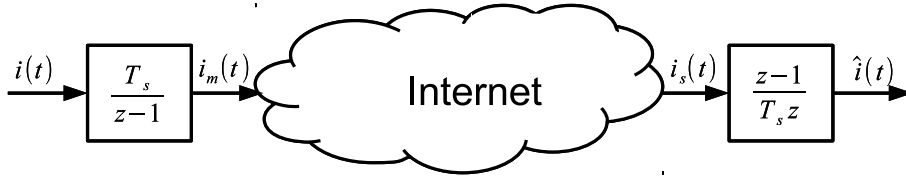


Figure 3.4 : Teleoperation Control Signal Correction Scheme.

The developed novel CSCS scheme is inspired by the LTI properties forced on the slave plant and aims for the slave output to track the master output accurately under network delay. The approach is based on the conservation of the effect created by the control input created on the master side, as closely as possible on the slave side at the infinity, to guarantee the accurate tracking between the master and slave outputs despite network delay and packet losses. To this aim, as a new approach, we propose to send a "cumulative" stimulation signal (control input) from the master to the slave, instead of the common control signal.

The proposed algorithm consists of a discrete time integrator (for generating the cumulative stimulation) at the master side, and a discrete time differentiator (to generate the decoded stimulation) on the slave side, as depicted in Fig. 3.4. As a result, the cumulative stimulation is conserved in synchrony with the input delivered through the Internet, and applied to the slave without loss, despite random delay or packet losses during transmission over the internet.

Below is a detailed discussion for CSCS implementation using four potential scenarios. In the first scenario, data is transmitted accurately (no data permutation nor packet loss) from the master to the slave with some static delay. Each data sample is transmitted from the master side and is received on the slave side after a constant delay. Table 3.3 shows this situation. As expected in this case, the integrator and differentiator cancel each other's effect, and the packets are received sequentially after going through the proposed process..

In the second scenario, only packet loss takes place. As can be seen in Table 3.4, messages Seq_1 and Seq_2 are lost. Here we see that for first message integrator-differentiator pair works fine and process gets the value i_0 . However for the following two sample because of packet loss differentiator produce 0 because its input doesn't change. After that, $i_0 + i_1 + i_2 + i_3$ from integrator is sent and received by differentiator. Differentiator produce $i_1 + i_2 + i_3$. We have previously prove that the output value of the process at infinity for input sequence $\langle i_0, i_1, i_2, i_3 \rangle$ is equal to $\langle i_0, 0, 0, i_1 + i_2 + i_3 \rangle$ based on the example in hand.

In the third scenario, only permutation is occurred. The sequence of messages Seq_1 and Seq_3 are exchanged. Again for the first sequence every thing is OK. It is shown in the previous section that, the effect of the permutation over steady θ_∞ value is nothing. This phenomena is also seen in the Table 3.5 *Desired Cumulative Contribution* and *Cumulative Contribution to θ_∞* columns of Seq_3 .

In the last scenario, as seen in the Table 3.6 both permutation and packetloss are occurred. While first and third message sequence are exchanged, also second message is lost. Again, it easily seen that the result, *Desired Cumulative Contribution* and *Cumulative Contribution to θ_∞* from Seq_3 get equals again as started in Seq_0 .

These cases are the all possible cases which can occur in the UDP/IP communication sequence. Therefore, here we have shown that the cumulative contribution of the input signal to θ_∞ is saved by using this simple discrete time integrator-differentiator topology.

Table 3.3 : Ordinary Case of CSCS.

Sequence	Received Cumulative Signal	Differentiator Input	Diff. Output	Cum. Contribution to θ_∞	Desired Cum. Contribution
0	$(i_0)T$	$(i_0)T$	i_0	$(i_0)K$	$(i_0)K$
1	$(i_0 + i_1)T$	$(i_0 + i_1)T$	i_1	$(i_0 + i_1)K$	$(i_0 + i_1)K$
2	$(i_0 + i_1 + i_2)T$	$(i_0 + i_1 + i_2)T$	i_2	$(i_0 + i_1 + i_2)K$	$(i_0 + i_1 + i_2)K$
3	$(i_0 + i_1 + i_2 + i_3)T$	$(i_0 + i_1 + i_2 + i_3)T$	i_3	$(i_0 + i_1 + i_2 + i_3)K$	$(i_0 + i_1 + i_2 + i_3)K$
4	$(i_0 + i_1 + i_2 + i_3 + i_4)T$	$(i_0 + i_1 + i_2 + i_3 + i_4)T$	i_4	$(i_0 + i_1 + i_2 + i_3 + i_4)K$	$(i_0 + i_1 + i_2 + i_3 + i_4)K$

Table 3.4 : Just with Packetloss Case of CSCS.

Sequence	Received Cumulative Signal	Differentiator Input	Diff. Output	Cum. Contribution to θ_∞	Desired Cum. Contribution
0	$(i_0)T$	$(i_0)T$	i_0	$(i_0)K$	$(i_0)K$
1	$(i_0 + i_1)T$	$(i_0)T$	0	$(i_0)K$	$(i_0 + i_1)K$
2	$(i_0 + i_1 + i_2)T$	$(i_0)T$	0	$(i_0)K$	$(i_0 + i_1 + i_2)K$
3	$(i_0 + i_1 + i_2 + i_3)T$	$(i_0 + i_1 + i_2 + i_3)T$	$i_1 + i_2 + i_3$	$(i_0 + i_1 + i_2 + i_3)K$	$(i_0 + i_1 + i_2 + i_3)K$
4	$(i_0 + i_1 + i_2 + i_3 + i_4)T$	$(i_0 + i_1 + i_2 + i_3 + i_4)T$	i_4	$(i_0 + i_1 + i_2 + i_3 + i_4)K$	$(i_0 + i_1 + i_2 + i_3 + i_4)K$

Table 3.5 : Just with Permutations Case of CSCS.

Sequence	Received Cumulative Signal	Differentiator Input	Diff. Output	Cum. Contribution to θ_∞	Desired Cum. Contribution
0	$(i_0)T$	$(i_0)T$	i_0	$(i_0)K$	$(i_0)K$
1	$(i_0 + i_1 + i_2 + i_3)T$	$(i_0 + i_1 + i_2 + i_3)T$	$i_1 + i_2 + i_3$	$(i_0 + i_1 + i_2 + i_3)K$	$(i_0 + i_1)K$
2	$(i_0 + i_1 + i_2)T$	$(i_0 + i_1 + i_2)T$	$-i_3$	$(i_0 + i_1 + i_2)K$	$(i_0 + i_1 + i_2)K$
3	$(i_0 + i_1)T$	$(i_0 + i_1)T$	$-i_2$	$(i_0 + i_1)K$	$(i_0 + i_1 + i_2 + i_3)K$
4	$(i_0 + i_1 + i_2 + i_3 + i_4)T$	$(i_0 + i_1 + i_2 + i_3 + i_4)T$	$i_2 + i_3 + i_4$	$(i_0 + i_1 + i_2 + i_3 + i_4)K$	$(i_0 + i_1 + i_2 + i_3 + i_4)K$

Table 3.6 : Both with Permutations and Packetloss Case of CSCS.

Sequence	Received Cumulative Signal	Differentiator Input	Diff. Output	Cum. Contribution to θ_∞	Desired Cum. Contribution
0	$(i_0)T$	$(i_0)T$	i_0	$(i_0)K$	$(i_0)K$
1	$(i_0 + i_1 + i_2 + i_3)T$	$(i_0 + i_1 + i_2 + i_3)T$	$i_1 + i_2 + i_3$	$(i_0 + i_1 + i_2 + i_3)K$	$(i_0 + i_1)K$
2	$(i_0 + i_1 + i_2)T$	$(i_0 + i_1 + i_2 + i_3)T$	0	$(i_0 + i_1 + i_2 + i_3)K$	$(i_0 + i_1 + i_2)K$
3	$(i_0 + i_1)T$	$(i_0 + i_1)T$	$-i_2 - i_3$	$(i_0 + i_1)K$	$(i_0 + i_1 + i_2 + i_3)K$
4	$(i_0 + i_1 + i_2 + i_3 + i_4)T$	$(i_0 + i_1 + i_2 + i_3 + i_4)T$	$i_2 + i_3 + i_4$	$(i_0 + i_1 + i_2 + i_3 + i_4)K$	$(i_0 + i_1 + i_2 + i_3 + i_4)K$

3.4 Simulation Results

In this section to manifest the contribution this novel add-on we compare it with add-on-less and similar add-on cases. Fig. 3.9 shows the angular displacement and velocity results for each case, and Fig. 3.8 shows control torque results for each case.

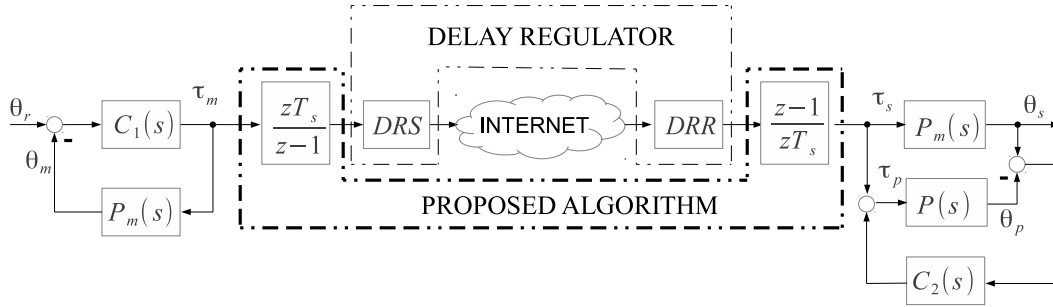


Figure 3.5 : Configuration Diagram for Teleoperation Simulations.

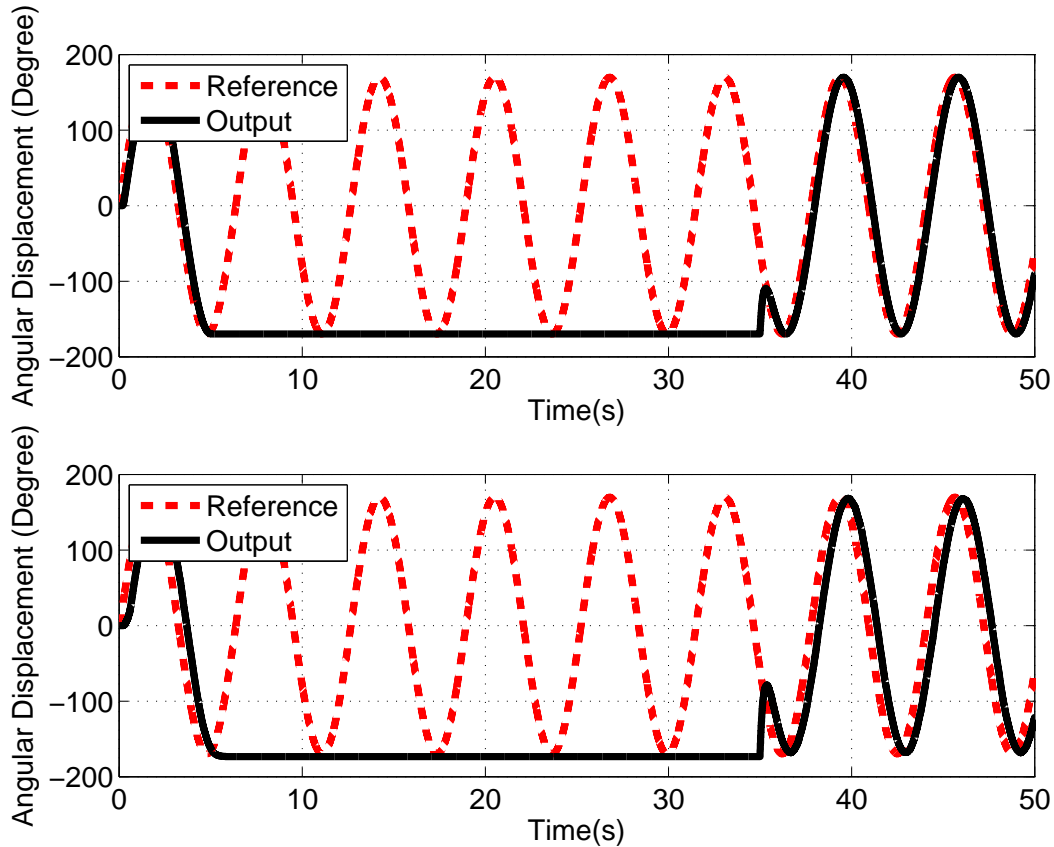


Figure 3.6 : Angular Displacements while 30s Internet Break a-)at constant delay b-)at variable delay.

Six different cases are simulated to evaluate the performance of the proposed approach. For all the cases discussed below the same notation is used for the references, and

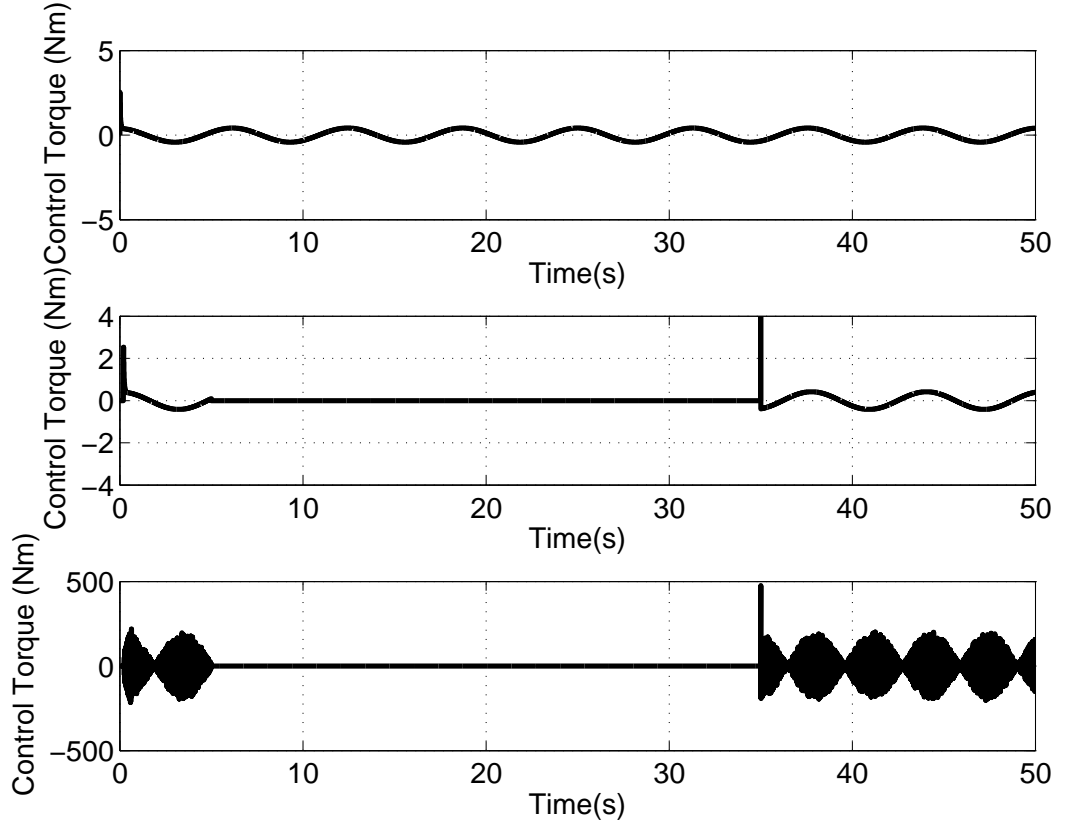


Figure 3.7 : Control Torques while 30s Internet Break a-)reference b-)at constant delay c-)at variable delay.

actual performances. Except Fig. 3.9a in each case a model plant is forced to track the trajectory plotted dashed in master side, and the torque generated from this model is sent over Internet, and again applied on a model plant which has the exactly same an parameters. For each subfigures in Fig. 3.9 except Fig. 3.9a dashed lines are represents the output of the model plant at master side which we also called reference trajectory. Also the straight lines are the output of the model plant at slave side. For each subfigures in Fig. 3.8, dashed lines are the torque signal which force the model plant at master side to track reference trajectory and sent to slave side over Internet, and the straight lines are the outputs of the correction algorithm if exists.

First case; just the reference trajectory is sent over Internet. This situation is seen in Fig. 3.9a. It is seen that while the system is stable, both angular velocity and angular displacement is effected very much from the disturbance because of network effects.

Second case; here just the torque signal sent over Internet without any correction. Because of perturbations and packetlosses in torque transmission seen in Fig. 3.8a,

the slave side couldn't track the master side in transient and steady state as seen in Fig. 3.9b.

Third case; here just the delay regulator is used for correction and delay time regulation. The results are seen in Fig. 3.9c and in Fig. 3.8b. All results are perfect, both displacement and velocity tracks the master without corruption. However, it should be noted that in that situation the maximum delay prediction is well suited for this networking environment which is a very hard case for real world because of Internet unpredictable delay behavior.

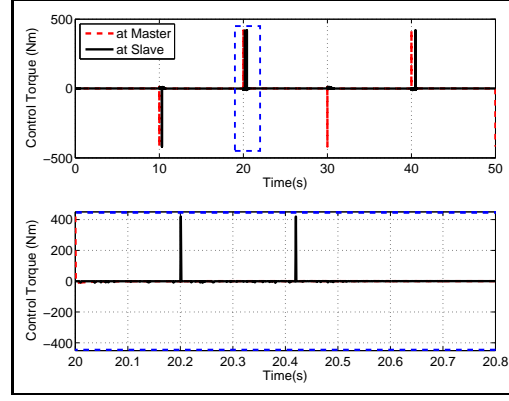
Forth case; again just the delay regulator is used for correction and delay time regulation. However, in that case the buffer is overflow. Because of perturbations and packetlosses in torque transmission seen in Fig. 3.8c, the slave side couldn't track the master side in transient and steady state as seen in Fig. 3.9d.

Fifth case; in that case proposed scheme is used for error correction. Here, it is interesting that while in Fig. 3.8d slave side torque signal does not exactly track the master side torque signal, as seen in Fig. 3.9e the slave side trajectory tracks master side reference trajectory with very low corruption in transient state and very close in steady state. This figure shows the major contribution of our proposed scheme over control signal transition. Instead of delay regulator, The aim of this approach is not saving the transmitted signal, the aim is saving the output signal.

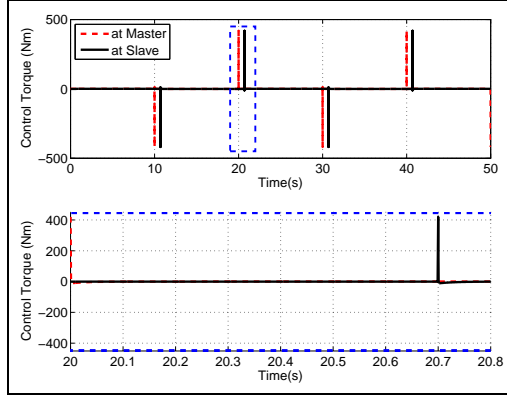
Sixth case; in that case proposed scheme is used with delay regulator. If the network delay is under the predicted value, because of integrator-differentiator process the output will be exactly same of the second case. Then here we are simulating overbuffer case like in third case. Instead of third case where the slave side could not track the master side trajectory in transient and steady state, here track perfect in steady state and with low corruption in transient.

3.5 NIL Results

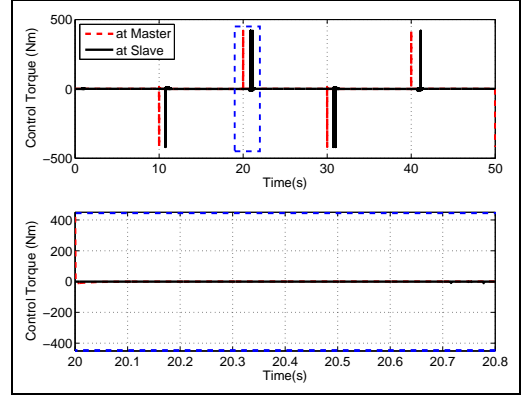
To analyze the performance of the proposed algorithm in further detail, we test the delay regulator only configuration and delay regulator plus CSCS algorithm on a network-in-the-loop (NIL) system [26]. In the NIL system, both the master and slave run on separate real time simulated systems (in our case MATLAB®'s XPCs), but the



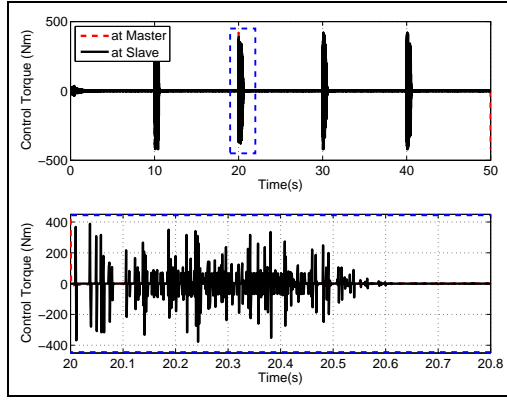
(a) Second Scenario



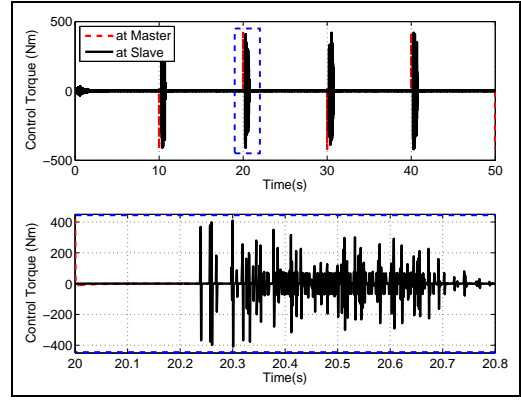
(b) Third Scenario



(c) Forth Scenario



(d) Fifth Scenario

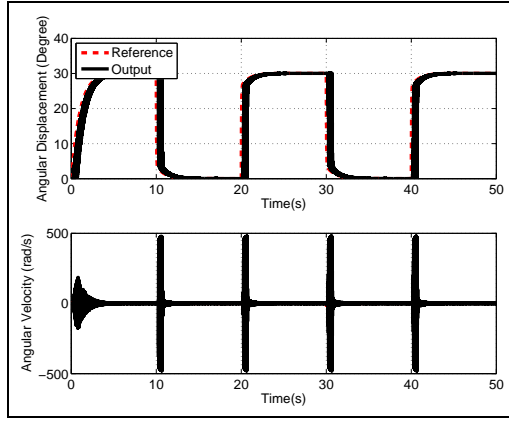


(e) Sixth Scenario

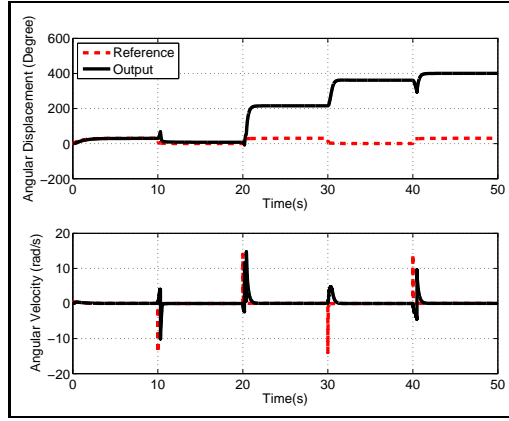
Figure 3.8 : Control Input Transmission Results.

network is the actual Internet. Thus, the “network” effects on the distributed system can be observed realistically and more distinctly, by isolating the effects of actual plant nonlinearities and uncertainties, as well as the measurement noise.

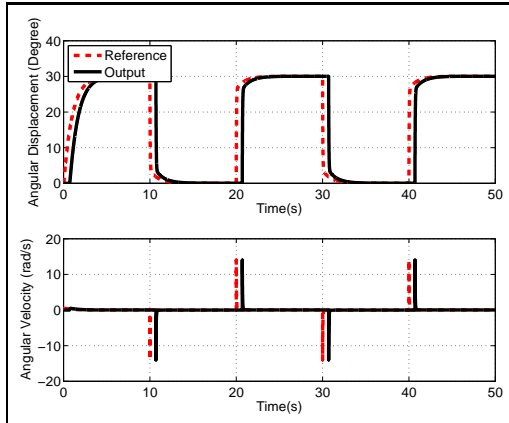
Fig. 3.11. depicts the comparative performance of the two approaches in terms of the angular displacement obtained via the NIL test bed. Here, Fig. 3.11a shows the angular displacement obtained from the delay regulator only(DR) configuration (with the delay



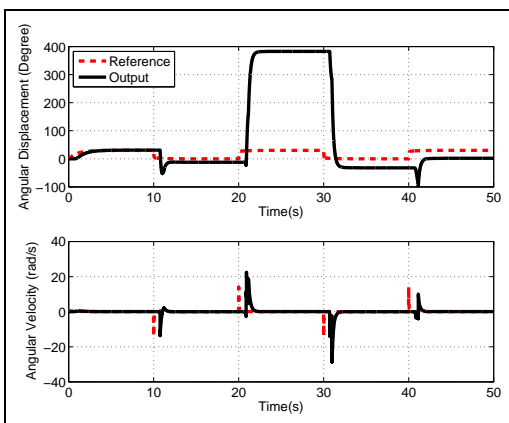
(a) First Scenario



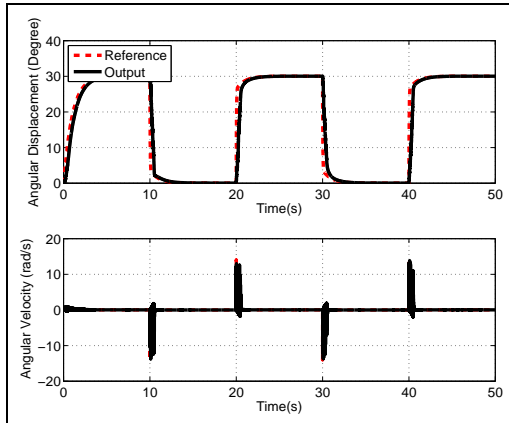
(b) Second Scenario



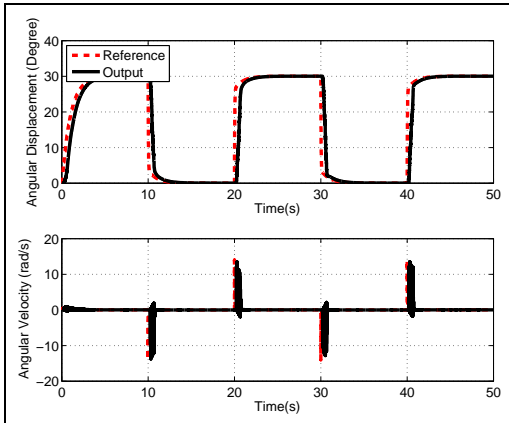
(c) Third Scenario



(d) Forth Scenario



(e) Fifth Scenario



(f) Sixth Scenario

Figure 3.9 : Angular Displacement Tracking Results.

exceeding the regulator's buffer length), and Fig. 3.11b demonstrates the results of the delay regulator plus CSCS (DR+CSCS) for the same time period (for the same case). While the delay regulator only configuration results in a drift, the addition of CSCS to the delay regulator contributes significantly to the tracking performance, especially eliminating the drift totally (hence, the effect of the double integrator) in steady-state.

Fig. 3.12 demonstrates the control (torque) inputs to the process for both cases. Here, Fig. 3.12a depicts the generated torque at the master side, while Fig. 3.12b and Fig. 3.12c demonstrate the torque input at the slave side for the delay regulator only scheme, and the integrated scheme, respectively. Some data corruption can be observed in Fig. 3.12b and Fig. 3.12c (around 5s). However, we also see signals around 5s in Fig. 3.12c which compensates the angular displacement from that corruption.

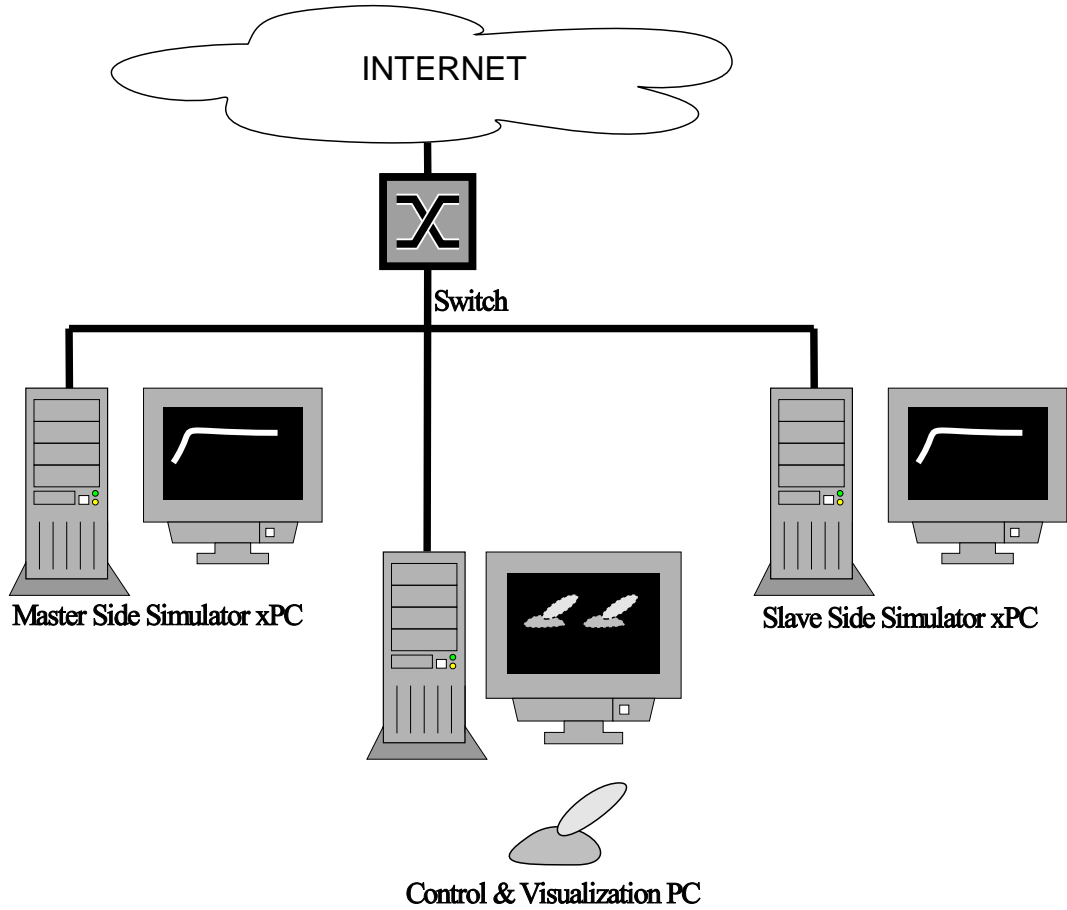


Figure 3.10 : NIL Setup Diagram.

3.6 Conclusion

In this chapter, different from most previous literature on teleoperation and bilateral control, the control (forward) path alone of the master-slave teleoperation system was taken into consideration and a novel approach, namely, the control signal correction scheme (CSCS) was proposed to remedy the performance deteriorating effects of the communication delays on the forward path. The developed scheme was integrated with the authors' previously proposed master-slave configuration, which converts the slave side to an LTI through a model tracking controller (MTC), thus justifying the

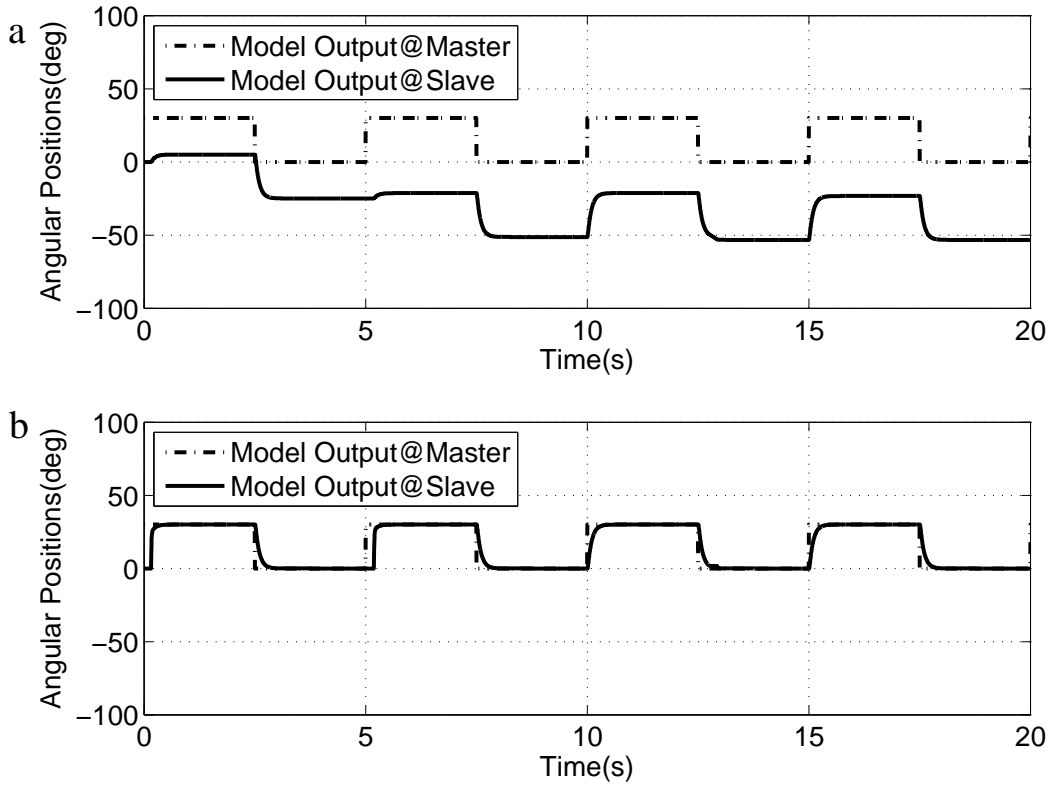


Figure 3.11 : NIL Angular Displacement Results a-)DR only b-)DR+CSCS.

development of the control signal correction scheme based on LTI principles. The CSCS is integrated with the previously developed master-slave configuration, which includes a delay regulator, a network delay compensation mechanism for the feedback path, and disturbance rejection scheme on the slave side, but no specific solution against the delay effects on the control path. The master-slave configuration with and without CSCS is tested under virtually created extreme network delays as well as under actual network conditions. The results demonstrate the delay regulator's contribution to perfect tracking in transient and steady-state as long as the delay remains within the limits of the buffer size; however, the unpredictable nature of the internet may result in the buffer size to be exceeded, resulting in instability. The control signal correction scheme faces no such limitations; hence, the integration of proposed CSCS with the delay regulator provides stability in this case. Using both in the same path, as a matter of fact, provides the best solution: When the delay is within the buffer limits, the delay regulator works fine and the proposed scheme has no contribution except two sample delays. However, when the buffer overflows, CSCS corrects the deviations of the output trajectory (caused due to losses) and supplies stability with very low error in the

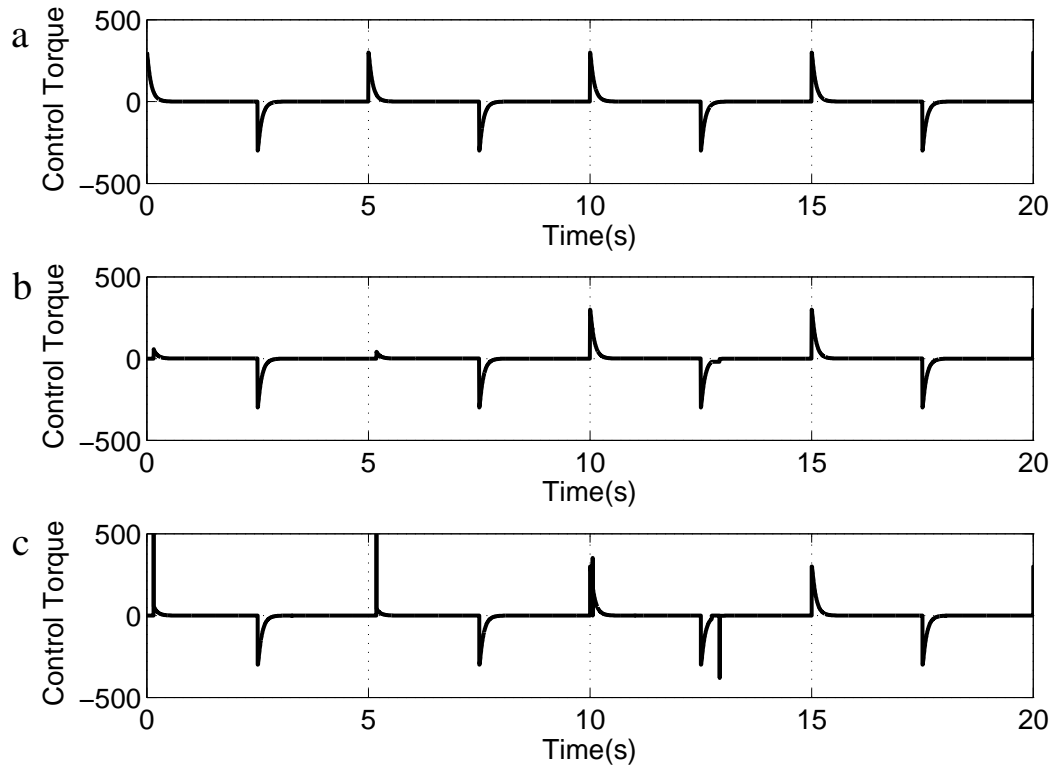


Figure 3.12 : NIL Control Torque Results a-)Torque at Master Side b-)Torque at Slave Side for DR only configuration c-)Torque at Slave Side for DR+CSCS configuration.

transient state. The CSCS could also function alone (with no delay regulator) yielding a small error in transient state, but perfect tracking in steady state, hence, could be integrated into master-slave motion control systems to increase position transparency under network delay. In the following chapter, we will add CSCS Addon to the core solution, and we will show closed loop behavior of CSCS by multi-dof experiments.

4. EXTENDING TO MULTI-DOF

The functionality of the improved delay regulator that was developed within this research is limited in terms of buffer size, thus requires additional modifications to be done. The previous chapter tackles all the problems by introducing a novel technique of dealing with the negative effects of delay on the control signals through CSCS (control signal energy conservation) between the initial control signal (conveyed from the master side) and the input of the control signal towards the slave. The suggested scheme is based on the notion that the main plant would closely monitor a desirable model of linear system, for instance, through MRAC (model reference adaptive control) or MTC (model tracking control).

Because the focus of the previous chapter is on the control path (forward path) only, here we have felt to demonstrate the closed loop CSCS concept with multi-dof, intercontinental experimental results.

4.1 A Configuration for the Networked Control System

Here we will introduce our proposed multi-dof networked control system configuration which is seen in Fig. 4.1. In the multi-dof configuration, the operator forces the master manipulator to a desired posture, which in turn will dictate the slave motion. In order for the slave to track the master motion in the closest possible way, on the master side, an Astrom Smith Predictor (*ASP*) generates the control signal for the model plant. The symbol and block diagram of the multi-dof *ASP* is seen in Fig. 4.3. Then the control signal generated on the master side, is transmitted to the slave side passing through a Delay Regulator Send unit (DRS_m) through the Internet to Delay Regulator Receive unit (DRR_s). On the slave side, a Model Tracking Control (*MTC*) algorithm inputs the received control to an other model process (same as the model plant at master side) and forces the slave manipulator to track the trajectory of the model plant. The symbol and block diagram of the multi-dof *MTC* is seen in Fig. 4.2. The angular displacement

output of the *MTC* is fed back to the *ASP* passing through a Delay Regulator Send unit (*DRS_s*) through the Internet to Delay Regulator Receive unit (*DRR_m*). [39]

Here $\tau_{oq\{1,2,3\}}$ denote the joint torques generated by the operator, $\tau_{qm\{1,2,3\}}$ denote the joint torques applied to the manipulator after the addition of $g_{qm\{1,2,3\}}$ gravitational compensation terms. $\tau_{mq\{1,2,3\}}$ denote the torque signals fed to *DRS_m* to be sent to slave side. $\bar{\tau}_{mq\{1,2,3\}}$ denote the delay regulated torque signals coming through the Internet from the master to the slave. $\tau_{cq\{1,2,3\}}$ denote the joint torques generated by *MTC*, $\tau_{qs\{1,2,3\}}$ denote the joint torques applied to the manipulator after the addition of $g_{qs\{1,2,3\}}$ gravitational compensation terms. Finally $q_{s\{1,2,3\}}$ denote the slave manipulator's joint angle (actual) positions.

Both manipulators can be modelled by Euler-Lagrange equation as a classical mechanical as follows

$$M(q).\ddot{q} + V(q, \dot{q}).\dot{q} + G(q) = \Gamma \quad (4.1)$$

where,

- q : $nx1$ position vector
- $M(q)$: nxn inertia matrix of the manipulator
- $V(q, \dot{q})$: $nx1$ vector of Centrifugal and Coriolis terms
- $G(q)$: $nx1$ vector of gravity terms
- Γ : $nx1$ vector of torques

Here, each manipulator system is taken on consideration as an independent control system after gravity compansation. Therefore, after gravity compansation, we assume each joint as an independent SISO system. All nonlinearities and couplings are taken as disturbance affection on each joint LTI SISO system. The only exception is gravity effect $G(q)$. For gravity effect we use compensator $\hat{G}_q \approx G(q)$ to cancel and/or reduce that effect.

4.2 Experimental System and Results

For this purpose two experimental setup is built. One is located in Istanbul, Turkey and the other is located in Alaska, USA. Those setups are connected to each other with ordinary Internet connection. The setup located in Alaska, contains a PUMA560

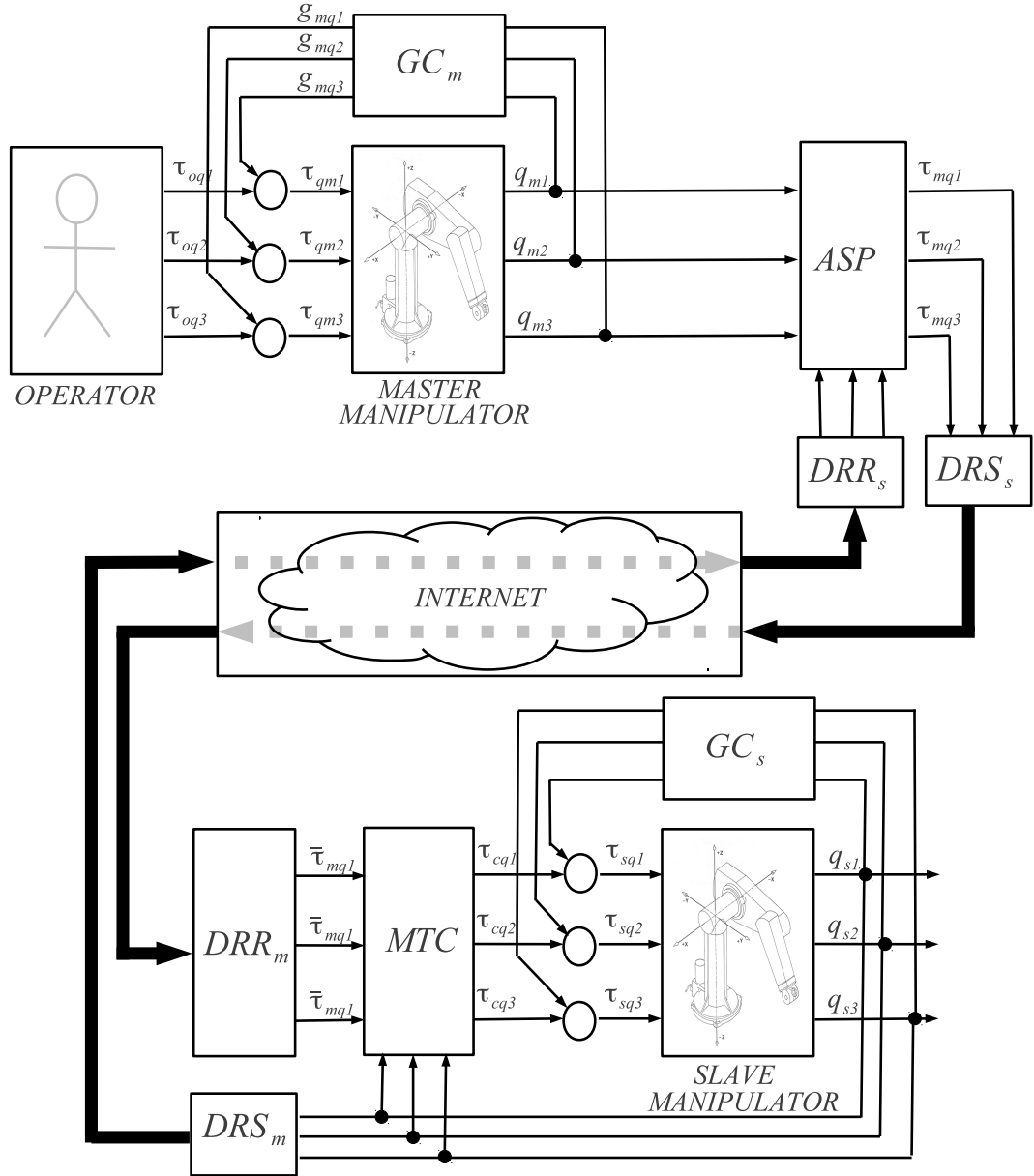


Figure 4.1 : Multi-DOF Position Control Scheme.

industrial robot used as master manipulator and moved by the operator. The setup located in Istanbul, contains a Staubli RX160 industrial robot used as slave manipulator which tracks the trajectory of the master manipulator with a time delay. Those setups are seen in Fig. 4.4.

Three kind of trajectory is tested in the experiments. For first case, $\tau_{oq\{1,2,3\}}$ is applied by and additional controller to force master manipulator track the pure sine trajectory. The results of this experiment is seen in Fig. 4.5. For the second case, $\tau_{oq\{1,2,3\}}$ is applied by and additional controller to force master manipulator track the bidirectional pulse trajectory. The results of this experiment is seen in Fig. 4.6. Finally, in the last

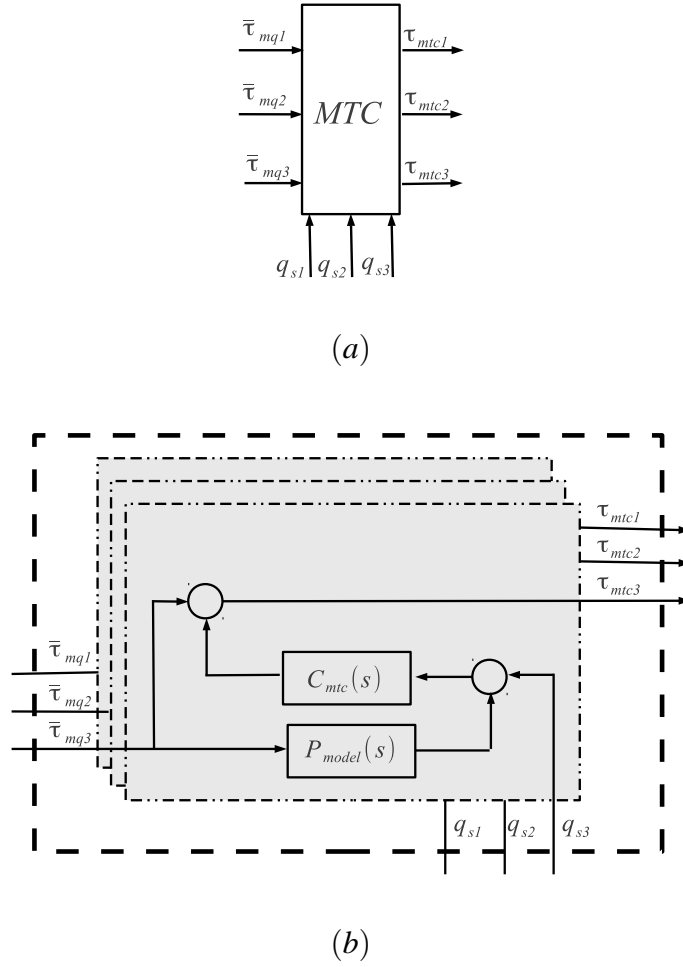


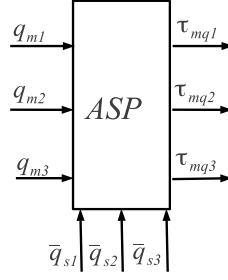
Figure 4.2 : Multi-Dof MTC; a) Symbol, b) Block Diagram.

case, an arbitrary signal is applied whit real operator. The result of that case is seen in Fig. 4.7. For each figures dashed lines represents the master side reference trajectory and the solid lines represents the actual trajectory in slave side. In each figure, it is easily seen that the slave manipulator tracks the master manipulator's trajectory successfully.

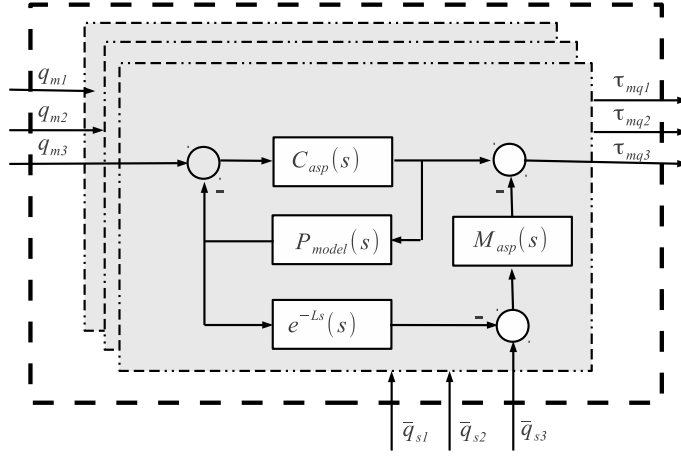
However, it should be mentioned that in our control topology, the effect of Centrifugal and Coriolis terms are ignored. Then, the system performs acceptable when the disturbances comming from those therms are small. For systems which runs higher speeds, also Centrifugal and Coriolis terms should be compensatsed like gravity.

4.3 Conclusion

In this study, a multi-dof networked control application of ASP-DR-MTC scheme and recently proposed CSCS algorithm, is presented. Then, the developed architecture is



(a)



(b)

Figure 4.3 : Multi-Dof ASP; a) Symbol, b) Block Diagram.

tested on an intercontinental test bed, one end is in Alaska, USA and the other is in Istanbul, Turkey. The experiment shows us the core solution plus CSCS Addon has sufficient maturity for real word applications where the robustness is essential. In the next chapter, we will focus on the networked control with the bandwidth limitaion view. We also propose a solution based on compression for that purpose.



Figure 4.4 : Setup for Multi-Dof Experiment.

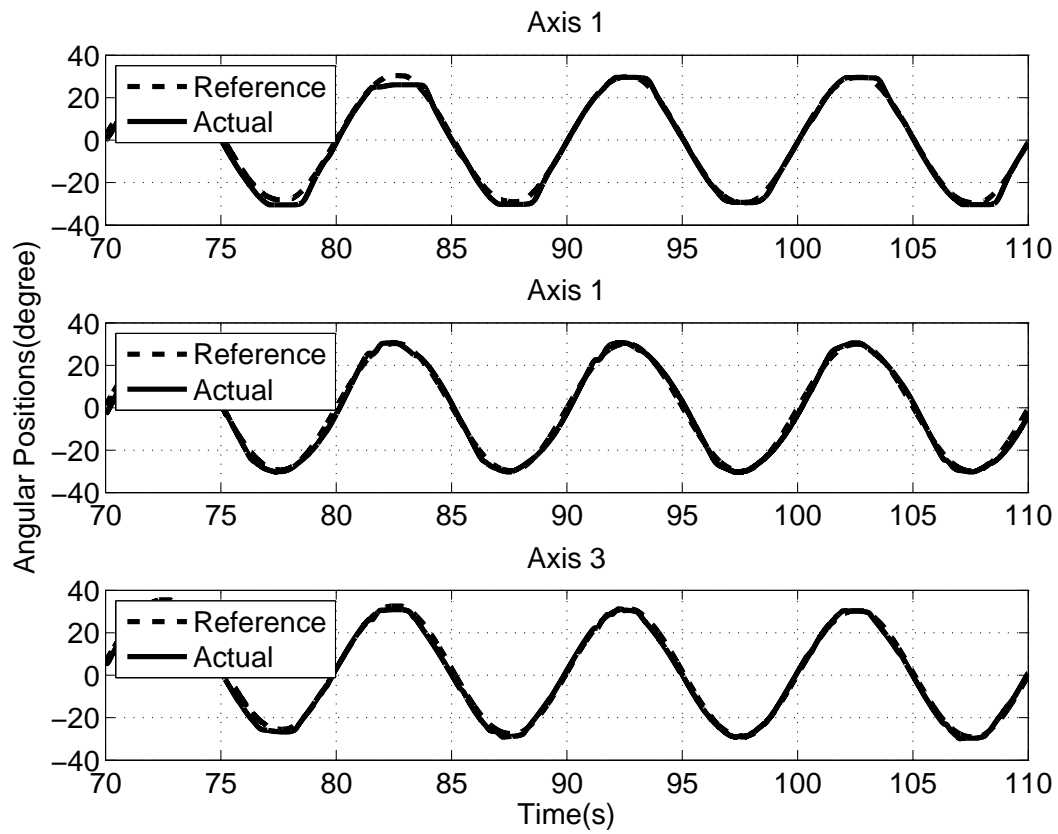


Figure 4.5 : Multi-DOF Position Control joint displacements for sine reference.

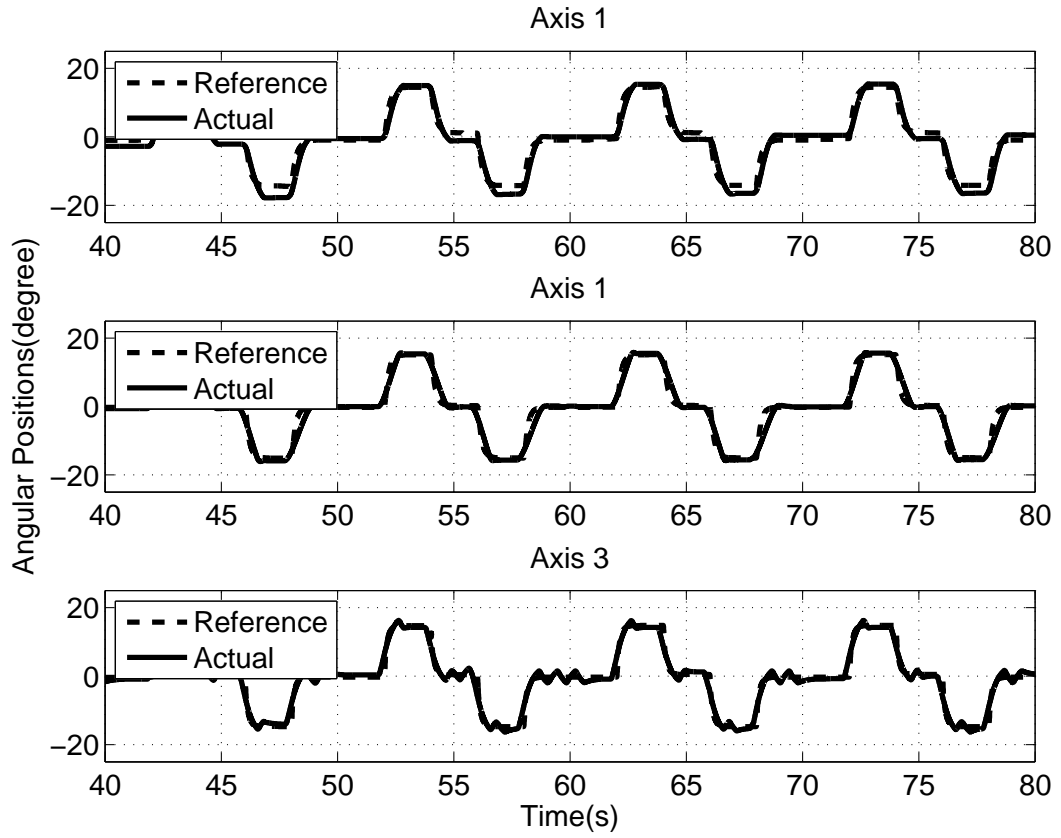


Figure 4.6 : Multi-DOF Position Control joint displacements for pulse reference.

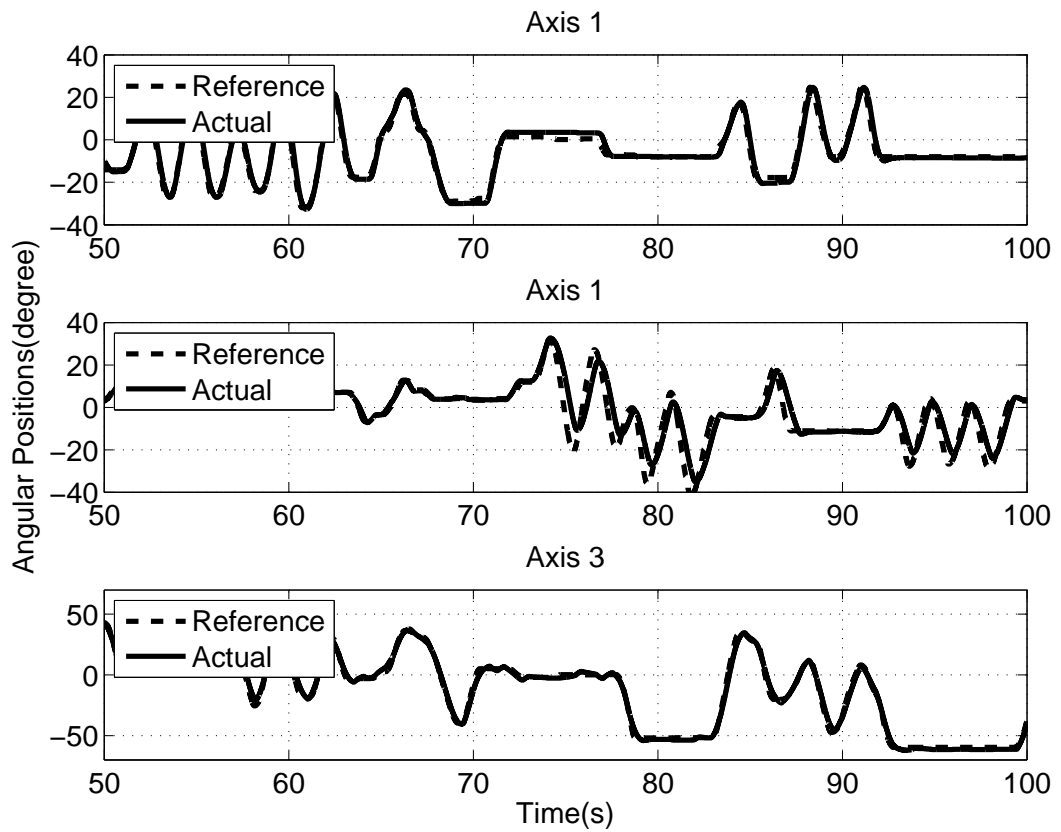


Figure 4.7 : Multi-DOF Position Control joint displacements for arbitrary reference.

5. THROUGHPUT IMPROVEMENT USING COMPRESSION

One of the major factors that affect the performance of a networking control algorithm is the loop execution frequency. The fact from Nyquist theory implies that the shorter sampling period yields the wider bandwidth of the signal [40]. The communication infrastructure of a teleoperation system, having consisted of communication lines and router devices, imposes significant limitations on packet transmission rates. Moreover, as a natural drawback of internet medium, network congestion risk increases when an interval of packet transmission is shortened. Because of network congestion, amount of communication delay and rate of packet loss increase significantly, which deteriorates the performance of overall control system. In order to overcome the effects of congestion, some compression based methods have been proposed that set the frequency of packet transmission lower than that of the control loop [41], [42], [43]. Utilization of compression algorithms implies the existence of two Nyquist frequencies for the acquisition of a signal; one that is determined by the sampling period for the control, and the other being determined by the packet transmission rate.

A similar problem can be observed in biomedical sciences when trying to transmit bio-potential signals, such as electrocardiogram (ECG) data, over the network. For those systems, compression schemes are used that implicitly make use of some transformations. Some examples of these compression structures include the discrete cosine transform (DCT), Walsh transform, Karhunen-Loeve transform (KLT), and wavelet transform. The contribution made by using a transformation for compression comes from the ability to concentrate the energy of the original signal in smaller sized data packages. With the particular selection of the transformation scheme, it becomes feasible to represent the signal by using small number of coefficients in exchange of small losses from the original data [44]. In that sense, mappings that would contain more of the energy from the original signal in smaller sized samples would perform better for the compression. The wavelet transform has a good localization property both in time and frequency domains and fits this purpose of the compression idea.

Furthermore, by appropriate selection of the wavelet function, representation of the same signal can be obtained with smaller error.

Despite being an important factor influencing performance, the use of compression approaches in the area of teleoperation and networking control are very rare [45], [46], [47] and are mostly based on DFT and DCT. The novel WPT codec scheme approach proposed by the authors was demonstrated to have a better performance over those approaches in the literature with its capability to track the original signal even at 90% compression rate [48]. This is an improved performance over existing compression approaches in the literature. In [49], the DFT approach was demonstrated by the authors to have a better performance over DCT, and yet to diverge even at 80% compression rate [48]. Besides its significantly improved performance, another advantage of the proposed WPT approach is its increased flexibility, which allows for a higher number of parameters to be adjusted (i.e. wavelet type, wavelet buffer, vanishing moments, and wavelet level) in comparison to DFT's single adjustment parameter, which is buffer length.

A short packet-sending period and a low communication delay are main requirements to achieve high synchronization in networking control. However, taking into consideration the bandwidth constraints, there is a tradeoff between packet-sending period and communication delay. Low frequency sampling deteriorates the transparency and stability whereas high frequency excitation of network increases the possibility of congestion and packet losses [41]. Making use of compression methods, flexible design possibility is introduced for adjusting the packet sending period taking into consideration the bandwidth limitations. Furthermore, since the network jitter is defined as communication delay variation over packet-sending period, use of a compression algorithm in real-time loop also reduces the jitter disturbing the system from network.

The main contribution of this chapter is a detailed performance analysis and experimental verification for the authors' WPT approach [48] proposed for teleoperation and networking control applications. To this aim, different wavelet families have been analyzed and experimentally tested at different buffer lengths, wavelet levels, and compression rates, also considering computational cost. The

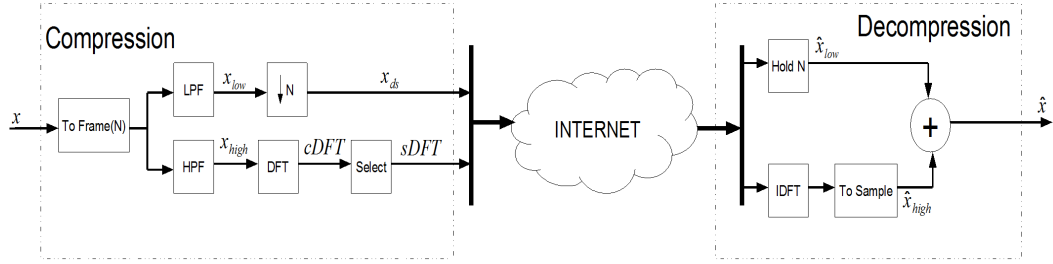


Figure 5.1 : Benchmark DFT Based Compression-Decompression Scheme.

analysis is based on the teleoperation system which was also used in the evaluation of the DFT and DCT approaches in the previous studies [49].

The organization of the chapter is as follows. Section 5.1 describes DFT based benchmark compression system. Section 5.2 introduces the Wavelet Packet Transform. Section 5.3 discusses the WPT based compression/decompression idea utilized for networking control. Section 5.4 compare DFT and WPT with experimental results. Section 5.5 analyses Wavelet basis functions . Section 5.6 analyses WPT in more detail with several parameters and basis function sweep. Finally, in 5.7 and 5.8, analytical discussion over experiment results and concluding remarks are presented respectively.

5.1 DFT Based Benchmark Compression System

A coding and decoding scheme based on the use of discrete Fourier transform (DFT) is proposed in the literature for bilateral control systems [40]. For convenience of the proposed architecture, an overview of the coding and decoding scheme that was proposed in this earlier study is presented in the following discussion. This method manages signal with low and high frequency components. The high frequency part is transmitted in terms of frequency spectrum and added to the low frequency part to increase the bandwidth of the decoded signals.

On the transmitting side, a signal lower than the Nyquist frequency (f_Q) of the original packet x_{low} is created by a low pass filter (LPF) as follows;

$$x_{low} = G_{LPF}(s)x \quad (5.1)$$

where, $G_{LPF}(s)$ denotes the low pass filter transfer function whose cutoff frequency is lower than f_Q . In addition to the extraction of x_{low} , DFT calculation is performed to

extract the frequency components from the following formula;

$$\begin{aligned} sDFT[k] &= \frac{1}{N} \sum_{n=0}^N x[n] e^{j2kn} \\ k &= \{k_{min}, k_{min} + 1, \dots, k_{max}\} \end{aligned} \quad (5.2)$$

where N is the number of data used for the DFT calculation. Larger N values provide a better frequency resolution, unfortunately with the cost of more calculations and larger memory requirement. When there is no compression, the minimum and maximum values of k are respectively set as $k_{min} = 0$ and $k_{max} = N$. In the case of compression, minimum value of k is selected to be $k_{min} = f_Q N T_s$ while the maximum value is determined from $\min(f_{sent}, f_Q)$ and the desired bandwidth for the compressed signal. Compression is performed by selecting k_{max} at a different value than N . Setting k_{max} to a large value increases the bandwidth, but also increases the calculation cost and the size of data transmitted over one packet. The transmitted packet includes the selected coefficients $sDFT$ and low frequency components x_{low} which are minimum necessary data to recover the compressed signal up to a certain precision. On the receiving side, the high frequency part \hat{x}_{high} is added to the low frequency part \hat{x}_{low} to reconstruct the original signal. \hat{x}_{high} is reconstructed by sDFT using inverse discrete Fourier transform (IDFT).

$$\begin{aligned} \hat{x}_{high}[k] &= \frac{1}{N} \sum_{n=0}^N x[n] e^{j2kn} \\ k &= \{1, 2, \dots, N\} \end{aligned} \quad (5.3)$$

where, N is the number of sampling points from the renewal of $sDFT$. The sum of \hat{x}_{low} and \hat{x}_{high} generates the decoded signal on the receiving side.

$$\hat{x} = \hat{x}_{low} + \hat{x}_{high} \quad (5.4)$$

The benchmark coding and decoding scheme described above enables the receiving side system use signals with frequency components higher than the Nyquist frequency which the network medium permits without compression. Moreover the scheme enables wide-band signal transmission even with severe limitations on the packet transmission interval. For convenience of the reader, a representative diagram of DFT based codec structure is given in Fig. 5.1.

5.2 Wavelet Packet Transform

In time-series, analysis can be handled by either in time domain perspective such as moments and correlations or can be handled in the frequency domain perspective such as energy spectra of signals. Wavelets yield a way to analyze these signals both in time and frequency domains by producing local spectral information about them [50]. Unlike the Fourier based waves, which covers the whole time axis, wavelets are localized in a bounded interval of time which satisfies a few requirements. This elasticity enables construction of new wavelets for new applications. The information from which the signal can be analyzed and reconstructed in the selected time and frequency span can be contained in the wavelet coefficients. Due to their advantages in providing local information, wavelets have been adopted to perform efficiently in many applications like identification and estimation [51].

Wavelets are defined by the wavelet function $\psi(t)$ also called the mother wavelet and scaling function $\phi(t)$ also called the father wavelet in the time domain. From a practical point of view, wavelet function acts like a band-pass filter with scaling. Hence, in order to cover the entire signal spectrum, one has to use an infinite number of wavelets. Mathematically speaking, the fundamental form of wavelets can be given as follows;

$$\psi(t) = \sqrt{2} \sum_{n \in \mathbb{Z}} g(n) \phi(2t - n) \quad (5.5)$$

$$\phi(t) = \sqrt{2} \sum_{n \in \mathbb{Z}} h(n) \phi(2t - n) \quad (5.6)$$

where, $g(n)$ and $h(n)$ stand for the high pass and low pass filters respectively which, together constitute a pair of conjugate quadrature filters [52].

Application of wavelets on practical systems is very similar to the realization of sub-band coders. In this approach, the signal is separated into low and high frequency parts that are called approximation and detail respectively. In 1988, Mallat produced a fast wavelet decomposition and reconstruction algorithm [53]. The Mallat algorithm for Discrete Wavelet Transform (DWT) is a two channel sub-band coder which uses conjugate quadrature filters (CQFs) or quadrature mirror filters (QMFs). The one-level

DWT algorithm, which is usually denoted as the decomposition algorithm, is shown in Fig. 5.2 below.

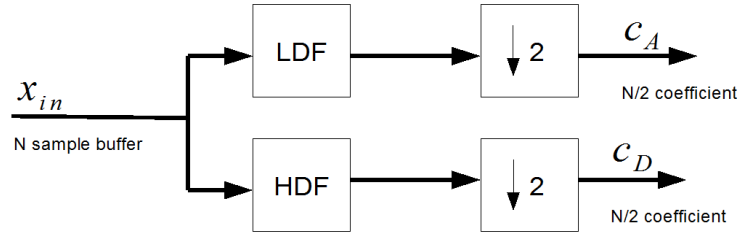


Figure 5.2 : Wavelet Decomposition Algorithm.

Here, LDF denotes low pass decomposition filter and HDF denotes high pass decomposition filter which are orthogonal to each other, " \downarrow " operator denotes down-sampling process, c_A denotes approximate wavelet coefficients and c_D denotes detailed wavelet coefficients. We will call this one-level discrete wavelet transform in the rest of the chapter as DWT1.

The inversion of the process is similar to the forward case and can be done by just exchanging down-sampling to up-sampling and quadrature filters to quadrature mirror filters as shown in Fig. 5.3.

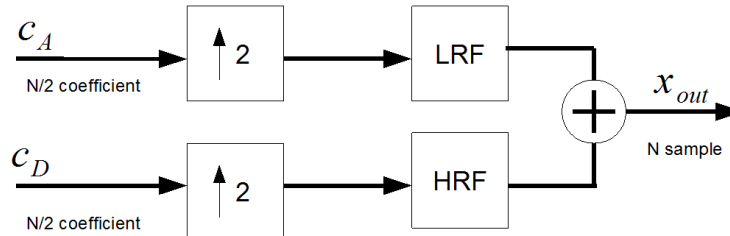


Figure 5.3 : Wavelet Reconstruction Algorithm.

Here, LRF and HRF represent the low-pass reconstruction filter and high pass reconstruction filter respectively, which are again orthogonal to each other, and likewise " \uparrow " operator denotes up-sampling process. Similar to the forward case, this one level inverse discrete wavelet transform will be abbreviated as IDWT1 in the context of this chapter.

5.3 WPT Based Compression System for Bilateral Control

The wavelet packet method involves decomposing the signal using wavelets in binary tree form. For the selected orthogonal wavelet function (LDF and HDF), we generate a set of bases called wavelet packet bases. Every set has particular features of the original signal. The wavelet packets can be used for lots of expansions of a given signal.

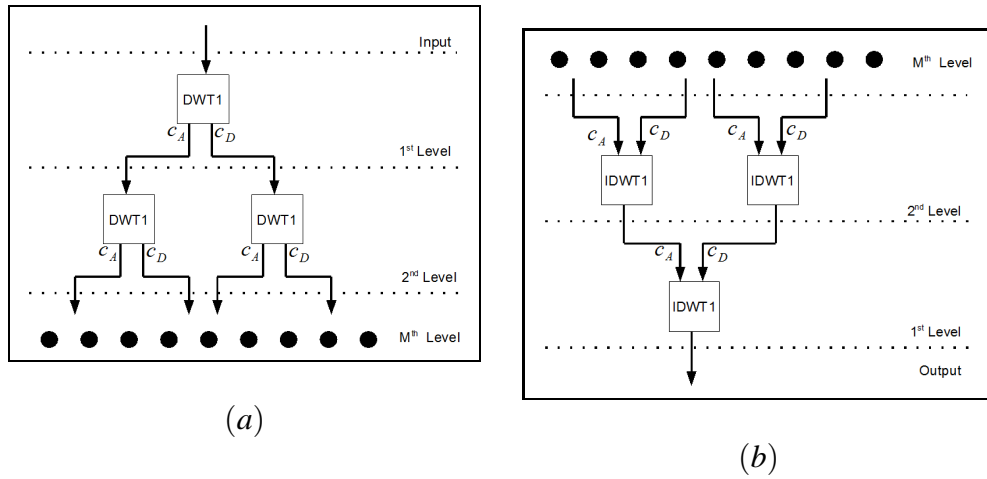


Figure 5.4 : Wavelet Packet Transform Tree; a) Decomposition, b) Reconstruction.

In the orthogonal wavelet decomposition procedure, the approximation coefficients are always separated into two parts, resulting in a vector of approximation coefficients and a vector of detail coefficients, both of which work at a coarser scale. Then, the approximation coefficient vector is separated again, but details are not reanalyzed anymore. Hence, the information loss is in the detailed side. In case of wavelet packet transmission, both detail and approximation coefficient vectors are separated, hence offering the richest analysis capability. The complete binary tree is produced in this way as given in the Fig. 5.4 (A) and (B) below.

In the WPT based compression architecture, wavelet packet tree system is used to decompose and reconstruct the signal. Once again, the signal is separated into its low and high frequency parts. Following this separation, the low frequency component of the signal is down-sampled and the high frequency component of the signal is compressed according to algorithm which saves the predefined amount of maximum wavelet component and cancels others.

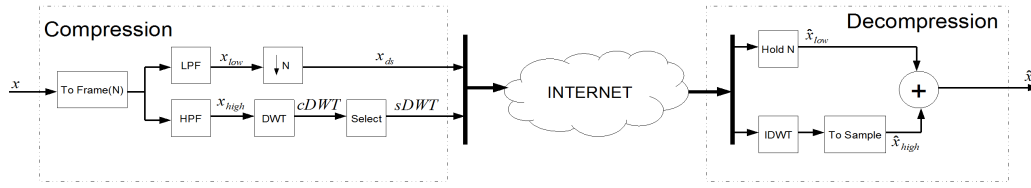


Figure 5.5 : Proposed DWT Based Compression-Decompression Scheme.

For the decompression process, the low frequency part and high frequency components are decompressed separately and then combined together. It is adequate to hold each sample of low frequency signal for N times. For decompression of the high frequency side, the inverse wavelet packet transform is applied to the wavelet packet tree. The selection process means saving maximum predefined amount of components. Having acquired the two components constituting the original signal, low frequency components are summed with decompressed high frequency signals and the recovery of the original data is completed. The whole process is shown in Fig. 5.5.

5.4 DFT vs DWT Experimental Compression Results

Verification of the proposed compression scheme is performed on an experimental setup consisting of linear motors. Two Hitachi-ADA series linear AC motors and drivers are used as the experimental platform. The linear motors had Renishaw RGH41 type incremental encoders with $1\mu m$ resolution. The implementation of the algorithm is made over C code and real time processing was enabled by a D-Space DS1103 card. The experiments are conducted with time delays that have constant and varying components in both measurement and control channels and the compression is made using the two schemes presented in the preceding sections. A sampling frequency of 1KHz was used for both the benchmark DFT based algorithm and proposed DWT based codec scheme. A picture of the experimental setup is given below in Fig.5.6.

In the experiments, the master operator is controlled by the computer under a sinusoidal position reference and the input current i_c from the same sine position tracking command is used in the algorithms. Selection of the input current has particular importance since it is the fastest varying signal of the overall control loop (i.e. the signal for which high frequency components carry the most important information). One segment of the compressed control current is given in Fig 5.12 below while the

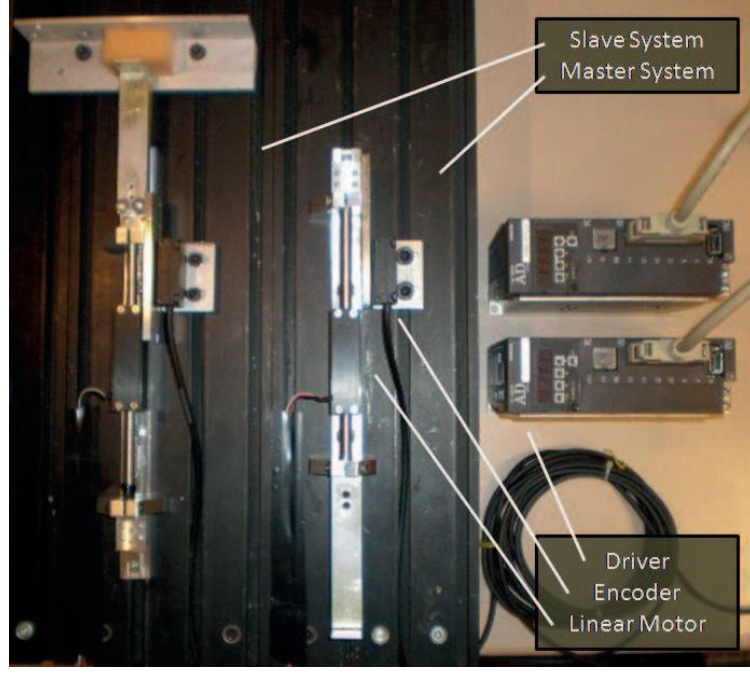


Figure 5.6 : Experimental Setup.

detailed plots obtained by zooming on the marked region of this figure is given in Fig 5.8.

The results shown in Fig 5.8 are obtained using different compression ratios varying from %80 to %95 having kept the buffer size at a constant value of 64. From the figure, it is observed that the reconstructed signal from the proposed codec scheme can track the original signal up to around %90 compression. On the other hand, responses from DFT based codec diverge from the original signal even at %80 compression rate.

In order have better evaluation of performance for the proposed architecture, power error comparisons with the existing method (i.e. DFT based codec scheme) are made using the same signals in both methods. In that sense, both of the algorithms are tried with buffer lengths of 16, 32, 64 and 128 data points. In each buffer length, the compression ratio is changed from %0 to %100 and the results are plotted with respect to the following power error E_P ;

$$E_P = \frac{P_{Original} - P_{Decomposed}}{P_{Original}} \times 100 \quad (5.7)$$

where $P_{Original}$ and $P_{Decomposed}$ respectively stand for the power of original and decomposed signals. Results of the power errors are plotted in Fig 5.9. From these plots, it is obvious that the proposed algorithm outperforms the benchmark algorithm used for the compression of haptic data. Moreover, it can be seen from these figures

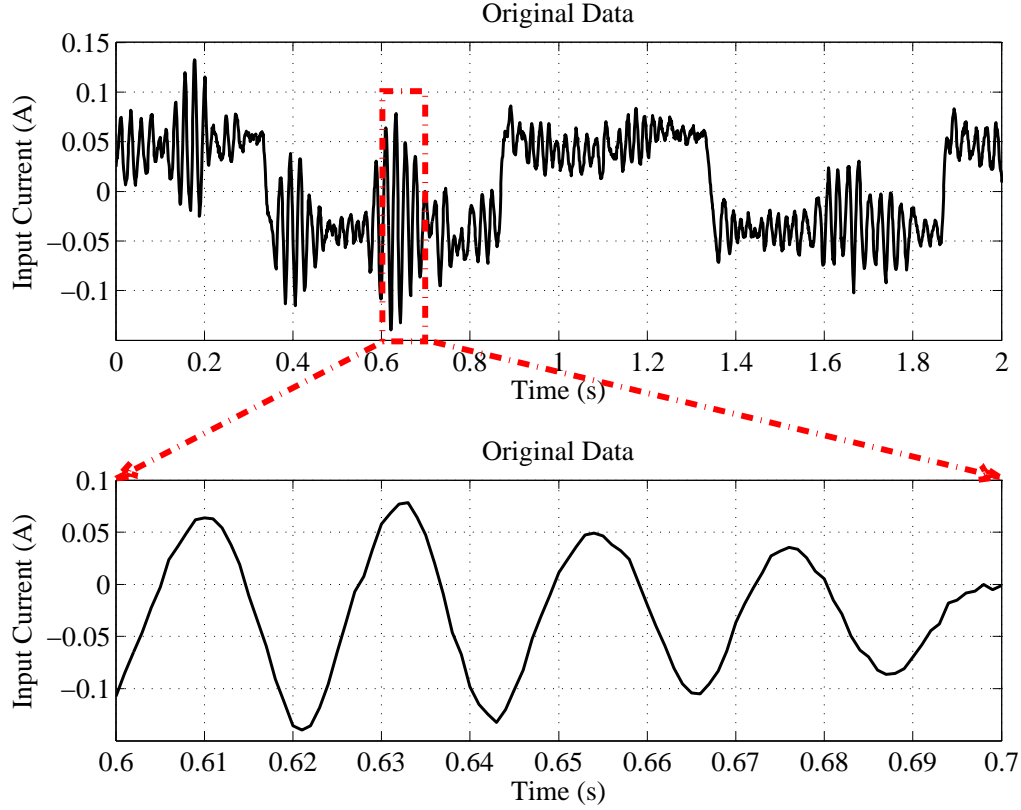


Figure 5.7 : Original Signal Used for Compression-Decompression.

that for the same signal, increasing the buffer size after 32 samples have almost negligible effect on the power error for the same values of compression rates. Having considered the computational requirements for larger buffer sizes, one can deduce the fact that the best performance of the system is obtained for buffer size of 32 samples in DWT based codec scheme.

5.5 DWT Basis Functions

In wavelet transform, the acquisition of information localized within the signal is dependent on the selection of the basis functions (i.e. wavelets). Based on the structure hidden in the basis function, the information is retrieved via dilations and shifting operations. Hence, it is important to decide on the correct wavelet for particular type of application since some basis functions might reveal deeper content from the same signal. For convenience of the reader, we provide below a brief summary of the most commonly used DWT basis functions. The derivations and construction procedures of these wavelets require a much deeper discussion, which is beyond the scope of the work presented here.

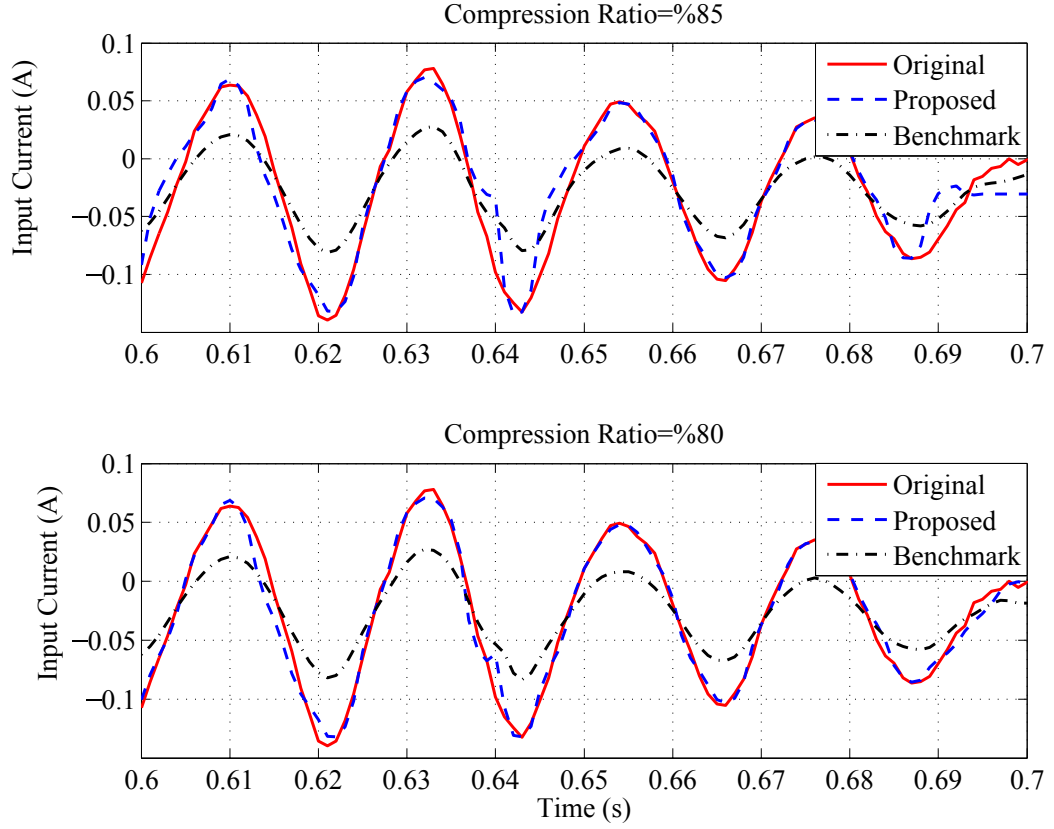


Figure 5.8 : Reconstructions from the Original Signal.

5.5.1 Haar

Haar wavelet family is combination of a sequence of square shaped functions scaled to construct a basis for transformation [54]. This family constitute the simplest possible wavelets that exists in the literature and can be shown to be a special case of Daubechies wavelet (i.e. D2). The Haar family wavelets are not continuous and therefore are not differentiable which provide advantage in analyzing suddenly changing signals. The mother function $\psi(t)$ and the corresponding scaling function $\phi(t)$ for the Haar wavelet family can be given as follows;

$$\psi(t) = \begin{cases} 1 & 0 \leq t < 1/2 \\ -1 & 1/2 \leq t < 1 \\ 0 & \text{otherwise} \end{cases} \quad (5.8)$$

$$\phi(t) = \begin{cases} 1 & 0 \leq t < 1 \\ 0 & \text{otherwise} \end{cases} \quad (5.9)$$

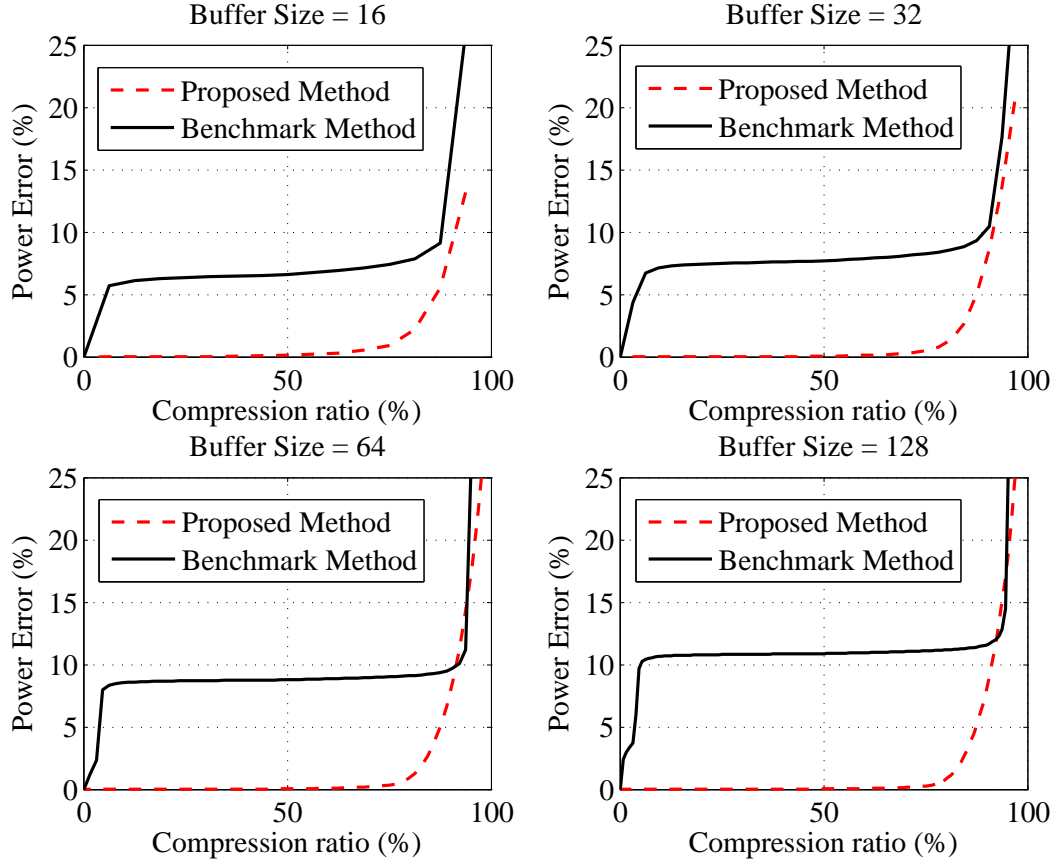


Figure 5.9 : Reconstruction Power Errors.

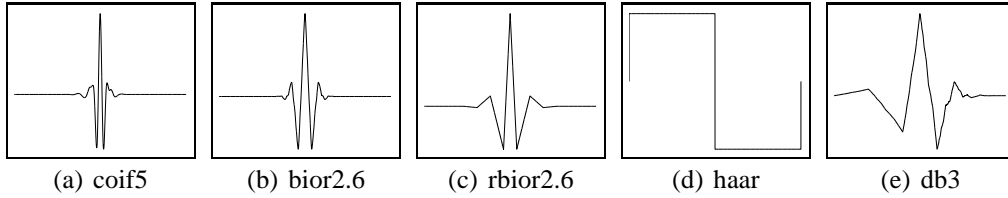


Figure 5.10 : General Shapes of Wavelet Basis Functions.

5.5.2 Coiflets

Coiflets constitute another set of discrete wavelet basis functions which have scaling functions with vanishing moments [55]. Vanishing moments are the degrees of the polynomials representing a linear combination of the smoothing function and its translation. It determines the convergence rate of wavelet approximation. Mathematically, the mother and scaling functions of generalized Coiflet of order l (denoted as $\psi_{l,\mu}$ and $\phi_{l,\mu}$) for some $\mu \in \mathbb{R}$, is supposed to satisfy;

$$\int_{\mathbb{R}} t^p \psi_{l,\mu}(t) dt = 0 \quad (5.10)$$

$$\int_{\mathbb{R}} (t - \mu)^p \phi_{l,\mu}(t) dt = \delta_p \quad (5.11)$$

where, $p = 0, 1, \dots, l-1$ and μ is the center of mass of scaling function $\phi_{l,\mu}(t)$ [52].

5.5.3 Daubechies

Daubechies family constitute an orthogonal wavelet basis which is characterized by a maximum amount of vanishing moments for some given support N . These wavelets are widely used for analysis of self similarity or signal discontinuity problems. An easy way to realize Daubechies wavelets practically is to make use of Fast Wavelet Transform [56]. Unlike other wavelets, in Daubechies wavelets the mother function is dependent on the scaling function and the scaling function can be obtained from a recursion equation [57]. Mathematically, for $N \in \mathbb{N}$, Daubechies wavelet of class D-2N can be obtained from the following mother and scaling functions;

$$\psi(x) = \sqrt{2} \sum_{k=0}^{2N-1} (-1)^k h_{2N-1-k} \phi(2x-k) \quad (5.12)$$

$$\phi(x) = \sqrt{2} \sum_{k=0}^{2N-1} h_k \phi(2x-k) \quad (5.13)$$

where, $h_0, h_1, \dots, h_{2N-1}$ are the constant coefficients of filter satisfying the following conditions;

$$\sum_{k=0}^{N-1} h_{2k} = \sum_{k=0}^{N-1} h_{2k+1} = \frac{1}{\sqrt{2}} \quad (5.14)$$

$$\sum_{k=2l}^{2N-1+2l} h_k h_{k-2l} = \begin{cases} 1 & \text{if } l = 0 \\ 0 & \text{if } l \neq 0 \end{cases} \quad (5.15)$$

with $l = 0, 1, \dots, N-1$. As obvious from equation (5.12), in order to obtain the wavelet, first the recursion given in equation (5.13) has to be solved for $x \in \mathbb{R} \setminus [0, 2N-1[$.

5.5.4 Bior

The Biorthogonal wavelet family differs from the function side since they are not based on vanishing moments [58]. Although they are very different from the Daubechies wavelets in terms of shape and properties, their construction idea is exactly same. Moreover, all generators and wavelets in this family are symmetric. Mathematically, the form of the corresponding mother and scaling functions [59] for Bior wavelet family can be given as;

$$\psi(t) = \sum_{k=0}^N 2g^r(k)\phi(2t-k) \quad (5.16)$$

$$\phi(t) = \sum_{k=0}^N h^r(k)\phi(2t-k) \quad (5.17)$$

where, $g^r(k)$ and $h^r(k)$ stand for the reverse of the original filters $g(k)$ and $h(k)$ respectively.

5.5.5 Rbior

Reverse Biorthogonal wavelet functions are generated by interchanging decomposition and reconstruction filters of the original Biorthogonal wavelet functions. The mother and scaling functions of these wavelets share the same mathematical representation with the original Biorthogonal wavelets as given in equations (5.16) and (5.17) respectively. Rbior wavelets are widely used for system identification.

The variations between the wavelet functions result in differences in terms of compression rates and computational complexities introducing a pay-off to select the best wavelet function for the particular application in hand. The dependency of compression rate is more closely related to the shape of the signal being compressed and the shape of the wavelet used for the transformation. On the other hand, having chosen a particular wavelet structure for application, problems related to computational complexity may come into picture based on the selected vanishing moment, buffer size and compression level. In order to provide a consistent analysis of the selected

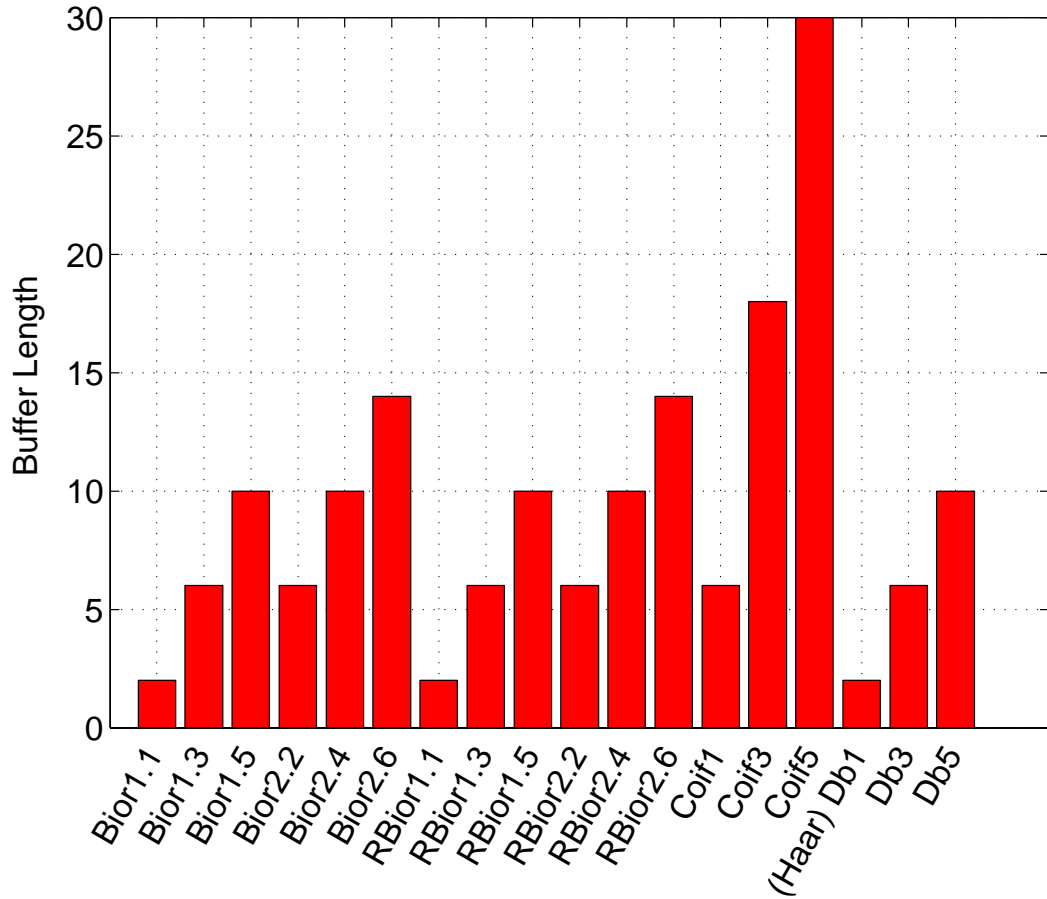


Figure 5.11 : Filter Length of Wavelets.

wavelets, the general shapes of these wavelets and the information related to their buffer sizes are provided in Fig. 5.10 and Fig. 5.11 respectively.

5.6 Detailed WPT Experimental Analysis

In the experiments, artificially generated time delays that have constant and varying components in both measurement and control channels are employed between master and slave operators. During experiments, the compression and decompression is made using the WPT based compression algorithm running in various parameter sweep conditions to test their effects on the overall performance. These conditions include wavelet family, compression level (i.e. depth), buffer size and compression ratio. A picture of the experimental setup is given below in Fig.5.6.

In the experiments, the master operator is computer controlled with sinusoidal position reference and the corresponding control current $i_c(t)$ from the same sine position tracking command is used in the compression algorithm since in bilateral control

current of the master system is the primary data that is sent to the remote system. Selection of the input current has one more important aspect. Since current input is the fastest varying signal within the control loop (i.e. the signal for which high frequency components carry the most important information) the performance of the compression algorithm can best be seen on this data. Fig. 5.12 shows one segment of the compressed control current while the detailed plots obtained by zooming on the marked region is provided over the same figure.

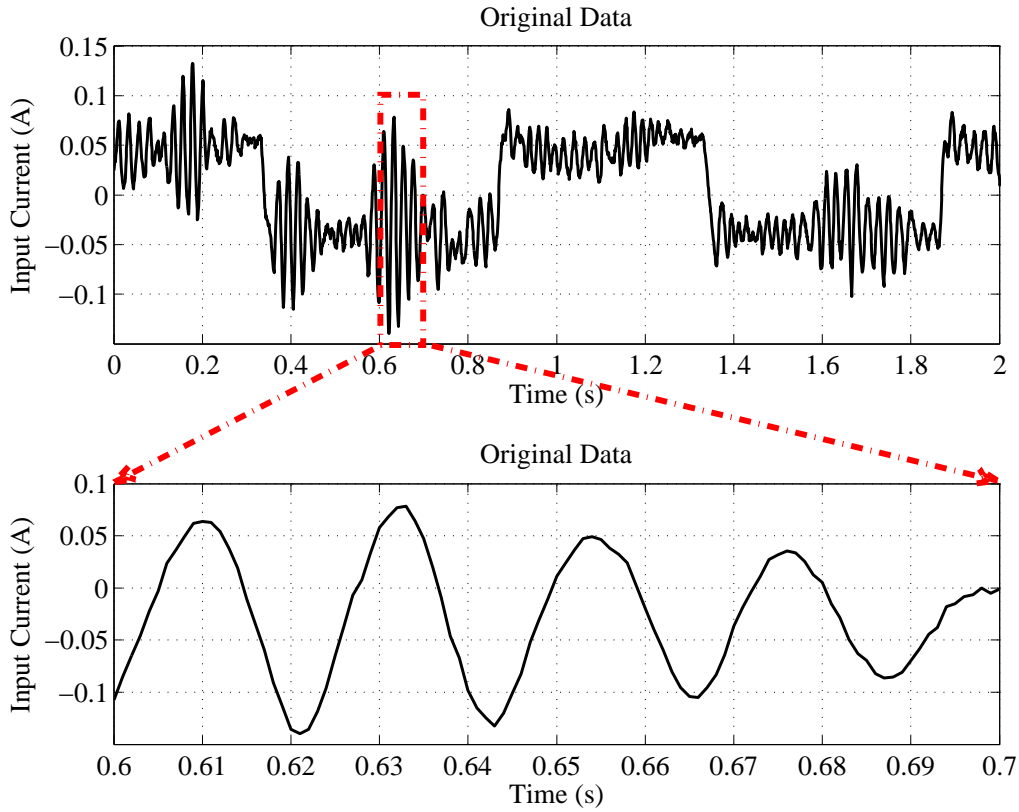


Figure 5.12 : Original Signal Used for Compression-Decompression.

In order have better evaluation of performance, power error comparisons are made using the same signals for every different scenario. For each case, the compression ratio is changed from 0% to 100% and the results are plotted with respect to the following power error E_P ;

$$E_P = \frac{P_{Original} - P_{Decomposed}}{P_{Original}} \times 100 \quad (5.18)$$

where, $P_{Original}$ and $P_{Decomposed}$ respectively stand for the power of original and decomposed signals.

Since the number of parameters that affect the overall algorithmic performance are relatively high, here we adopt a methodological way to observe the effects of these parameters by carrying out separate analysis for each different factor. For that purpose, three different experiment sets are carried out and explained below.

5.6.1 Experiment Set-1

The first experiment set covers analysis with respect to the wavelet family and compression depth for which the results are given in Fig. 5.13. In these figures, the main objective is to see the change in responses via changing the vanishing moments of the corresponding family and changing the compression depth (i.e. level) under constant vanishing moment of the corresponding family. The families used in the experiment content include Biorthogonal 1.x, Biorthogonal 2.x, Reverse Biorthogonal 1.x, Reverse Biorthogonal 2.x, Coiflets and Daubechies, given in Fig 5.13-(a), Fig 5.13-(b), Fig 5.13-(c), Fig 5.13-(d), Fig 5.13-(e) and Fig 5.13-(f) respectively. In these figures, for each family, upper subfigure shows the effect of family parameter on power error with respect to comparison ratio and lower subfigure shows the effect of wavelet depth on power error with respect to comparison ratio.

Referring to the upper subfigures, one can conclude that the compression error decrease slightly with increasing vanishing moments for every wavelet family. On the other hand, the computational complexity comes into picture when talking about increasing vanishing moments since that means increasing the length of reconstruction and decomposition filters as seen in Fig. 5.11. Hence, one has to take into consideration the relative change in the required computational power for a small enhancement in the compression performance.

On the other hand, having observed the lower subfigures, one can deduce that increasing the wavelet depth results in better performance regardless of the wavelet structure. This result is consistent with the intuitional expectation, since at every additional level more coefficients are generated to represent the same signal. However, here again one has to consider the increasing computational complexity with the increasing depth. Theoretically the computational requirements double as the compression depth is increased one step forth. Hence, selection of compression

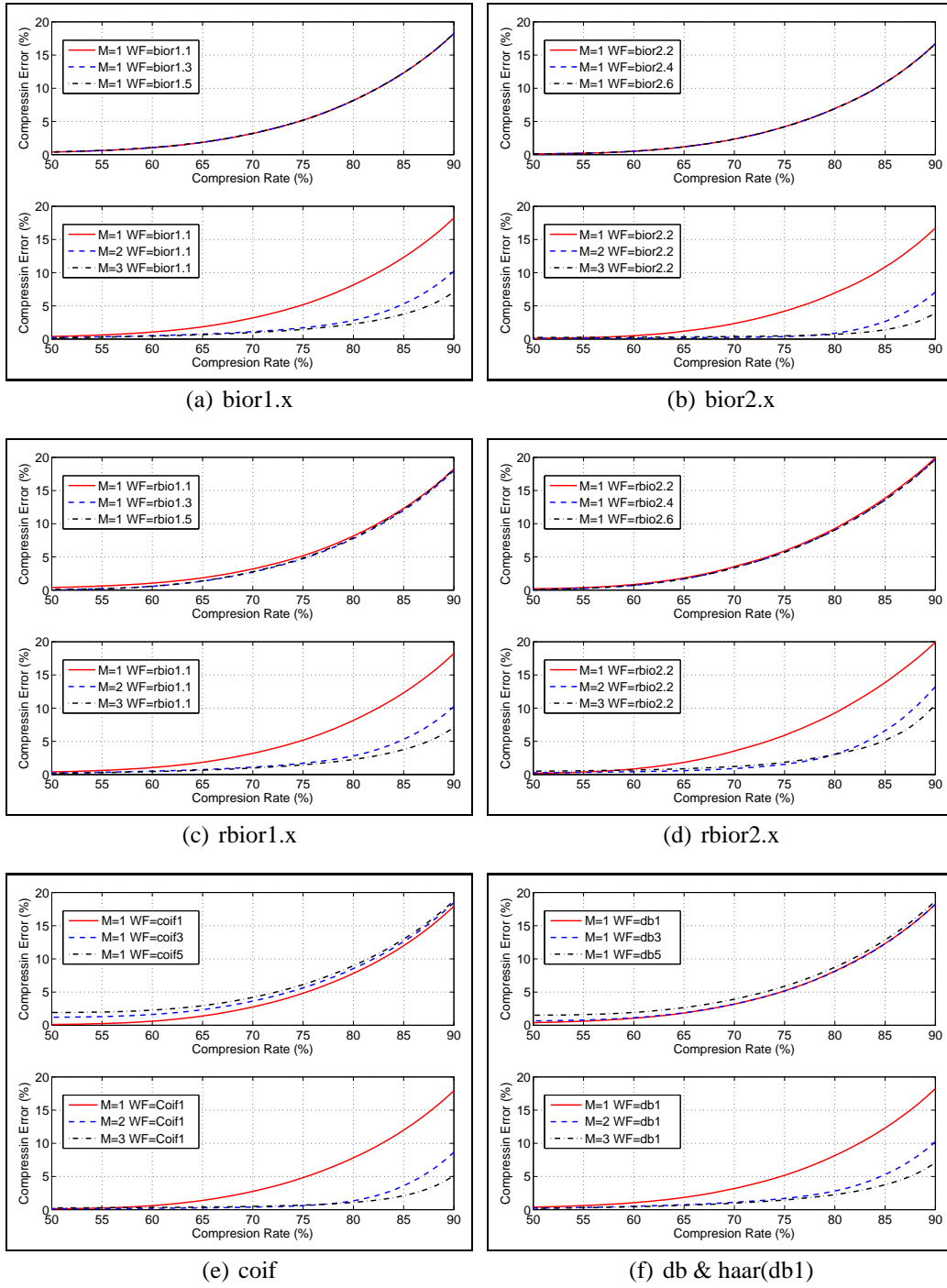


Figure 5.13 : Comparison of Wavelet Families With Respect to Vanishing Moments and Compression Levels.

depth is a matter of decision based on the available computational power that can be permitted by the real time processing unit under certain sampling time constraint.

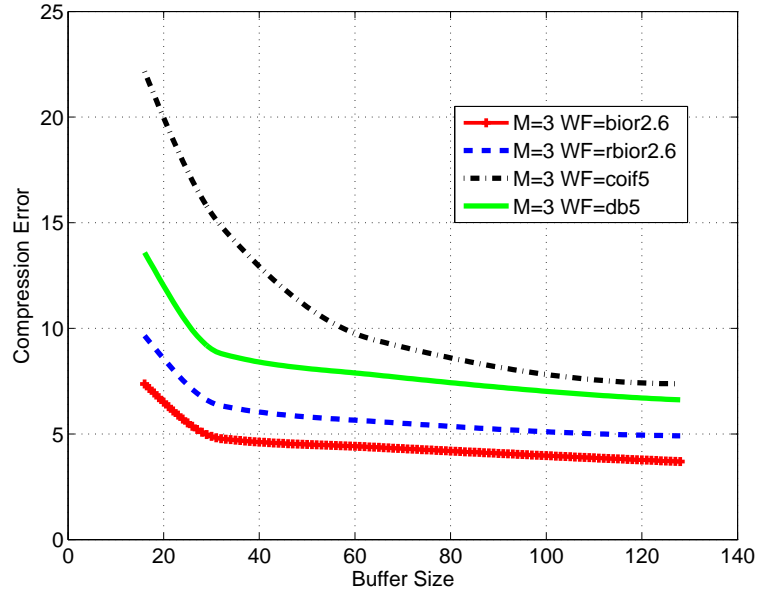


Figure 5.14 : Comparison of Wavelet Families With Respect to Buffer Size.

5.6.2 Experiment Set-2

Another set of experiments is made to observe the relationship between compression ratio and the size (i.e. length) of buffer used for storing and reconstructing the data under constant compression depth for wavelet families Biorthogonal 2.6, Reverse Biorthogonal 2.6, Coiflets 5 and Daubechies 5. Once again reconstruction power error is taken as the major metric to analyze the results which are shown in Fig. 5.14. In this experiment set, the buffer length used in the algorithm is swept from 16 to 128 and the compression rate is kept at 90% for all wavelet families.

The results obtained from this experiment set show that the reconstruction error decays exponentially as the buffer size is increased. In other words, increasing buffer length after a certain point has almost negligible effect on the overall reconstruction performance of the signal. On the other hand, just like the compression depth, having larger buffer means increased computational cost.

Another important result obtained from Fig. 5.14 is the considerable change of reconstruction error between wavelet families. For the entire sweep range of buffer size, Bior family outperforms the other wavelet bases while the worst results are obtained from Coiflet family. Having considered the simpler structure of Bior with

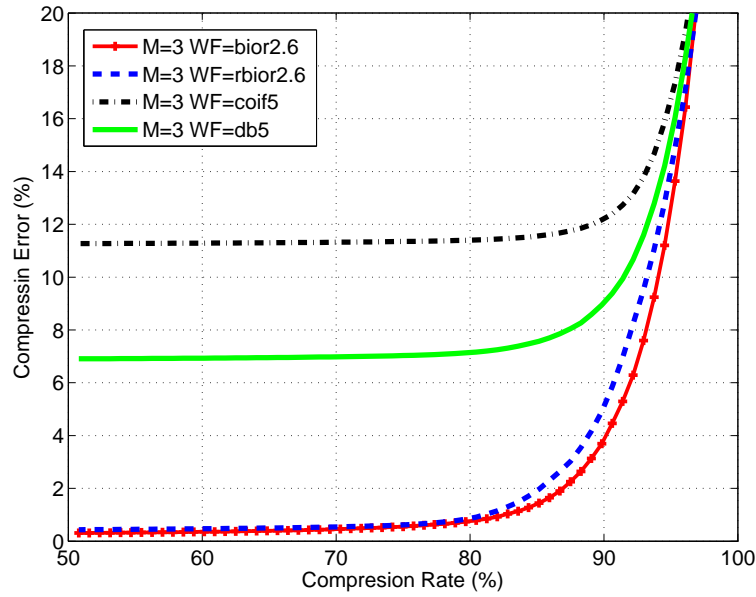


Figure 5.15 : Comparison of Wavelet Families With Respect to Compression Ratio.

respect to other families, one can conclude that it comes out as the best selection for the entire range of buffer length.

5.6.3 Experiment Set-3

The final set of experiments includes a comparison between the wavelet families with respect to power error under constant buffer size and constant level of compression. For that purpose, results obtained from families Biorthogonal 2.6, Reverse Biorthogonal 2.6, Coiflets 5, and Daubechies 5 are compared and shown in Fig. 5.15 all of which having buffer size equal to 128 and compression depth being equal to 3.

Based on the results shown in the figure, one can conclude that in terms of error performance, Bior family once again give the best response while Coiflet family performs worst. Families Rbior and Daubechies show intermediate responses. However, here one can also observe that for low ranges of compression, Rbior family gives almost the same response with Bior bases.

5.7 Discussion

Having evaluated the results shown in these experiments, few important conclusions can be summarized. The first result is the negligible effect of vanishing moments on the performance of the system. Since vanishing moments add up with further

computational complexity, for realization of the given framework, it is recommended to take the vanishing moments with the least complication. The second remarkable conclusion that can be observed from the system is improvement of performance with increasing compression depth. Based on the results, selection of compression depth at the level $M = 3$ seems to be a good solution as compression rates of 85% can be achieved within the error bounds of 5% with relatively low computational requirement. Another result obtained from the experiments indicate that increasing buffer size contributes on the reconstruction performance in an exponentially decaying manner. On the other hand like the vanishing moments and compression depth, buffer size also negatively affects the computational requirements of the system. As the computational requirements increase linearly with increasing buffer size, one can make a relatively easier selection. From the given results, a buffer size of 64 seems to be a good selection for bilateral control application. The final result that can be acquired from the last experiment set indicates that the reconstruction error remains same for most of the range of compression ratios. However, increasing the compression ratio beyond values of 80%, the power error starts to rise up exponentially with compression rate for all families. Having summarized all these results, a meaningful selection of the system configuration for the proposed WPT based compression scheme will be using the basis family Bior2 with the first vanishing moment (i.e. Bior2.2) and with compression depth of $M = 3$ and buffer size of 64.

In order to better illustrate the performance of the compression algorithm, the position responses of the master and slave manipulators are recorded and shown in this section. For that purpose, the master system is operated under a computer controlled sinusoidal position reference and the compressed control current is sent to the slave system over an artificially generated network delay of varying magnitude between $95ms$ and $105ms$. Following the discussion on the results obtained from experiments, the WPT based compression algorithm is tuned to have the configuration described at the end of the previous paragraph. The decompressed control signal is then used to drive the slave system based on the time delayed motion control algorithm. In order to observe the performance of the proposed codec scheme in real time control, the original master position signal is also transferred through the same amount of delay and plotted

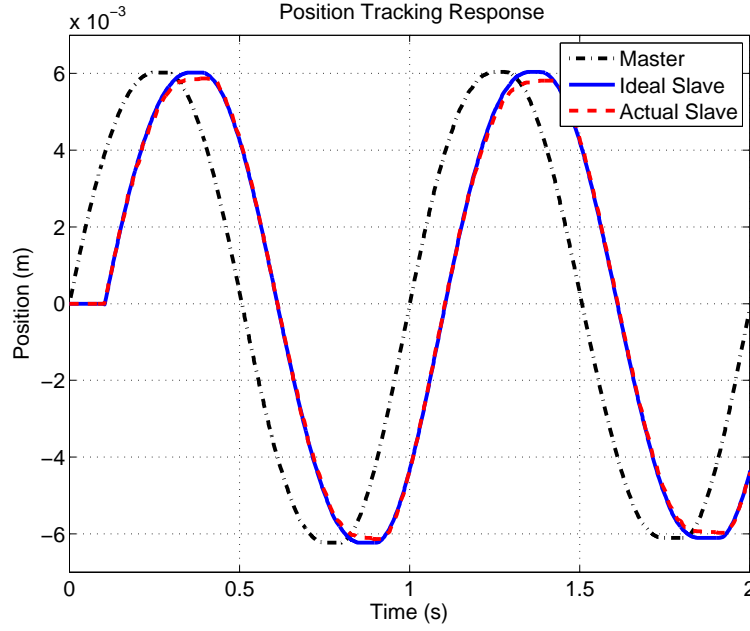


Figure 5.16 : Position Tracking Responses of the Master and Slave Systems.

together with the actual slave position response under the label "Ideal Slave" as shown in Fig. 5.16 below.

As obvious from the given plots, the proposed WPT based algorithm performs efficiently in compressing and decompressing the high frequency signals being used in network delayed teleoperation systems. For the sake of completeness, the actual slave motion data is analyzed in terms of power error with respect to the ideal slave motion data using the power error defined in equation (5.18). It turns out that the power error between ideal and actual slave motion is 4.81% meaning that the recovery of original data is made with an accuracy level above 95%. It should also be pointed out here that this error contains both the error due to the imperfections of estimation in network delayed control algorithm and the error due to compression and decompression in WPT based algorithm. Hence, the proposed algorithm alone is supposed to perform even better if all imperfections in the system are cleared out.

In order to show the effect of compression on transparency, the position and force responses of the master and slave manipulators are recorded making use of the proposed codec scheme and above-mentioned network controller. For that purpose, the master system is first moved by a human operator and the corresponding motion is recorded. Then, this recorded motion is given as reference to master system under

a computer controlled loop and the slave system is home positioned to have contact with remote environment. While, in the first scenario neither position nor force signal is compressed, in the second scenario both position and force signals are compressed and decompressed. The results are shown in Fig. 5.17 below. From the given figure, it is obvious that the effect of the proposed compression algorithm is negligible on the overall response of the system.

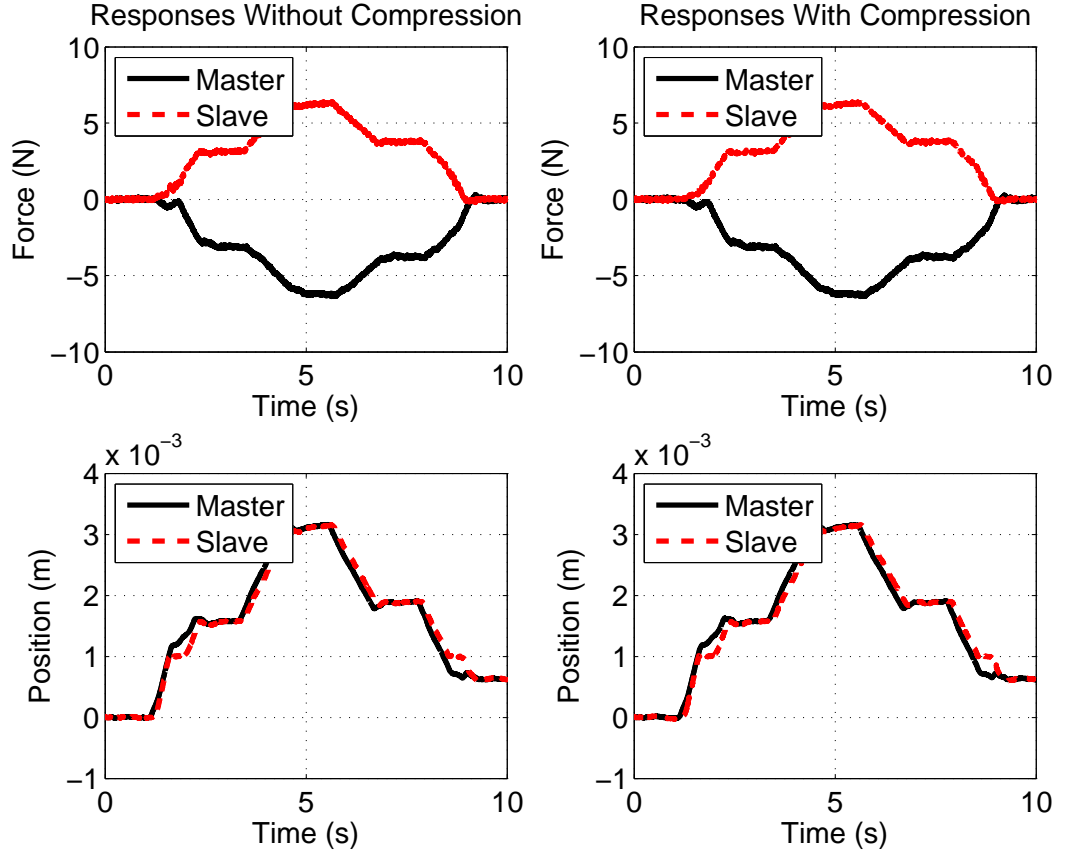


Figure 5.17 : Wavelet Position and Force Tracking Results under Hard Contact.

5.8 Conclusion

In this chapter, a compression-decompression algorithm using Wavelet Packet Transform is proposed as a novel approach for networked control and teleoperation systems. The derivation of the proposed codec scheme is followed by a detailed analysis of the factors and parameters affecting the performance of the system. For the convenience of the reader, brief summaries are provided for the controller structure and the wavelet families that are used in the context of this study. Detailed experimental results are evaluated in a comparative manner and several conclusions

are drawn to utilize the algorithm in teleoperation with the best possible performance. Network control systems can benefit from compression approaches due to the fact that compression allows for sampling rates that are higher than the network throughput by a multiple of the compression ratio. Moreover, this is achieved with very little loss in the control input power. The authors have already emphasized the benefits of this proposed novel compression approach comparatively with respect the DCT and DFT based compression approaches in the literature [45], [46], [47]. Different from previous studies, this chapter performs a comprehensive analysis of the novel compression approach in terms of its parameters and how they affect the system. Our analysis verified that increasing the buffer length affects the compression performance positively, while also increasing the network delay, as expected from compression approaches in general. The analysis performed among different wavelet families in terms of different parameters demonstrated the biorthogonal wavelets to have the best performance. An interesting conclusion was reached with another wavelet parameter known as vanishing moment, which, while increasing computational complexity, was observed to have little or no effect on the system performance. The compression depth, on the other hand was noted to improve performance. Consideration of the above outcomes favors the selection of wavelets with optimum buffer size, maximum compression depth, and a vanishing moment with minimum complexity. In the following chapter, we look at the networked control from an other view, which is called synchronization.

6. SYNCHRONIZATION IMPROVEMENT USING OPERATOR MOTION ESTIMATION

While the ultimate goal of the networked control is full synchronization, network delay between master and slave is a major obstacle for the desired performance, and network delays happen randomly. In teleoperation applications the reference is often provided by a human, known as the operator. Due to the nature of the human system, references provided by the human operator are of a much lower bandwidth when compared to common control reference inputs, and this can sometimes be problematic. All of the above mentioned studies discuss system stabilization under network delay [60], but do not address the operator delay, which also contributes to the delay between master and slave. Meanwhile, the prediction of the input delay (in this case, created by the human operator) has the potential to reduce this network latency. However, to the authors' best knowledge, the only study in the literature addressing this concept is [60], which uses a Taylor series based analytical approach to handle this problem. Taylor series simply performs the extrapolation of position based on velocity, meanwhile acceleration has significant effect on both velocity and position, and affects the prediction error negatively.

In this chapter, we propose a method based on Grey Prediction for Predictive Input Delay Compensation, and demonstrate experimentally the advantages of the proposed method over the one using Taylor Series in predicting the operator's motion. The Grey prediction not only performs extrapolation, but unlike the Taylor Method fits a differential equation to the system dynamics. As a result, grey prediction is more effective in considering the transients, hence, the acceleration.

6.1 Taylor based PIDC as Benchmark System

In this section, we will first discuss the benchmark PIDC approach based on Taylor Series. Subsystems of the human, such as skeleton, muscle, and neural systems behave similar to mass-spring-damper like structures, hence result in a high time constant for the operator. This also makes it acceptable to assume the human motion output to be continuously differentiable in time [60].

By accepting this assumption, future signal values can be predicted using simple geometric approaches. The prediction formula is

$$\lim_{T \rightarrow 0} q_{mi}(n+k) \approx (k+1)q_{mi}(n) - kq_{mi}(n-1) \quad (6.1)$$

Here $q_{mi}(n+k)$ denotes k step further value, $q_{mi}(n)$ denotes current value and finally $q_{mi}(n-1)$ denotes previous value. We must mention that, there are just two error source which is neglected. One is high order terms and the second is discretization.

6.2 Grey based PIDC

Grey system theory [61] is developed for systems characterized by uncertain information. Grey Prediction is a scientific quantitative prediction method which is based on the theoretical treatment of the original data to determine the future output of the system [62]. Basically, it can be defined as a local curve fitting extrapolation method, which requires four data sets only. In Grey Systems, $GM(n, m)$ denotes a grey model. Here n denotes the order of the difference equation, and m is the number of the variables. The commonly used Grey Model is of the $GM(1, 1)$ type. It represents the first order derivative, and one input variable is used for prediction purposes. The process of the Grey Prediction can be given as below:

Step 1: Collecting the original data sequence, and using generalized coordinate, q_{mi} for the master manipulator's i^{th} joint angle position,

$$q_{mi}^{(0)} = \{q_{mi}^{(0)}(1), q_{mi}^{(0)}(2), \dots, q_{mi}^{(0)}(n)\}, n \geq 4 \quad (6.2)$$

Step 2: Conducting an accumulated generation operation, AGO, on the original data sequence in order to diminish the effect of data uncertainty;

$$q_{mi}^{(1)} = \{q_{mi}^{(1)}(1), q_{mi}^{(1)}(2), \dots, q_{mi}^{(1)}(n)\}, n \geq 4 \quad (6.3)$$

Where

$$q_{mi}^{(1)}(k) = \sum_{i=1}^k q_{mi}^{(0)}(i), k = 1, 2, \dots, n \quad (6.4)$$

Step 3: Establishing the Grey difference equation and then calculating its background values;

$$q_{mi}^{(0)}(k) = -a_i z_i^{(1)}(k) + b_i \quad (6.5)$$

$$z_i^{(1)}(k) = 0.5 \{q_{mi}^{(1)}(k) + q_{mi}^{(1)}(k-1)\} \quad (6.6)$$

Step 4: Constructing data matrix B and data vector Y;

$$B = \begin{bmatrix} -z_i^{(1)}(2) & 1 \\ -z_i^{(1)}(3) & 1 \\ \vdots & \vdots \\ -z_i^{(1)}(n) & 1 \end{bmatrix} \quad (6.7)$$

$$Y_{Ni} = [q_{mi}^{(0)}(2), q_{mi}^{(0)}(3), \dots, q_{mi}^{(0)}(n)]^T \quad (6.8)$$

Step 5: Resolving the matrix;

$$Y_{Ni} = B_i \hat{a}_i \quad (6.9)$$

$$\hat{a}_i = B_i^T B_i^{-1} B_i^T Y_{Ni} = \begin{bmatrix} a_i \\ b_i \end{bmatrix} \quad (6.10)$$

Step 6: Deriving the solution to the Grey difference equation;

$$q_{mi}^{(1)}(k+1) = \left[q_{mi}^{(0)}(1) - \frac{b_i}{a_i} \right] e^{-a_i k} + \frac{b_i}{a_i} \quad (6.11)$$

$$q_{mi}^{(1)}(k+1) = \left[q_{mi}^{(0)}(1) - \frac{b_i}{a_i} \right] e^{-a_i k} (1 - e^{a_i}) \quad (6.12)$$

Step 7: Conducting the inverse accumulated generation operation to obtain a prediction value

$$q_{mi}^{(1)}(k+H) = \left[q_{mi}^{(0)}(1) - \frac{b_i}{a_i} \right] e^{-a_i(k+H-1)} (1 - e^{a_i}) \quad (6.13)$$

$$\hat{q}_{mi}(k) = q_{mi}^{(1)}(k+H) \quad (6.14)$$

Here we will introduce our proposed networked control system configuration to explain the requirement and the performance measure of the Predictive Input Delay Compensator (*PIDC*) algorithms. However first, we will introduce our standard configuration without the *PIDC*. In the standard configuration, the operator forces the master manipulator to a desired posture, which in turn will dictate the slave motion. In order for the slave to track the master motion in the closest possible way, on the master side, an Astrom Smith Predictor (*ASP*) generates the control signal for the model plant. Then the control signal generated on the master side, is transmitted to the slave side passing through a Delay Regulator Send unit (*DRS_m*)" through the Internet to Delay Regulator Receive unit (*DRR_s*). On the slave side, a Model Tracking Control (*MTC*) algorithm inputs the received control to an other model process (same as the model plant at master side) and forces the slave manipulator to track the trajectory of the model plant. The angular displacement output of the *MTC* is fed back to the *ASP* passing through a Delay Regulator Send unit (*DRS_s*) through the Internet to Delay Regulator Receive unit (*DRR_m*). [39]

Here $\tau_{oq\{1,2,3\}}$ denote the joint torques generated by the operator, $\tau_{qm\{1,2,3\}}$ denote the joint torques applied to the manipulator after the addition of $g_{qm\{1,2,3\}}$ gravitational compensation terms. $\tau_{mq\{1,2,3\}}$ denote the torque signals fed to *DRS_m* to be sent to slave side. $\bar{\tau}_{mq\{1,2,3\}}$ denote the delay regulated torque signals coming through the Internet from the master to the slave. $\tau_{cq\{1,2,3\}}$ denote the joint torques generated by *MTC*, $\tau_{qs\{1,2,3\}}$ denote the joint torques applied to the manipulator after the addition of $g_{qs\{1,2,3\}}$ gravitational compensation terms. Finally $q_{s\{1,2,3\}}$ denote the slave manipulator's joint angle (actual) positions.

In this study, the Predictive Input Delay Compensator (*PIDC*) unit is added to this configuration between the operator and *ASP*. With this addition, it is now possible to

predict and compensate the delay caused by the operator, which will allow sending the master side information to the slave side with less delay. This reduced delay increases the synchronization between the master and slave trajectories. To reduce nonlinearities of the master and slave manipulators, namely to increase the compliance on the master side and compensate the gravity on the slave side, gravity compensation blocks GC_m and GC_s added, respectively. The overall master-slave architecture is given in Fig. 6.1. However the function detail of each block is outside the scope of this study, and will not be discussed.

6.3 Experimental System and Results

Next, experiments have been performed to conduct a comparative performance evaluation for the Taylor based and Grey prediction approaches. The 6-DOF PUMA560 Industrial Robot is used for experimentation. The manipulator is operated as a 3-DOF system by the operator as can be seen in Fig. 6.2.

The well-known Euler-Lagrange based dynamic model of the manipulator has the following general form:

$$M(q).\ddot{q} + V(q, \dot{q}).\dot{q} + G(q) = \Gamma \quad (6.15)$$

where,

- q : $nx1$ position vector
- $M(q)$: nxn inertia matrix of the manipulator
- $V(q, \dot{q})$: $nx1$ vector of Centrifugal and Coriolis terms
- $G(q)$: $nx1$ vector of gravity terms
- Γ : $nx1$ vector of torques

In this study the system will be taken on the consideration as an independent joint control system. This approach allows each manipulator joint to be controlled independently as a SISO system, with the nonlinearities and couplings taken as a disturbance affecting each joint actuator.

For our experimental system, since the human speed is considerably low, the main nonlinearities come from the gravity effect $G(q)$. For that reason, in our experiments

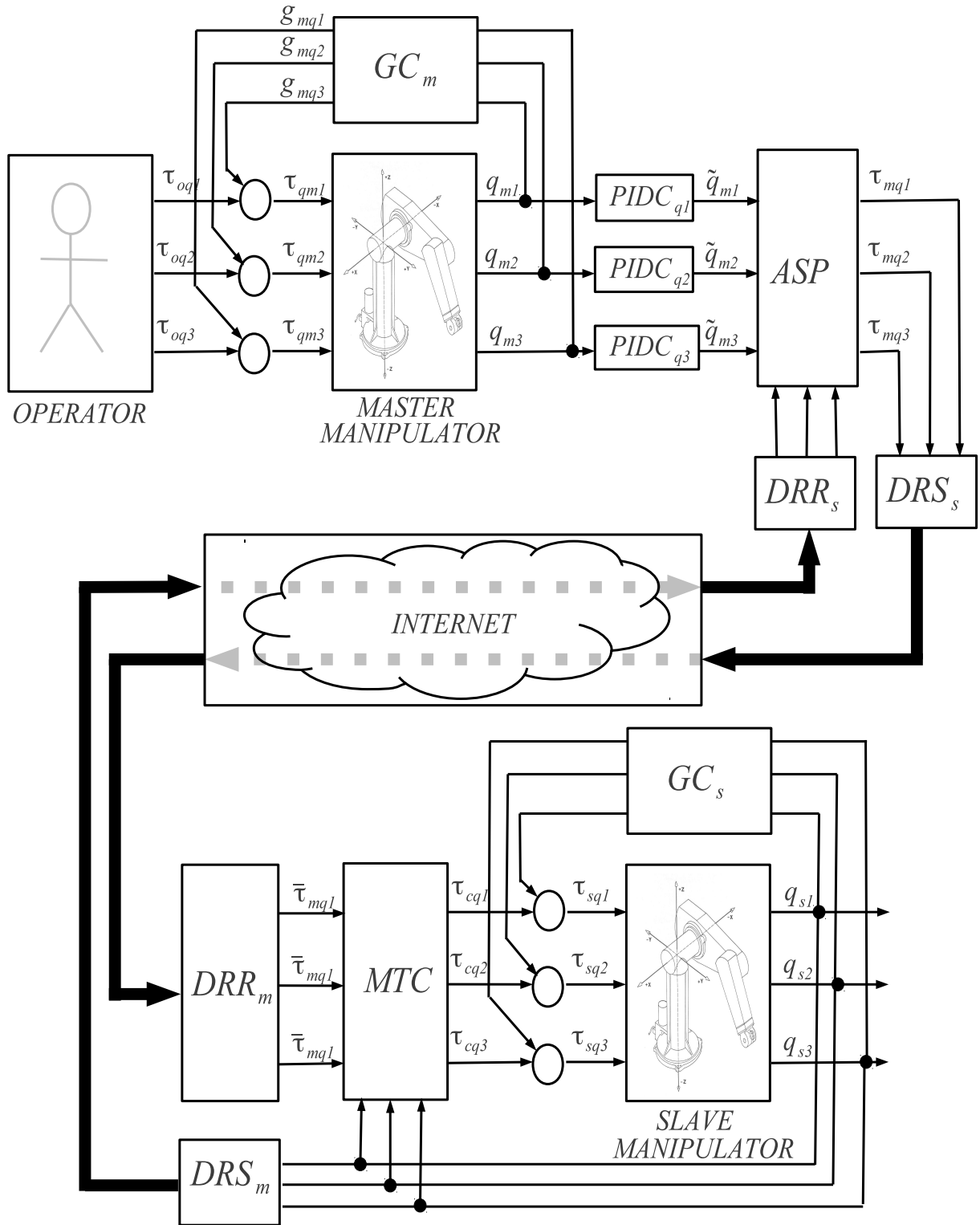


Figure 6.1 : Extended Control Scheme of Networked Control for Grey Prediction.

we apply system gravity compensation $\tilde{G}(q) \approx G(q)$, to cancel and/or reduce the gravity effect on the experimental system to a negligible level.



Figure 6.2 : Experimental Setup for Grey Prediction.

The use of an independent joint control system approach, simplifies the system to be estimated to a one-degree-of-freedom process.

The results of those experiments are seen in Fig. 6.3. Here, Fig. 6.3a and Fig. 6.3b depict the results for the first joint, Fig. 6.3c and Fig. 6.3d for the second joint, Fig. 6.3e and Fig. 6.3f for the third joint. The performance of each joint is further demonstrated by also highlighting the zoomed version of the region marked in red. The figures in the right are zoomed versions for the highlighted sections in the diagrams on the left side. For each figure, the grey line represents the operator motion, which is taken as the reference motion to be predicted. The solid line depicts the Grey Predictor's output, and finally dashed line demonstrates the output of the benchmark Taylor Series based predictor. In each figure, it is easily seen that when the angular velocity is low, both algorithms demonstrate similar performance. However when the acceleration increases, the performances show differences. Only operation intervals where there is significant operator motion have been selected in the zooms of Fig. 6.3b, Fig. 6.3d and Fig. 6.3f. In all three figures, we see that the Grey Prediction method achieves a faster prediction of $100ms$ on average when compared with the Taylor based approach. On the other hand, the benchmark method demonstrates a prediction performance that varies between $10ms$ and $100ms$, and demonstrates a poor performance in tracking transients as indicated by the high amplitude oscillation observed in Fig. 6.3d starting at $5.7ms$, and in Fig. 6.3d starting at $2.8ms$ for the

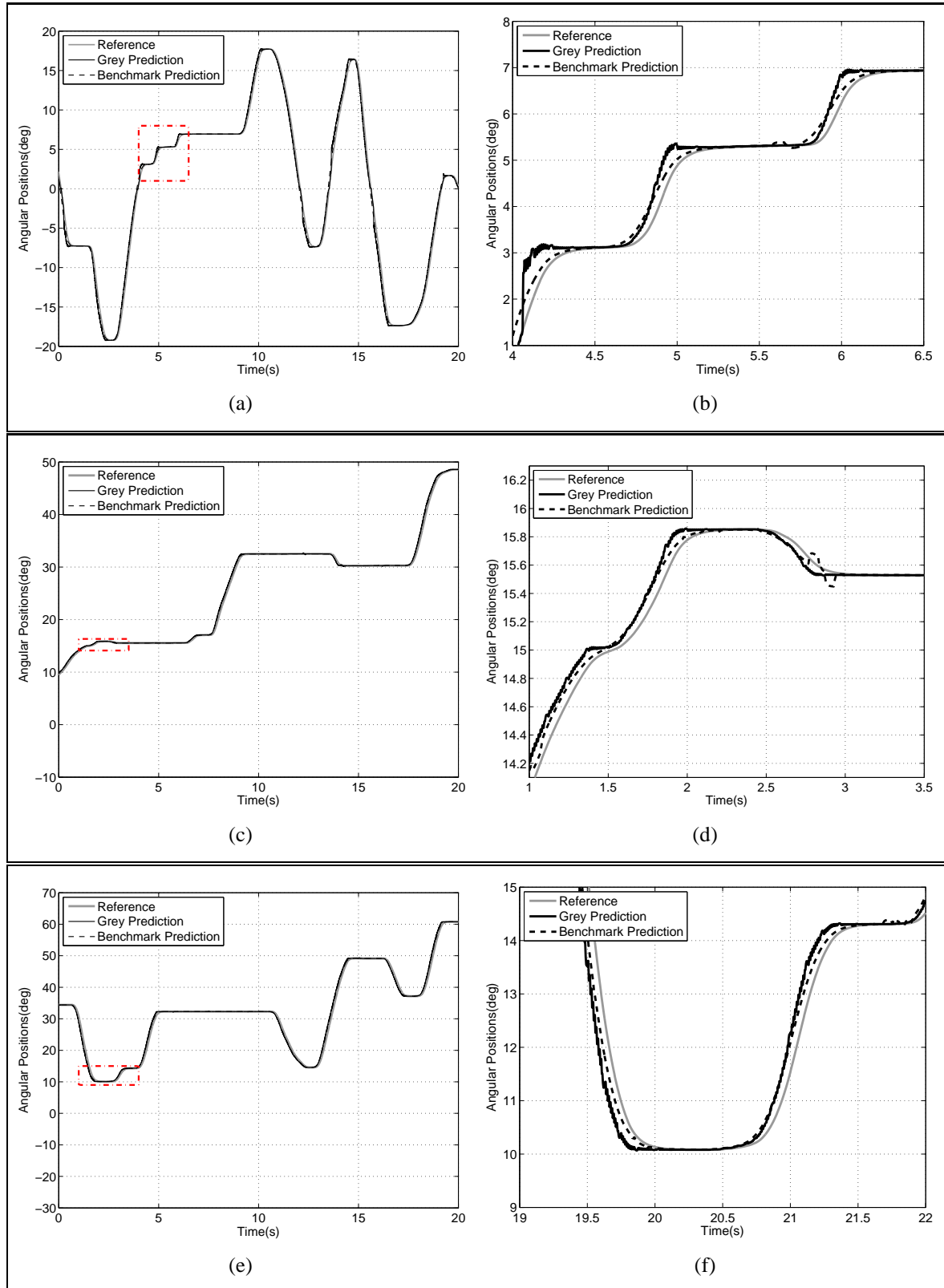


Figure 6.3 : Measured and Predicted Angular Positions of each joint and zoomed versions a) joint 1, b) zoomed area of joint 1, c) joint 2, d) zoomed area of joint 2, e) joint 3, f) zoomed area of joint 3.

benchmark system output. Hence, it can be said that the proposed Grey based *PIDC* demonstrates a faster and more accurate prediction performance than the Taylor based *PIDC*.

6.4 Conclusion

In this study, a Grey system theory based *PIDC* is developed and implemented for the prediction of the master manipulator motion in order to reduce the transmission latency between the master and slave. Our philosophy is to reduce the latency in every way possible within our capability, considering network latency is unavoidable and random.

Experiments are conducted on a PUMA 560 manipulator which is just compensated for gravitational force to allow easy manipulation for the operator. The operator randomly manipulates the arm, while both the benchmark and proposed schemes predict the future trajectory of the robot motion created by the operator. The proposed approach outperforms the Taylor Series based benchmark approach, by predicting the joint motions approximately 100ms ahead on average, while the benchmark's predictor performance varies between 2.8ms-100ms. Based on these results, it can be concluded that Grey Prediction meets our motion prediction requirements better than the Taylor Series based approach, which is currently the only other study in the literature to address input delay compensation.

In the next chapter we will focus on force feedback control, and propose a novel method for that purpose.

7. ADDING FORCE FEEDBACK INTO LOOP

Until this chapter, we have analyzed position control aspects. Here, we enhance the architecture proposed in the position control chapters and make possible to handle force control issues. Our proposed architecture for force is weakly coupled with the previously defined position control loop. Therefore the design can be done separately. In position control loop, the master manipulator has acted as sensor role and slave manipulator has acted as actuator role. Similarly, for force loop the slave manipulator will act as sensor role and master manipulator will act as actuator role. Additionally, in our proposed force control architecture we will use laser range sensor for reacting proactively.

The organization of the chapter is as follows. Section 7.1 overviews the proposed bilateral configuration. Section 7.2, Section 7.3, Section 7.4 introduces the force feedback loop main elements called Reactive Force Observer (RFOB), Environment Parameter Estimator (EPE), and Reactive Force Generator (RFG) respectively. Section 7.5 analyses proposed novel architecture with experimental results. Finally, in 7.6 concluding remarks are presented.

7.1 System Configuration

The general configuration of the master-slave system considered in this study is given in Fig. 7.1. In this master-slave bilateral configuration, the human operator forces the master manipulator and generates a reference trajectory on the master side. This reference trajectory, together with the trajectory data coming from the slave side through Internet is considered by the master controller in the generation of the control signal. The control signal is generated to be sent to the slave side. On the slave side, the control signal coming from the master side through Internet and the actual slave trajectory data is processed by the slave controller and actual control signal is generated. The information sent from the master side to the slave side is a message package containing the tapped control input signal (the reference current value) and a sequence

ID. On slave side, more specifically, on the received side of the slave regulator, this information is processed to get the actual current input signal to be applied as reference to the slave side. As a result of this process, the input current signal is now compensated for data losses and the delay is regulated to a constant value.

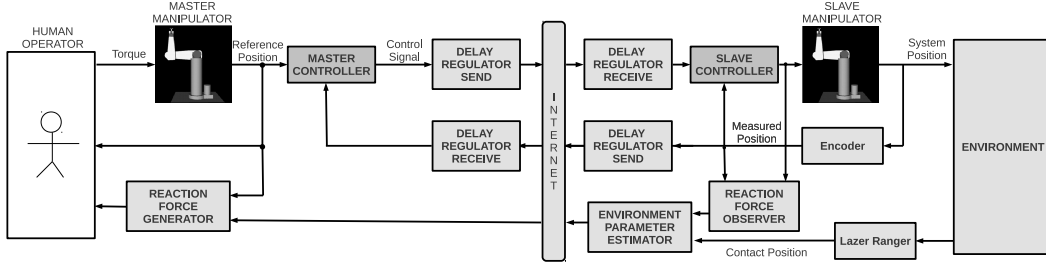


Figure 7.1 : Configuration of the bilateral control system with communication delays both in control and feedback paths.

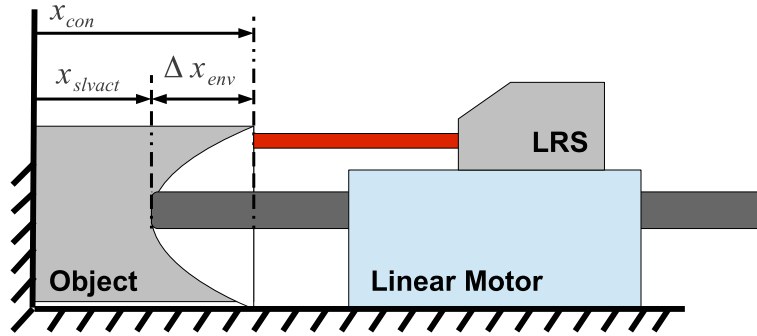


Figure 7.2 : Interaction between object and slave manipulator.

Force control is handled by an open loop. Coupling with master and slave side is supplied by environment parameters; contact point position with respect to origin, damping coefficient, linear and nonlinear stiffness coefficients. In slave side there exist a lazer range meter to measure contact point position with respect to origin directly. Also there exist a reaction force observer block which extracts reaction force information from from motor current and position information. Those contact point position with respect to origin and reaction force data are processed to in environment parameter estimation block and the parameters mentioned before are generated. Those parameters are sent to master side to master side though Internet. It isn't necessary to send them through Delay Regulators because those parameters are not varying frequently. In master side those information and the actual master manipulator position are fused and force feedback information is created, also applied to the operator by using master manipulator.

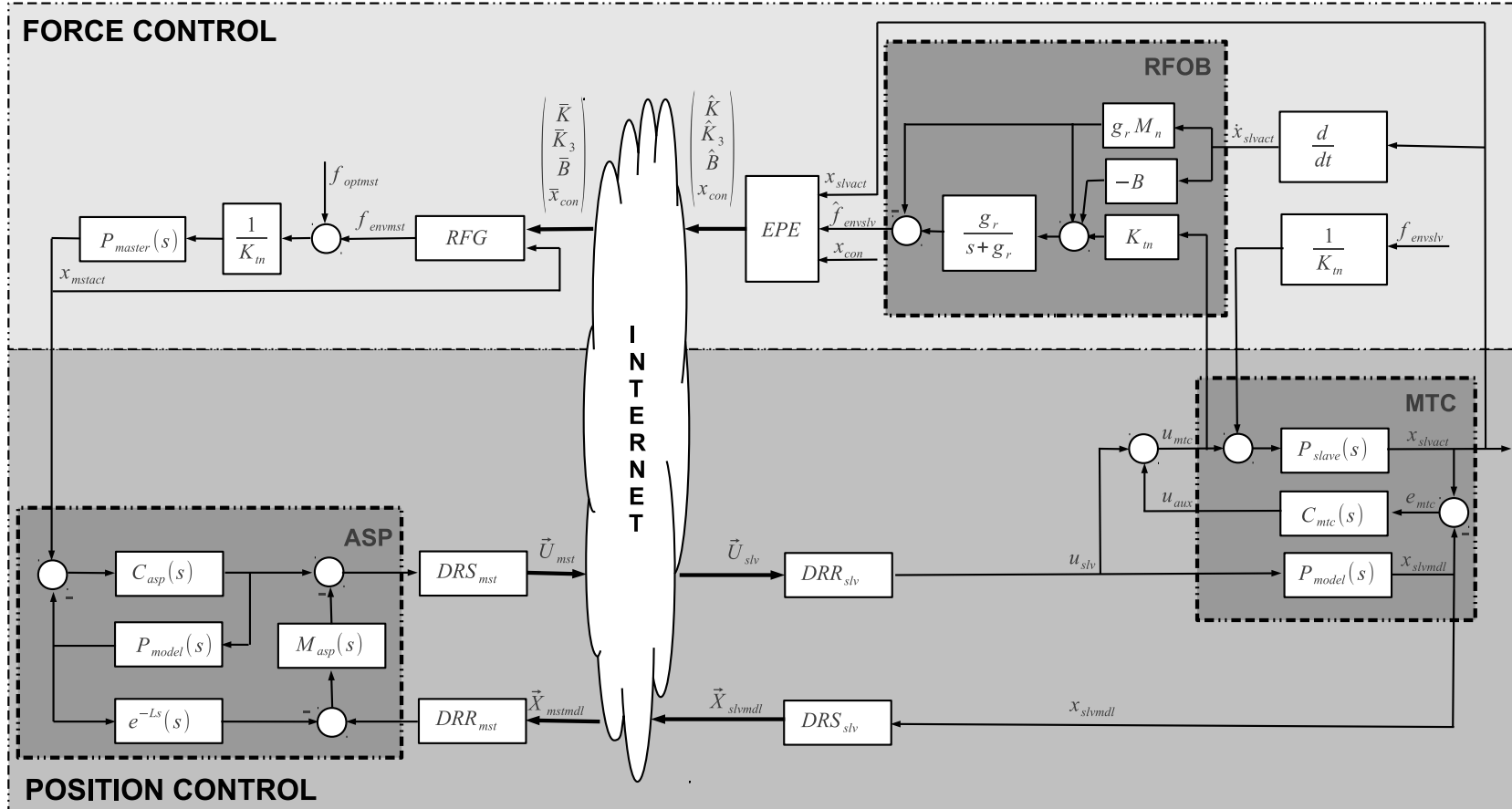


Figure 7.3 : Bilateral Control Architecture Block Diagram.

7.2 Reaction Force Observer (RFOB)

One of the vital block of force control is reactive force observer. It observes reaction forces generated by the environment which interacts with the manipulator. For that aim, one can modify the disturbance observer structure to estimate the external force acting on the system. [63]. Mathematically, the reaction force can be estimated as:

$$\hat{f}_{envslv} = \{f_{slv} - (B(x_{slvact}, \dot{x}_{slvact})\dot{x}_{slvact} + G(x))\} \frac{g_r}{s + g_r} \quad (7.1)$$

$$f_{slv} = K_{tn}u_{mtc} \quad (7.2)$$

Where B denotes viscous friction and G denotes gravity, and g_r denotes corner angular frequency. Assuming that the fluctuations in the nominal inertia and the nominal torque constant are negligibly small (i.e. $\Delta K_n, \Delta M_n \approx 0$),

Similar to the disturbance observer, the estimation accuracy relies on the corner angular frequency g_r . A depiction of RFOB is given in Figure 7.4.

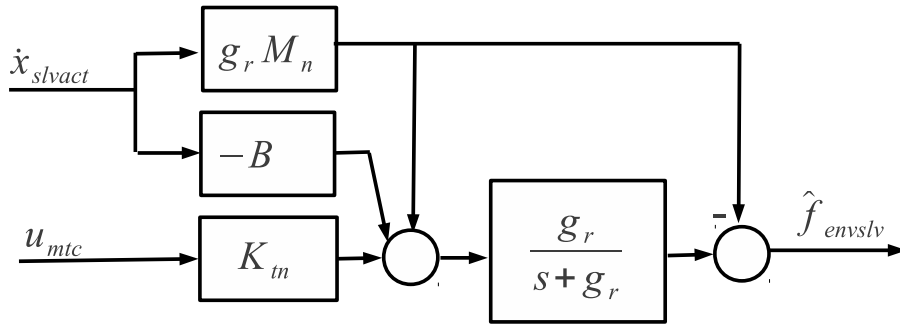


Figure 7.4 : Structure of the Reaction Force Observer.

Keeping the low pass filter gain g_r high, the force estimation can be made accurately and fast since the observer uses only the input current and velocity measurement of the system. The bandwidth limitations of RFOB related to the selection of filter gain is analyzed in detail in [63].

7.3 Environment Parameter Estimator (EPE)

In this section, the details related to the least squares based environment parameter estimation method will be discussed. The estimator makes use of the estimated reaction force \hat{f}_{envslv} in RFOB, the contact position x_{con} of remote environment measured with the laser range sensor and the position x_{slv} of the slave manipulator. The aim of the estimator is, estimating linear stiffness coefficient, K , nonlinear stiffness coefficient, K_3 , and damping coefficient B of the object in contact. To implement the algorithm we should first calculate the deflection of the object at the slave contact point position with respect to origin.

$$\Delta x_{env} = x_{con} - x_{slvact} \quad (7.3)$$

$$\Delta \dot{x}_{env} = -\dot{x}_{slvact} \quad (7.4)$$

Here Δx_{env} denotes the deflection of the object after contact. For each sample of the real time control loop, one can write general nonlinear-spring damper equation as follows;

$$f_{envslv1} = K\Delta x_{env1} + K_3\Delta x_{env1}^3 + B\Delta \dot{x}_{env1} \quad (7.5)$$

$$f_{envslv2} = K\Delta x_{env2} + K_3\Delta x_{env2}^3 + B\Delta \dot{x}_{env2} \quad (7.6)$$

...

$$f_{envslvN} = K\Delta x_{envN} + K_3\Delta x_{envN}^3 + B\Delta \dot{x}_{envN} \quad (7.7)$$

The matrix ΔX_{env} which contains measurable values in the equation () to () can be defined as;

$$\Delta X_{env} = \begin{bmatrix} \Delta x_{env1} & \Delta x_{env1}^3 & \Delta \dot{x}_{env1} \\ \Delta x_{env2} & \Delta x_{env2}^3 & \Delta \dot{x}_{env2} \\ \dots & \dots & \dots \\ \Delta x_{envN} & \Delta x_{envN}^3 & \Delta \dot{x}_{envN} \end{bmatrix} \quad (7.8)$$

With this definition, the equation given in () to () can be represented in the following simpler form;

$$\begin{bmatrix} f_{envslv1} \\ f_{envslv2} \\ \dots \\ f_{envslvN} \end{bmatrix} = \Delta X_{env} \cdot \begin{bmatrix} K \\ K_3 \\ B \end{bmatrix} \quad (7.9)$$

Following a least squares based methodology, the environment parameters can be estimated using the pseudo inverse of matrix ΔX_{env} ;

$$\begin{bmatrix} \hat{K} \\ \hat{K}_3 \\ \hat{B} \end{bmatrix} = pinv(\Delta X_{env}) \cdot \begin{bmatrix} f_{envslv1} \\ f_{envslv2} \\ \dots \\ f_{envslvN} \end{bmatrix} \quad (7.10)$$

Here \hat{K} , \hat{K}_3 and \hat{B} denote estimated values of linear spring coefficient, nonlinear spring coefficient and damping coefficient, respectively.

7.4 Reaction Force Generator (RFG)

Reaction force generation process can be imagined as the inverse process of the EPE. This process is triggered when the master manipulator's position exceeds the contact point position with respect to origin and outputs zero force to the operator when there is no contact. However, when the master manipulator's position exceeds contact point position with respect to origin then the reaction is applied to the operator by using general nonlinear spring-damper equation. The process of reaction force generation can be mathematically represented with the following equation;

$$f_{envmst} = \begin{cases} \bar{K} [\bar{x}_{con} - x_{mstact}] + \bar{K}_3 [\bar{x}_{con} - x_{mstact}]^3 + \bar{B} \dot{x}_{mstact} & \text{if } x_{mstact} < \bar{x}_{con} \\ 0 & \text{if } x_{mstact} \geq \bar{x}_{con} \end{cases} \quad (7.11)$$

Here $\bar{*}$ operator denotes the data $*$ received to master side from the slave through Internet with a time delay. Here, again \bar{K} , \bar{K}_3 and \bar{B} respectively stand for the linear spring coefficient, nonlinear spring coefficient and damping coefficient of the object with which the slave manipulator interacts. With this process the transparency condition of the bilateral control system can be satisfied.

7.5 Experimental Results

In this section experimental results will be provided for validation of proposed bilateral control scheme. For this purpose, an experimental setup, including two direct drive motors and a laser range sensor is used. The motors are linear brushless DC type from Faulhaber LM series with integrated hall effect sensors. The position readout are enabled via the use of Renishaw incremental encoders of resolution $1\mu m$. In

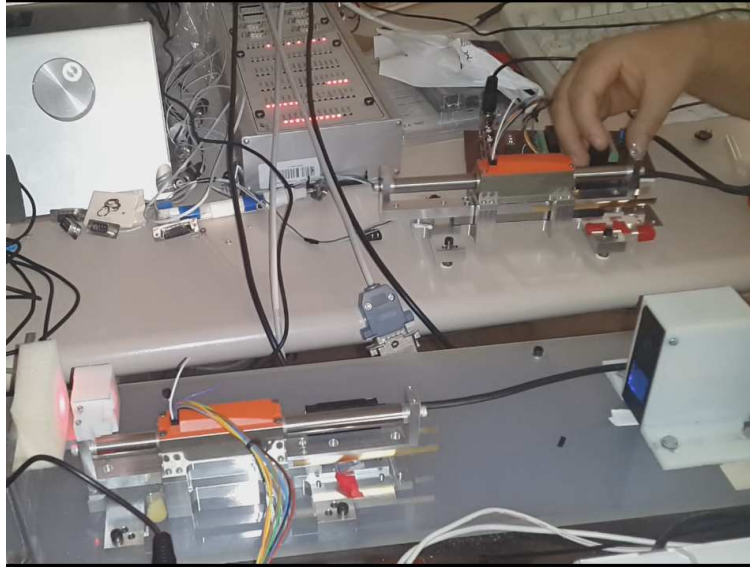


Figure 7.5 : Experimental Setup for Bilateral Control.

the experiments artificially generated time delays that have constant and varying components in both measurement and control channels are used between master and slave sides.

In the experiments, master manipulator is operated by a human operator arbitrarily. In slave side there exist an object, which is fixed from one side and on which slave manipulator can contact from the other side. Three experiments are made for testing the performances of non-contact, soft-contact and hard-contact cases. The results obtained from these experiments are given below from Fig. 7.6 to Fig. 7.8. In these figures, black lines represents master side position or force data, red lines represents slave side position or force data.

Results of the first experiment are given in Fig. 7.6. Here there is just free movement, no contact. As seen in the force results in Fig. 7.6a there is no noise in reaction force applied to the operator at slave side. Moreover in the position results seen in Fig. 7.6b, it is easily seen that position tracking is very accurate. In the second experiment, a sponge is used as an object and the results are illustrated in Fig. 7.7. As can also be observed in the results shown in Fig. 7.7a force tracking is acceptable while position tracking is again very accurate as shown in Fig. 7.7b. In the last experiment, there is hard contact with a hard plastic object and results are given in Fig. 7.8. As shown in the force results in Fig. 7.8a, force tracking performance is considerably reduced, but there is no instability. Reason of this performance deterioration is that; in hard contact

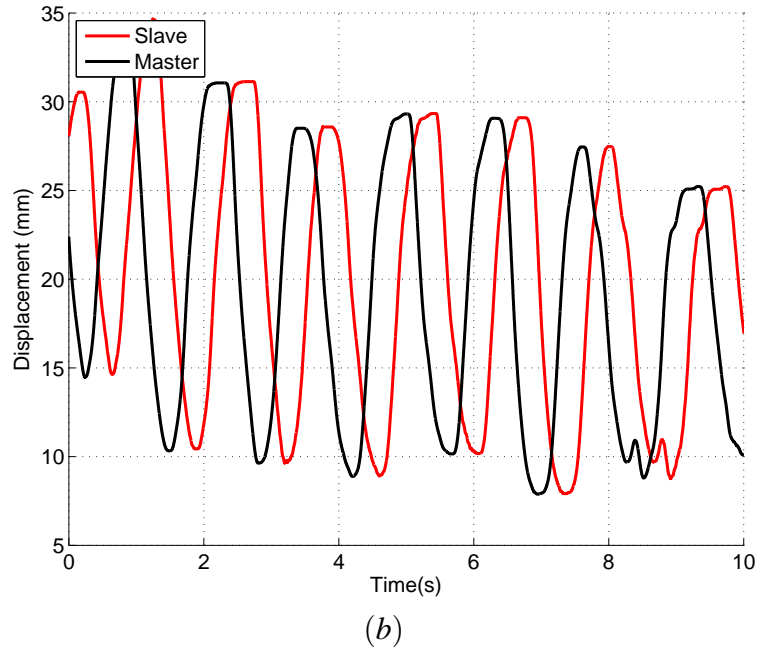
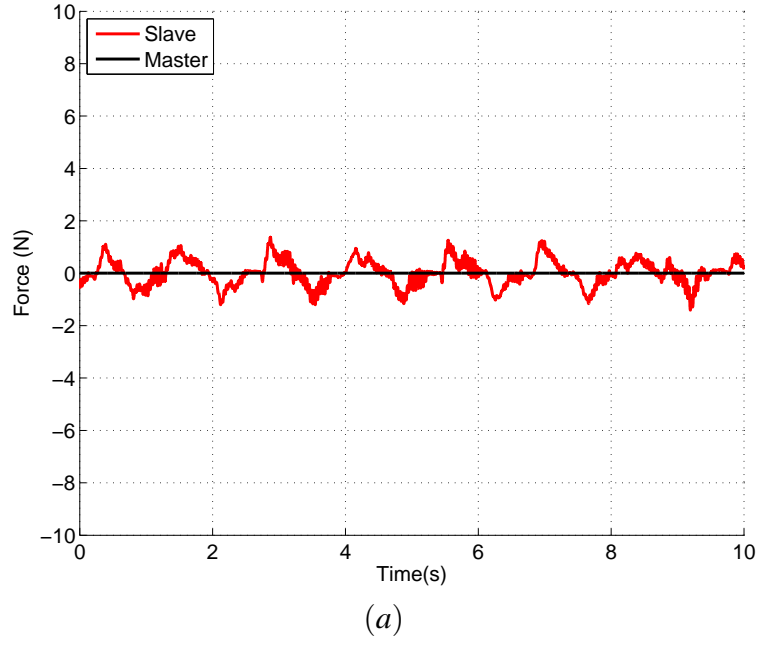
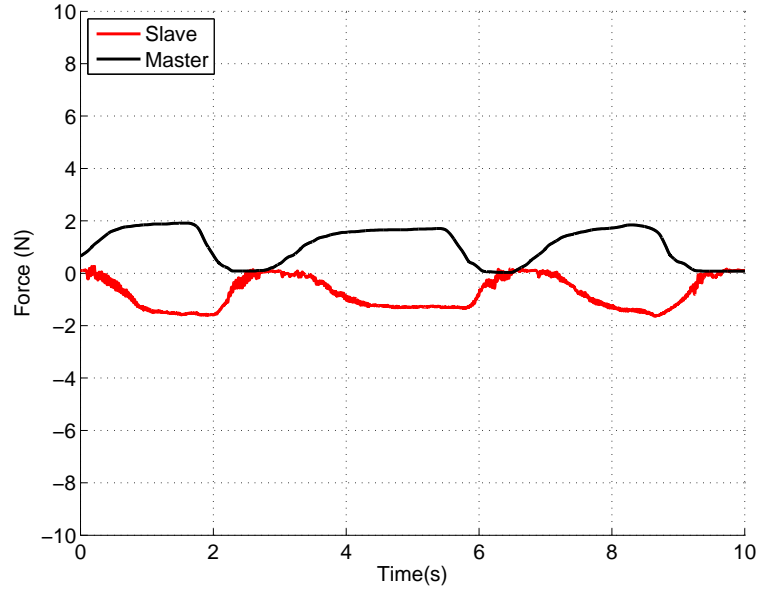


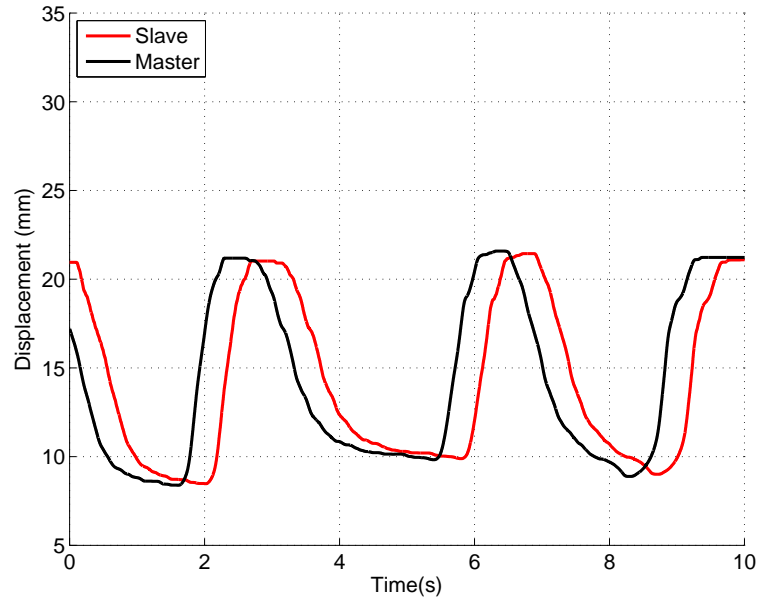
Figure 7.6 : No-contact Force Feedback Results; a) Forces, b) Displacements.

case, while the deflections are so small, the effect of the deflection measurement error can rise even though position tracking is not affected from this hard contact situation as shown in Fig. 7.8b.

It is important to point out that, in the applications like medical operations, interaction between the manipulator and object can be classified as the aspect of overall controller with secondary importance. Hard contact occurs when the manipulator interact with bones, in those cases, it is important to transmit the sense of hard contact to the operator



a)



b)

Figure 7.7 : Soft-contact Force Feedback Results; a) Forces, b) Displacements.

even though the actual value of the reaction force cannot be fully reflected. Keeping in mind that position tracking objective has priority over the force tracking in high precision surgery applications, a system with superior performance in position control loop with relatively lower performance in the force control loop is more preferable than a system with better conditioning of force control in exchange of deteriorated position control performance.

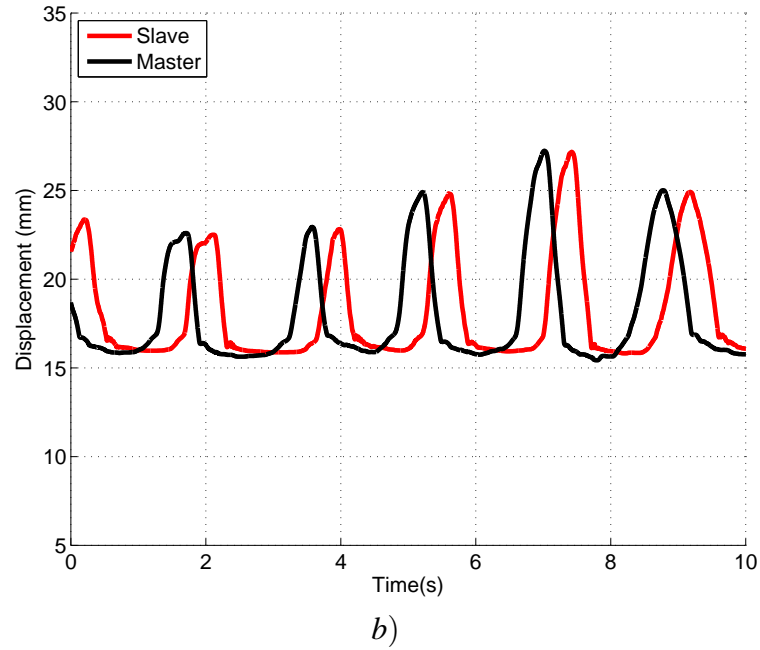
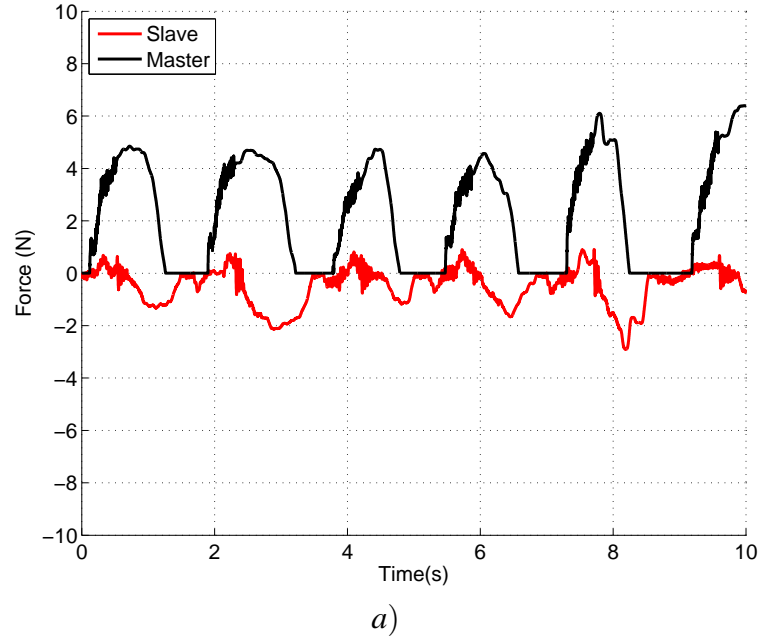


Figure 7.8 : Hard-contact Force Feedback Results; a) Forces, b) Displacements.

7.6 Conclusions

This study builds on model based networked control approach. Here, we enhance that architecture from position control to bilateral teleoperation, again by a model based perspective. The reaction force, which is applied to the operator is generated on the master side by using a nonlinear spring-damper environment model. This environment model uses contact point position, damping coefficient, linear and nonlinear spring coefficients as the parameters to reconstruct the slave system interaction force. Those

parameters, except contact point, are estimated on slave side by least square estimation technique. Only the contact point is measured by laser range sensor.

Experiments are conducted on two direct drive linear manipulator system under time-varying network delay of between 100 and 350 *ms* that impacts both measurement and control loop. Proposed system behaves very accurate in position tracking and shows acceptable force tracking performance. This property is very important, since the contact location is more important than the exact value of applied force, especially in medical operations.

The other advantage of the proposed system is its economic bandwidth usage while feeding back the force from slave to master side. While in a variety of bilateral control systems, bandwidth is the key factor determining the performance of force tracking, here the performance of the force tracking is independent from bandwidth. This is because, the force feedback is supplied by parameters that has relatively steady values. Moreover, the reaction force applied to the operator is generated by using master position. Therefore the reaction force can be generated before the actual slave system contact occurs since the system estimates the environment parameters prior to contact after the first interaction with the slave environment.

Accurate position tracking performance, low bandwidth usage and pro-activity properties are superiority of the proposed architecture against the other works in the literature.

8. CONCLUSIONS AND FUTURE WORKS

8.1 Conclusions

This thesis focuses on solving four major performance problems of networked control systems. These problems are availability, robustness, bandwidth efficiency and synchronization problems. First of all, an expandable core solution is proposed. This solution satisfies the basic performance requirements of networked control. The proposed core system builds on the disturbance observer based approach in bilateral control and contributes to significant improvements in both control and communication issues faced with position control aspects of bilateral control systems. To this aim, two novel master-slave configurations are proposed: one based on a sliding-mode observer and model-tracking controller (MTC), and the other based on Astrom's Smith Predictor on the master side. Both configurations benefit from a delay regulator, which regulates the random network delay into a constant delay. Both configurations also use a MTC designed for the slave side disturbance rejection and trajectory tracking. Experiments are conducted on a single-link arm system under variable gravitational effects and a randomly varied network delay of 100-400 ms that impacts both the feedback and control loop. While the Astrom's Smith Predictor (ASP) is a more capable version of the standard SP against disturbances stemming from network and slave uncertainties, the much reduced system uncertainties via the proposed combination of the delay regulator and MTC contribute significantly to the overall performance. The delay regulator and MTC have also benefited the SMO based configuration significantly, which has been shown to demonstrate a poor tracking performance under variable network and slave disturbances in the authors' previous studies, while achieving perfect tracking under no load and constant network delay. Hence, both configurations demonstrate a significantly improved tracking performance against model-mismatch and randomly varying network delay (within 100-400ms) and can handle feedback loop deteriorations arising from the limited buffer size of the delay

regulator. Also, this structure can reconstruct the states of the control system even after an internet outage. Therefore, the proposed core solution is a novel solution which solves availability problems in networking control. The weakness of the proposed core system is that it can get unstable when the delay exceeds the maximum delay constraint in the control signal path. This is a problem not well-addressed in the literature. To handle that problem, we offer a novel control signal correction scheme (CSCS) to support delay regulator, which can also be used alone. The effects of the proposed scheme are analyzed under all possible extreme scenarios in terms of network and disturbance issues. It is shown that CSCS is effective against all such extremities. Delay regulator (DR) gives perfect results even if the delay variance is under assumption. When over-buffer occurs DR is useless. Using only CSCS is also useful for steady state case, however it gives small error in transient state. Using CSCS and DR in the same path is the best ever solution. Because when delay is under the assumed limits, the delay regulator works fine and the proposed scheme has no contribution to the performance, outside of generating two sample delays. However when the buffer size is exceeded, the proposed scheme corrects the process trajectory and maintains the stability with very low error in the transient state. This is the second problem we have addressed in this thesis, and classified it as robustness problem. The CSCS method is also a novel contribution of this thesis. For bandwidth optimization problem, the thesis proposes a compression-decompression system using Wavelet Packet Tree as a novel approach for bilateral control systems. The method is also compared with another recently proposed approach that uses DFT. Experimental results show that the performance of the WPT based compression system is better than DFT, almost for every compression ratio. Networked controlled systems can benefit from compression approaches due to the fact that compression allows for sampling rates that are higher than the network throughput by a multiple of the compression ratio. Moreover, this is achieved with very little loss in the control input power. The authors have already emphasized the benefits of this proposed novel compression approach comparatively with respect the DCT and DFT based compression approaches in the literature [45], [46], [47]. DWT based compression in network controlled systems is also the contribution of this thesis. For the synchronization problem, a Grey system theory based PIDC is developed and implemented for the prediction of the master manipulator motion in order to reduce the transmission latency between the

master and slave. Our philosophy is to reduce the latency in every way possible within our capability, considering network latency is unavoidable and random. Also, it is shown that Grey Prediction meets our motion prediction requirements better than the Taylor Series based approach, which is currently the only other study in the literature to address input delay compensation. Other than those solutions for performance problems in availability, robustness, bandwidth efficiency and synchronization, the thesis has also contributed to the force feedback problem of the networked control systems. To this aim, we proposed a novel method which measures the contact point position with respect to origin before contact occurs. As a result, the reaction force on the slave side is applied at the correct position. Also, for force feedback, the whole force data is not transmitted from slave side to master side, but only the contact point position with respect to origin and environment parameters. Therefore the bandwidth requirement of our system to supply force feedback is lower than other methods in the literature. With those properties, our force feedback approach is also novel. Although we propose several solutions to several problems of the networked control, it is not necessary to use all in every networked control system. The last contribution of the proposed architecture is its modularity. This modular approach allows for the implemented topology to be optimized for the requirements of the each networked system application in consideration. However, there is no exact best solution which solves all the problems. Each addon has drawbacks such as added computational cost, added delay, and information lost. Here, It can be said that, we propose a set of tools which can be glued to a core solution, so the designer can optimize it for his/her needs. We show that the proposed new methods have significant advantages and experimental results are very promising for future studies.

8.2 Future Works

In the future works, we wish to work on developing some techniques for contactless estimation of environment parameters. For this purpose, we will develop an electro-pneumatic and acousto-optic measurement devices for environment estimation.

REFERENCES

- [1] **Munir, S. and Book, W.** (2002). Internet-based teleoperation using wave variables with prediction, *Mechatronics, IEEE/ASME Transactions on*, **7**(2), 124–133.
- [2] **Jin, H., Hu, Y., Tian, W., Zhang, P., Zhang, J. and Li, B.** (2014). Safety analysis and control of a robotic spinal surgical system, *Mechatronics*, **24**(1), 55–65.
- [3] **Tennekoon, R., Wijekoon, J., Harahap, E., Nishi, H., Saito, E. and Katsura, S.** (2014). Per hop data encryption protocol for transmission of motion control data over public networks, *Advanced Motion Control (AMC), 2014 IEEE 13th International Workshop on*, pp.128–133.
- [4] **Vollmer, T. and Manic, M.** (2014). Cyber-Physical System Security With Deceptive Virtual Hosts for Industrial Control Networks, *Industrial Informatics, IEEE Transactions on*, **10**(2), 1337–1347.
- [5] **Mersha, A., Stramigioli, S. and Carloni, R.** (2014). On Bilateral Teleoperation of Aerial Robots, *Robotics, IEEE Transactions on*, **30**(1), 258–274.
- [6] **Nakajima, Y., Nozaki, T. and Ohnishi, K.** (2014). Heartbeat Synchronization With Haptic Feedback for Telesurgical Robot, *Industrial Electronics, IEEE Transactions on*, **61**(7), 3753–3764.
- [7] **Pajic, M., Mangharam, R., Sokolsky, O., Arney, D., Goldman, J. and Lee, I.** (2014). Model-Driven Safety Analysis of Closed-Loop Medical Systems, *Industrial Informatics, IEEE Transactions on*, **10**(1), 3–16.
- [8] **Mori, T.** (2012). Modified bilateral control by using intervention impedance based on passivity of flexible master-slave manipulators and its design methods, *Control, Automation and Systems (ICCAS), 2012 12th International Conference on*, pp.748–753.
- [9] **Munir, S. and Book, W.** (2001). Wave-based teleoperation with prediction, *American Control Conference, 2001. Proceedings of the 2001*, volume 6, pp.4605–4611 vol.6.
- [10] **Gadamsetty, B., Bogosyan, S., Gokasan, M. and Sabanovic, A.** (2009). Novel observers for compensation of communication delay in bilateral control systems, *Industrial Electronics, 2009. IECON '09. 35th Annual Conference of IEEE*, pp.3019–3026.
- [11] **Gadamsetty, B., Bogosyan, S., Gokasan, M. and Sabanovic, A.** (2010). Sliding mode and EKF observers for communication delay compensation

- in bilateral control systems, *Industrial Electronics (ISIE), 2010 IEEE International Symposium on*, pp.328–333.
- [12] **Shen, W., Gu, J. and Feng, Z.** (2007). A Stable tele-robotic neurosurgical system based on SMC, *Robotics and Biomimetics, 2007. ROBIO 2007. IEEE International Conference on*, pp.150–155.
- [13] **Hung, L.C., Wang, C.Y. and Chung, H.Y.** (2005). Sliding mode control for uncertain time-delay systems with sector nonlinearities via fuzzy rule, *Systems, Man and Cybernetics, 2005 IEEE International Conference on*, volume 1, pp.251–256 Vol. 1.
- [14] **Yu, X., Han, Q., Li, X. and Wang, C.** (2008). Time-delay effect on equivalent control based single-input sliding mode control systems, *Variable Structure Systems, 2008. VSS '08. International Workshop on*, pp.13–17.
- [15] **Garcia-Valdovinos, L., Parra-Vega, V. and Arteaga, M.** (2006). Observer-based Higher-Order Sliding Mode Impedance Control of Bilateral Teleoperation under Constant Unknown Time Delay, *Intelligent Robots and Systems, 2006 IEEE/RSJ International Conference on*, pp.1692–1699.
- [16] **Sabanovic, A., Elitas, M. and Ohnishi, K.** (2008). Sliding Modes in Constrained Systems Control, *Industrial Electronics, IEEE Transactions on*, **55**(9), 3332–3339.
- [17] **Smith, O.J.** (1959). A controller to overcome dead time, *ISA Journal*, **6**(2), 28–33.
- [18] **Astrom, K., Hang, C.C. and Lim, B.C.** (1994). A new Smith predictor for controlling a process with an integrator and long dead-time, *Automatic Control, IEEE Transactions on*, **39**(2), 343–345.
- [19] **Natori, K., Oboe, R. and Ohnishi, K.** (2008). Stability Analysis and Practical Design Procedure of Time Delayed Control Systems With Communication Disturbance Observer, *Industrial Informatics, IEEE Transactions on*, **4**(3), 185–197.
- [20] **Natori, K. and Ohnishi, K.** (2008). A Design Method of Communication Disturbance Observer for Time-Delay Compensation, Taking the Dynamic Property of Network Disturbance Into Account, *Industrial Electronics, IEEE Transactions on*, **55**(5), 2152–2168.
- [21] **Isermann, R.** (2007). *Mechatronic systems: fundamentals*, Springer Science & Business Media.
- [22] **Natori, K., Tsuji, T., Ohnishi, K., Hace, A. and Jezernik, K.** (2004). Robust bilateral control with internet communication, *Industrial Electronics Society, 2004. IECON 2004. 30th Annual Conference of IEEE*, volume 3, IEEE, pp.2321–2326.
- [23] **Suzuki, A. and Ohnishi, K.** (2013). Novel four-channel bilateral control design for haptic communication under time delay based on modal space analysis, *Control Systems Technology, IEEE Transactions on*, **21**(3), 882–890.

- [24] **Natori, K., Tsuji, T., Ohnishi, K., Hace, A. and Jezernik, K.** (2010). Time-delay compensation by communication disturbance observer for bilateral teleoperation under time-varying delay, *Industrial Electronics, IEEE Transactions on*, **57**(3), 1050–1062.
- [25] **Matsuo, K., Miura, T. and Taniguchi, T.** (2007). A speed control method of small DC motor through IP network considering packet loss, *IEEJ Transactions on Electrical and Electronic Engineering*, **2**(6), 657–659.
- [26] **Kuzu, A., Bogosyan, S. and Gokasan, M.** (2012). Network in the loop platform for research and training in bilateral control, *Advanced Motion Control (AMC), 2012 12th IEEE International Workshop on*, pp.1–6.
- [27] **Watanabe, K. and Ito, M.** (1981). A process-model control for linear systems with delay, *Automatic Control, IEEE Transactions on*, **26**(6), 1261–1269.
- [28] **Chen, Y.D., Tung, P.C. and Fuh, C.C.** (2007). Modified Smith predictor scheme for periodic disturbance reduction in linear delay systems, *Journal of process control*, **17**(10), 799–804.
- [29] **Zhang, W.D. and Sun, Y.X.** (1996). Modified Smith predictor for controlling integrator/time delay processes, *Industrial & engineering chemistry research*, **35**(8), 2769–2772.
- [30] **Wang, Y.G., Shao, H.H. and Wang, J.** (2000). PI tuning for processes with large dead time, *American Control Conference, 2000. Proceedings of the 2000*, volume 6, pp.4274–4278 vol.6.
- [31] **Ziegler, J. and Nichols, N.** (1942). Optimum settings for automatic controllers, *trans. ASME*, **64**(11).
- [32] **Åström, K., Hägglund, T., Hang, C.C. and Ho, W.** (1993). Automatic tuning and adaptation for PID controllers-a survey, *Control Engineering Practice*, **1**(4), 699–714.
- [33] **Leonardi, F. and Da Cruz, J.** (2002). Robust model tracking and 2-D control design, *Proc. of the 10th Mediterranean Conference on Control and Automation*.
- [34] **Kuzu, A., Bogosyan, S., Gokasan, M. and Sabonovic, A.** (2011). Control and measurement delay compensation in bilateral position control, *Mechatronics (ICM), 2011 IEEE International Conference on*, pp.1003–1010.
- [35] **Juanping, Z. and Xianwen, G.** (2009). Time-delay analysis and estimation of internet-based robot teleoperation system, *Control and Decision Conference, 2009. CCDC'09. Chinese*, IEEE, pp.4643–4646.
- [36] **Kuzu, A., Bogosyan, S., Gokasan, M. and Sabanovic, A.** (2014). Experimental Evaluation of Novel Master-Slave Configurations for Position Control under Random Network Delay and Variable Load for Teleoperation, *Mathematical Problems in Engineering*.

- [37] **Natori, K., Oboe, R. and Ohnishi, K.** (2008). Stability analysis and practical design procedure of time delayed control systems with communication disturbance observer, *Industrial Informatics, IEEE Transactions on*, **4**(3), 185–197.
- [38] **Gadamsetty, B., Bogosyan, S., Gokasan, M. and Sabanovic, A.** (2010). Sliding mode and EKF observers for communication delay compensation in bilateral control systems, *Industrial Electronics (ISIE), 2010 IEEE International Symposium on*, pp.328–333.
- [39] **Kuzu, A., Bogosyan, S., Gokasan, M. and Sabonovic, A.** (2011). Control and measurement delay compensation in bilateral position control, *Mechatronics (ICM), 2011 IEEE International Conference on*, pp.1003–1010.
- [40] **Mizuochi, M. and Ohnishi, K.** (2012). Coding and decoding scheme for wide-band bilateral teleoperation, *Advanced Motion Control (AMC), 2012 12th IEEE International Workshop on*, IEEE, pp.1–6.
- [41] **Yashiro, D. and Ohnishi, K.** (2011). Performance analysis of bilateral control system with communication bandwidth constraint, *Industrial Electronics, IEEE Transactions on*, **58**(2), 436–443.
- [42] **Kuschel, M., Kremer, P. and Buss, M.** (2009). Passive haptic data-compression methods with perceptual coding for bilateral presence systems, *Systems, Man and Cybernetics, Part A: Systems and Humans, IEEE Transactions on*, **39**(6), 1142–1151.
- [43] **Lee, J.y. and Payandeh, S.** (2011). Performance evaluation of haptic data compression methods in teleoperation systems, *World Haptics Conference (WHC), 2011 IEEE*, IEEE, pp.137–142.
- [44] **Yokokura, Y., Katsura, S. and Ohishi, K.** (2009). Bilateral control using compressor/decompressor under the low-rate communication network, *Mechatronics, 2009. ICM 2009. IEEE International Conference on*, IEEE, pp.1–6.
- [45] **Tanaka, H. and Ohnishi, K.** (2009). Haptic data compression/decompression using DCT for motion copy system, *Mechatronics, 2009. ICM 2009. IEEE International Conference on*, IEEE, pp.1–6.
- [46] **Tanaka, H., Ohnishi, K. and Nishi, H.** (2010). Implementation of lossy haptic data compression using integer DCT to FPGA, *IECON 2010-36th Annual Conference on IEEE Industrial Electronics Society*, IEEE, pp.1726–1731.
- [47] **Yokokura, Y., Katsura, S. and Ohishi, K.** (2009). Bilateral control using compressor/decompressor under the low-rate communication network, *Mechatronics, 2009. ICM 2009. IEEE International Conference on*, IEEE, pp.1–6.
- [48] **Kuzu, A., Baran, E.A., Bogosyan, S., Gokasan, M. and Sabanovic, A.** (2013). WPT based compression for bilateral control, *Industrial Electronics Society, IECON 2013-39th Annual Conference of the IEEE*, IEEE, pp.5686–5691.

- [49] **Kuzu, A., Baran, E.A., Bogosyan, S., Gokasan, M. and Sabanovic, A.** (2013). Performance comparison of compression techniques used in bilateral control, *Industrial Electronics Society, IECON 2013-39th Annual Conference of the IEEE*, IEEE, pp.5674–5679.
- [50] **Yu, J. and Karlsson, S.** (2001). Local spectral analysis using wavelet packets, *Circuits, Systems and Signal Processing*, **20**(5), 497–528.
- [51] **Li, Y., Wei, H.I. and Billings, S.A.** (2011). Identification of time-varying systems using multi-wavelet basis functions, *Control Systems Technology, IEEE Transactions on*, **19**(3), 656–663.
- [52] **Wei, D., Bovik, A.C. and Evans, B.L.** (1997). Generalized coiflets: a new family of orthonormal wavelets, *Signals, Systems & Computers, 1997. Conference Record of the Thirty-First Asilomar Conference on*, volume 2, IEEE, pp.1259–1263.
- [53] **Mallat, S.G.** (1989). A theory for multiresolution signal decomposition: the wavelet representation, *Pattern Analysis and Machine Intelligence, IEEE Transactions on*, **11**(7), 674–693.
- [54] **Lee, B.** (1999). Application of the discrete wavelet transform to the monitoring of tool failure in end milling using the spindle motor current, *The International Journal of Advanced Manufacturing Technology*, **15**(4), 238–243.
- [55] **Beylkin, G., Coifman, R. and Rokhlin, V.** (1991). Fast wavelet transforms and numerical algorithms I, *Communications on pure and applied mathematics*, **44**(2), 141–183.
- [56] **Shen, J. and Strang, G.** (1998). Asymptotics of daubechies filters, scaling functions, and wavelets, *Applied and Computational Harmonic Analysis*, **5**(3), 312–331.
- [57] **Daubechies, I.** (1988). Orthonormal bases of compactly supported wavelets, *Communications on pure and applied mathematics*, **41**(7), 909–996.
- [58] **Cohen, A., Daubechies, I. and Feauveau, J.C.** (1992). Biorthogonal bases of compactly supported wavelets, *Communications on pure and applied mathematics*, **45**(5), 485–560.
- [59] **Karam, J.** (2012). On the Zeros of Daubechies Orthogonal and Biorthogonal Wavelets., *Applied Mathematics*, **3**(7).
- [60] **Baran, E. and Sabanovic, A.** (2012). Predictive input delay compensation for motion control systems, *Advanced Motion Control (AMC), 2012 12th IEEE International Workshop on*, pp.1–6.
- [61] **Ju-Long, D.** (1982). Control problems of grey systems, *Systems & Control Letters*, **1**(5), 288–294.
- [62] **Liu, S. and Lin, Y.** (2006). *Grey information: theory and practical applications*, Springer.

- [63] **Ohnishi, K., Shibata, M. and Murakami, T.** (1996). Motion control for advanced mechatronics, *Mechatronics, IEEE/ASME Transactions on*, **1**(1), 56–67.

CURRICULUM VITAE



Name Surname: Ahmet Kuzu

Place and Date of Birth: ÇORLU/TEKİRDAĞ - 7 December 1978

Address: TÜBİTAK BİLGEM BTE 41470 Gebze Kocaeli

E-Mail: ahmet.kuzu@tubitak.gov.tr

B.Sc.: ITU - Electronics and Telecommunication Engineering

M.Sc.: ITU - Mechatronics Engineering

Professional Experience and Rewards:

2012-	TUBITAK-BILGEM-BTE	Chief Researcher	Kocaeli
2007-2012	TUBITAK-BILGEM-BTE	Senior Researcher	Kocaeli
2004-2007	TUBITAK-MAM-BTE	Researcher	Kocaeli
2003-2004	SGM Elektronik	Technical Director/Founder	Istanbul
2002-2003	ENTES Elektronik	System Designer	Istanbul

List of Publications and Patents:

Journal Papers

- **Kuzu A.**, Bogosyan, S., Gokasan, M., 2011: High-order Sliding Mode Approach for the Control of MEM Optical Switches, *International Review of Automatic Control (IREACO)*, vol.4, no.3, pp.431-438
- **Kuzu A.**, Bogosyan, S., Gokasan, M., 2008: Novel Approach for Detection and Tracking of Explosive Carrying Mobile Humans with Odor-Sensor Based Multisensor Networks, *WSEAS Tran. on Systems and Control*, vol.3, pp.63-70
- **Kuzu A.**, Bogosyan, S., Gokasan, M., 2007: Survey: Detection, recognition and source localization of odor, *WSEAS Tran. on Systems*, vol.7, pp.611-621
- **Kuzu A.**, Bogosyan, S., Gokasan, M., 2007: Comparison of Multisensor Fusion Techniques for Improvement of multiple MEM Accelerometers on Single Die System, *WSEAS Tran. on Systems*, vol.6, pp.431-437
- **Kuzu A.**, Bogosyan, S., Gokasan, M., 2007: Novel Approach for Detection and Tracking of Explosive Carrying Mobile Humans with Odor-Sensor Based Multisensor Networks, *WSEAS Tran. on Systems*, vol.6, pp.449-454

Conference Papers

- **Kuzu A.**, Songuler, O., Ucan, F., 2014: Fuzzy Interval Type II Lateral Control of an Autonomous UAV, *IEEE ICUMT2012*

- **Kuzu A.**, Kuzu, A.T., Rahimzadeh, K., Bogosyan, S., Gokasan, M., Bakkal, M., 2014: Autonomous hole quality determination using image processing techniques, *IEEE ISIE2014*
- **Kuzu A.**, Danis, U., Kurt, E., Karabulut, E., Sahinkaya, D., Bilgic, E., Kaplaner, A., 2012: Laboratory and sea testing of difar sonobuoys, *IEEE ICUMT2012*
- **Kuzu A.**, Songuler, O., Bogosyan, S., Gokasan, M., 2012: Fast locking of PLLs using fuzzy scheduled SMC, *IEEE ICUMT2012*
- **Kuzu A.**, Danis, U., Kurt, E., Karabulut, E., Sahinkaya, D., Bilgic, E., Kaplaner, A., Birecik, S., 2012: Test and calibration of sonobuoys in the air environment, *IEEE SIU2012*
- **Kuzu A.**, Songuler, O., 2012: Novel fuzzy-Smith predictor hybrid scheme for periodic disturbance reduction in linear time delay systems, *IEEE AMC2012*
- **Kuzu A.**, Bogosyan, S., Gokasan, M., 2012: Network in the loop platform for research and training in bilateral control, *IEEE AMC2012*
- **Kuzu A.**, Danis, U., Kurt, E., Karabulut, E., Sahinkaya, D., Bilgic, E., Kaplaner, A., 2011: Calibration of DIFAR Sonobuoys, *IEEE ISIE2011*
- **Kuzu A.**, Songuler, O., Bogosyan, S., Gokasan, M., 2011: Fast Locking of PLLs using Fuzzy Gain Scheduling, *IEEE ISIE2011*
- **Kuzu A.**, Songuler, O., Turk, S., Sonat, A., 2011: Automatic Interlocking Table Generation from Railway Topology, *IEEE ICM2011*
- Turk, S., Sonat, A., **Kuzu A.**, Soylemez, M.T., Songuler, O., Taralp, T., 2011: Automated Interlocking Algorithm Generation From Interlocking Tables For Railway Signalization Systems, *IEEE ICM2011*
- **Kuzu A.**, Bogosyan, S., Gokasan, M., 2010: Comparative Evaluation of two Chattering-free Sliding Mode Controllers for the Control of MEMS Optical Switches, *IEEE ISIE2010*
- **Kuzu A.**, Bogosyan, S., Gokasan, M., Sahinkaya, D., 2009: Fast Locking of PLLs using Sliding Mode Control, *IEEE ISIE2009*
- **Kuzu A.**, Bogosyan, S., Gokasan, M., 2009: Multipurpose Wireless Sensor Network Platform for Research and Training in Data Fusion, and Multi-feature Target Tracking, *IEEE HSI2009*
- **Kuzu A.**, Gokasan, M., Bogosyan, S., 2008: Survey: Odor Source Localization, *WSEAS ACACOS2008*
- **Kuzu A.**, Bogosyan, S., Gokasan, M., 2009: Multipurpose Wireless Sensor Network Platform for Research and Training in Data Fusion, and Multi-feature Target Tracking, *IEEE HSI2009*
- **Kuzu A.**, Gokasan, M., Bogosyan, S., 2007: Detection and Tracking of an Explosives Carrying Human with Odor-Sensor Based Multisensor Networks, *16th WSEAS International Conference on System Science and Simulation in Engineering*
- **Kuzu A.**, Bogosyan, S., 2006: Control Comparison of Multisensor Fusion Techniques for Improvement of Measurement Accuracy with MEM Accelerometers, *WSEAS MECHANICS'06*

- **Kuzu A.**, Bogosyan, S., Gokasan, M., 2006: Control Strategies for Increased Reliability in MEM Comb' Drives, *WSEAS MECHANICS'06*

Granted and Pending Patents/Utility Model Applications

- **Kuzu A.**, Kuzu, E., Pekgoz, E., Bircek, A., 2005, TR200500822U, *TPE*
- Korurek, M, **Kuzu A.**, Kuzu, E., 2004, TR200402139, *TPE*
- Korurek, M, **Kuzu A.**, Kuzu, E., 2004, TR200402140U, *TPE*

PUBLICATIONS/PRESENTATIONS ON THE THESIS

- **Kuzu A.**, Baran, E.A., Bogosyan, S., Gokasan, M., Sabanovic, A., 2015: Wavelet packet transform based compression for teleoperation, *Proceedings of the Institution of Mechanical Engineers, Part I: Journal of Systems and Control Engineering*, doi:10.1177/0959651815575438
- **Kuzu A.**, Bogosyan S., Gokasan M., and Sabanovic A., 2014: Experimental Evaluation of Novel Master-Slave Configurations for Position Control under Random Network Delay and Variable Load for Teleoperation, *Mathematical Problems in Engineering*, doi:10.1155/2014/608208.
- **Kuzu A.**, Baran, E.A., Bogosyan, S., Gokasan, M., Sabanovic, A., 2013: WPT based compression for bilateral control, *Industrial Electronics Society, IECON 2013 - 39th Annual Conference of the IEEE*, pp.5686-5691, doi:10.1109/IECON.2013.6700066
- **Kuzu A.**, Baran, E.A., Bogosyan, S., Gokasan, M., Sabanovic, A., 2013: Performance comparison of compression techniques used in bilateral control, *Industrial Electronics Society, IECON 2013 - 39th Annual Conference of the IEEE*, pp.5674-5679, doi:10.1109/IECON.2013.6700064
- **Kuzu A.**, Bogosyan, S., Gokasan, M., 2012: Network in the loop platform for research and training in bilateral control, *12th IEEE International Workshop on Advanced Motion Control (AMC), 2012*, pp.1-6, doi:10.1109/AMC.2012.6197132
- **Kuzu A.**, Bogosyan, S., Gokasan, M., Sabonovic, A., 2011: Control and measurement delay compensation in bilateral position control, *IEEE International Conference on Mechatronics (ICM)*, pp.1003-1010, doi: 10.1109/ICMECH.2011.5971263